# Effects of exogenously introduced miRNA molecules on CD274 expression in human tumor cell lines of various entities

Effekte exogen eingeschleuster miRNA Moleküle auf die CD274-Expression in humanen Zelllinien unterschiedlicher Krebsarten

Master Thesis of Melisa Nurcan Wartusch | 2934093

**Master of Science Biomolecular Engineering** 



Melisa Nurcan Wartusch

Matrikelnummer: 2934093

Studiengang: Master of Science Biomolecular Engineering – Molekulare Biotechnologie

#### **Masterthesis:**

Effekte exogen eingeschleuster miRNA Moleküle auf die CD274-Expression in humanen Zelllinien unterschiedlicher Krebsarten

# **Eingereicht:**

Interne Erstprüferin: Externer Zweitprüfer:

Prof. Dr. Beatrix Süß Prof. Dr. Stefan Eichmüller

Technische Universität Darmstadt Deutsches Krebsforschungszentrum

Fachbereich Biologie GMP & T Zelltherapie (Einheit D210)

Schnittspahnstraße 10 Im Neuenheimer Feld 280

64287 Darmstadt 69120 Heidelberg

i

Erklärung zur Abschlussarbeit gemäß § 22 Abs. 7 APB TU Darmstadt

Hiermit versichere ich, Melisa Nurcan Wartusch, die vorliegende Master-Thesis gemäß § 22 Abs. 7 APB

der TU Darmstadt ohne Hilfe Dritter und nur mit den angegebenen Quellen und Hilfsmitteln angefertigt

zu haben. Alle Stellen, die Quellen entnommen wurden, sind als solche kenntlich gemacht worden. Diese

Arbeit hat in gleicher oder ähnlicher Form noch keiner Prüfungsbehörde vorgelegen.

Mir ist bekannt, dass im Falle eines Plagiats (§38 Abs.2 APB) ein Täuschungsversuch vorliegt, der dazu

führt, dass die Arbeit mit 5,0 bewertet und damit ein Prüfungsversuch verbraucht wird.

Abschlussarbeiten dürfen nur einmal wiederholt werden.

Thesis Statement pursuant to § 22 paragraph 7 of APB TU Darmstadt

I herewith formally declare that I, Melisa Nurcan Wartusch, have written the submitted thesis

independently pursuant to § 22 paragraph 7 of APB TU Darmstadt. I did not use any outside support

except for the quoted literature and other sources mentioned in the paper. I clearly marked and

separately listed all of the literature and all of the other sources which I employed when producing this

academic work, either literally or in content. This thesis has not been handed in or published before in

the same or similar form.

I am aware, that in case of an attempt at deception based on plagiarism (§38 Abs. 2 APB), the thesis

would be graded with 5,0 and counted as one failed examination attempt. The thesis may only be

repeated once.

Datum / Date:

Unterschrift/Signature:

15.05.2023

Melisa N. Wartusch

ii

# Table of contents

1	. Overview	1
	1.1. Abstract	1
	1.2. Zusammenfassung	3
2	. Introduction	5
	2.1.microRNAs: small but powerful	5
	2.1.1. The function of microRNAs	5
	2.1.2. Biogenesis of microRNAs	5
	2.1.3. Cancer and microRNAs	7
	2.2. The role of immune checkpoint molecules	8
	2.2.1. At the intersection of programmed cell death	8
	2.2.2. NT5E expression and the formation of immunosuppressive microenvironments	10
	2.3. miRNA library for the regulation of PD-L1	12
	2.4. Aim of this study	13
3	. Methods	14
	3.1.Cell culture	14
	3.1.1. Standard cell culture conditions	14
	3.2.miRNA Transfection	15
	3.3.RT-qPCR	16
	3.3.1. Harvest of cells for RT-qPCR	16
	3.3.2. Isolation of RNA	16
	3.3.3. Quantification of RNA	16
	3.3.4. Synthesis of cDNA	17
	3.3.5. RT-qPCR	17
	3.3.6. RT-qPCR analysis	18
	3.4. Flow cytometry	19
	3.4.1. Harvest of cells for FACS	19
	3.4.2. Immunofluorescence staining and FACS measurement	19
	3.4.3. Analysis of FACS data	20
	3.5.XTT Assay	21
	3.6.3'-UTR reporter assay	22

3.7.Statistical analysis
4 Results
4.1. Comparison of immune checkpoint molecule expression profiles
4.2. Quantification of miRNA library transfection effects on PD-L1 and NT5E25
4.3. Validation of selected miRNA candidates
4.4. Investigation of miRNA effects on cell viability
4.5. Validation of direct interactions between miRNAs and PD-L1
5 Discussion
5.1.1. miRNA-mediated inhibition of PD-L1 expression in breast cancer cells
5.1.2. Effect of miRNA library on PD-L1 expression in human cell lines41
5.1.3. miRNA library and the regulation of NT5E42
5.1.4. Investigation of miRNA library induced cell viability effects
5.1.5. Validation of direct interactions between miRNAs and the 3'-UTR of PD-L1
5.1.6. miRNA candidates and impervious PD-L1 and NT5E levels
6 Conclusion
6.1.Outlook
7 Bibliography52
8 Appendix66
8.1. Supplementary figures
8.2. Figures
8.2.1. List of figures
8.2.2. List of supplementary figures75
8.3. List of tables
8.4. Abbreviations
8.5. Chemicals and materials
8.6. Acknowledgements84

# 1. Overview

#### 1.1. Abstract

The overexpression of the programmed cell death-protein 1 (PD-1) and its ligand PD-L1 play a key role in development and progression of cancer by inhibiting T cell activation, proliferation and survival. To date, targeting of the PD-1-PD-L1 axis harbors great therapeutic potential in the treatment of tumors by reversing cancer cell-driven immune escape and improving disease prognosis. Moreover, the aberrant expression of the immunoregulatory enzyme ecto-5'-nucleotidase (NT5E) in tumor tissue is strongly associated with the promotion of an anti-inflammatory state by inhibiting T cell-critical cytokine secretion and encouraging the generation of tumor tolerant type 2 macrophages. The dysregulated expression of PD-L1 and NT5E in cancer is linked to tumor growth, progression and reoccurrence resulting in overall poor survival rates. Unfortunately, recent studies have reported that the employment of common radiotherapy against solid tumors elevated PD-L1 and NT5E expression levels. Altogether, this unequivocally necessitates the elucidation of novel therapeutic approaches that effectively target the immense oncogenic potential of the immune checkpoint molecules PD-L1 and NT5E.

This thesis in particular investigated miRNA-mediated aberrant immune checkpoint molecule expression in human cell lines of three tumor entities through fluorescence-activated cell sorting (FACS) and quantitative real-time polymerase chain reaction (RT-qPCR). This study identified and characterized two novel tumor-suppressive miRNA candidates from a preselected library for the common inhibition of PD-L1 in all investigated cell lines: Both miR-3117-3p and miR-1273c significantly downregulated PD-L1 surface levels, indicating the miRNA-driven blockage of target mRNA transcript translation. For miR-3117-3p the results suggest that the presence of three predicted target binding sites within the three prime untranslated region (3'-UTR) of the PD-L1 mRNA further result in an overall decrease of target mRNA levels through transcript degradation. Adjacently, miR-3117-3p upregulated NT5E levels through binding site-independent effects in the breast cancer cell line. Furthermore, the molecular interactions between miR-1273c and the 3'-UTR of the PD-L1 mRNA were validated in a luciferase reporter assay, explaining the observed interference with PD-L1 surface levels through direct 3'-UTR binding events. Moreover, this investigation elucidated two multi-functional inhibitors for the simultaneous downregulation of PD-L1 and NT5E in the tumor cell lines tested: miR-155-5p and miR-512-3p decreased the surface expression of both targets via predicted binding sites. This study verified the in silico predicted binding site of miR-512-3p for the ligand PD-L1 via the conducted reporter assay. Interestingly, miR-512-3p transfection elevated NT5E enzyme levels exclusively in the melanoma cell line.

In conclusion, this study provided better insight into the regulation of miRNA-mediated immune checkpoint molecule expression in different human tumor entities. Thereby, several novel tumor-suppressive miRNA candidates were validated and characterized *in vitro* for the immune checkpoint molecules PD-L1 and NT5E. The elucidation of novel inhibitory miRNAs and their targets broadens our understanding of tumor development while bearing therapeutic potential for clinical application. In particular, the presented discovery of PD-L1 inhibiting miRNAs could be implemented as a new tool in combined radiotherapy approaches against tumors to mitigate PD-L1 enhancing side effects.

#### miRNAs affecting PD-L1 and NT5E expression

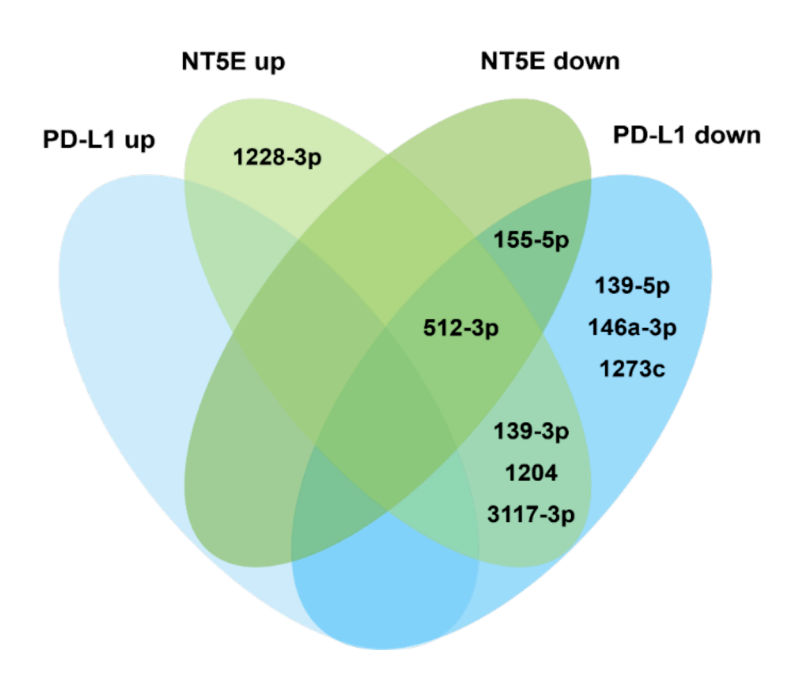


Figure 1: Summary of miRNA effects on PD-L1 and NT5E mRNA and surface level expression. Display of miRNAs significantly affecting both immunoregulatory target molecules in three human tumor entities. Flow cytometric and RT-qPCR data was acquired for the breast cancer cell line MDA-MB-231, the lung adenocarcinoma cell line CRL-5826 and the metastatic melanoma cell line MaMel86b, as well as the normal proximal tubular kidney cell line HK-2.

#### 1.2. Zusammenfassung

Die Überexpression des programmierten Zelltod-Proteins 1 (PD-1) und seines Liganden PD-L1 spielen eine Schlüsselrolle in der Entstehung von Krebs, indem sie die Aktivierung, die Vermehrung und das Überleben von T-Zellen hemmen. Das Eingreifen in die der PD-1-PD-L1-Achse birgt bislang ein großes therapeutisches Potenzial für die Behandlung von Tumoren, da man so die Krebszell-induzierte Immunflucht umkehrten und die Krankheitsprognose verbessern kann. Darüber hinaus fördert die krankhafte Expression des immunregulatorischen Enzyms Ecto-5'-Nukleotidase (NT5E) im Tumorgewebe einen entzündungshemmenden Zustand, indem die T-Zell-kritische Zytokinsekretion gehemmt und die Bildung von tumortoleranten Typ-2-Makrophagen gefördert wird. Die Dysregulation von PD-L1 und NT5E in Krebs steht im direkten Zusammenhang mit Tumorwachstum, Fortschreiten und Wiederauftreten der Krankheit. Aktuelle Forschung berichtet, dass herkömmliche Strahlentherapie bei soliden Tumoren die PD-L1- und NT5E-Expressionswerte deutlich erhöht. Die Erforschung neuer therapeutischer Ansätze ist unabdinglich, um dem immensen onkogenen Potenzial der Immun-Checkpoint-Moleküle PD-L1 und NT5E effektiv entgegenzuwirken.

Diese Thesis hat sich insbesondere der miRNA-mediierten Expression von Immun-Checkpoint-Molekülen in drei menschlichen Tumorentitäten gewidmet, dabei wurden Effekte mittels Durchflusszytometrie (FACS) und quantitativer Echtzeit-Polymerasekettenreaktion (RT-qPCR) untersucht. Diese Arbeit hat zwei neue zwei tumorsuppressive miRNA-Kandidaten aus einer vorselektierten Bibliothek identifiziert und charakterisiert, die in allen untersuchten Zelllinien eine universelle Hemmung von PD-L1 verursacht haben: Sowohl miR-3117-3p als auch miR-1273c führten zu einer signifikanten Herabregulierung des Liganden an der Zelloberfläche, was auf eine miRNA-gesteuerte Blockade der Translation der Ziel-mRNA hinweist. Spezifisch für miR-3117-3p deuten die Ergebnisse darauf hin, dass das Vorhandensein von drei vorhergesagten Zielbindungsstellen in der 3' untranslatierten Region (3'-UTR) von PD-L1, für den Abbau des mRNA-Transkripts verantwortlich sind welches in der allgemeinen Verringerung des Ziel-mRNA-Spiegels ersichtlich war. Kontrastierend, hochreguliert miR-3117-3p das Enzym NT5E in Brustkrebszellen durch vermeidlich bindungsstellenunabhängige Effekte. Darüber hinaus wurden molekularen Wechselwirkungen zwischen miR-1273c und dem 3'-UTR von PD-L1 in einem Luciferase-Reporter-Assay validiert, die beobachtete Herabregulierung von PD-L1 kann somit durch die direkte Bindung des Liganden doziert werden. Zusätzlich wurden im Rahmen dieser Untersuchung zwei multifunktionale Tumorinhibitoren für die simultane Herunterregulierung von PD-L1 und NT5E in Krebszellen identifiziert: miR-155-5p und miR-512-3p verringerten signifikant die Oberflächenexpression beider Ziele mittels vorhergesagte Bindungsstellen. In dieser Studie wurde die in silico vorhergesagte Bindungsstelle von miR-512-3p für den Liganden PD-L1 durch den durchgeführten Reporter-Assay verifiziert. Interessanterweise erhöhte die miR-512-3p-Transfektion den NT5E-Enzymspiegel ausschließlich in der Melanom-Zelllinie.

Zusammenfassend lässt sich sagen, dass diese Studie dazu beigetragen hat, mehr Einblicke in die Regulierung der miRNA-vermittelten Immun-Checkpoint-Expression in verschiedenen menschlichen Tumorentitäten zu gewinnen. Dabei wurden mehrere neue tumorsuppressive miRNA-Kandidaten validiert und für die Immun-Checkpoint-Moleküle PD-L1 und NT5E *in vitro* charakterisiert. Die Erforschung neuartiger suppressiver miRNAs und ihrer Zielmoleküle erweitert unser Verständnis der Krankheitsentwicklung bei Krebs und birgt so ein großes therapeutisches Potenzial für die klinische Anwendung. Insbesondere die hier präsentierte Ermittlung von PD-L1-hemmenden miRNAs könnte als neues Instrument in der kombinierten Strahlentherapie eingesetzt werden, um PD-L1-verstärkende Nebenwirkungen entgegenzuwirken.

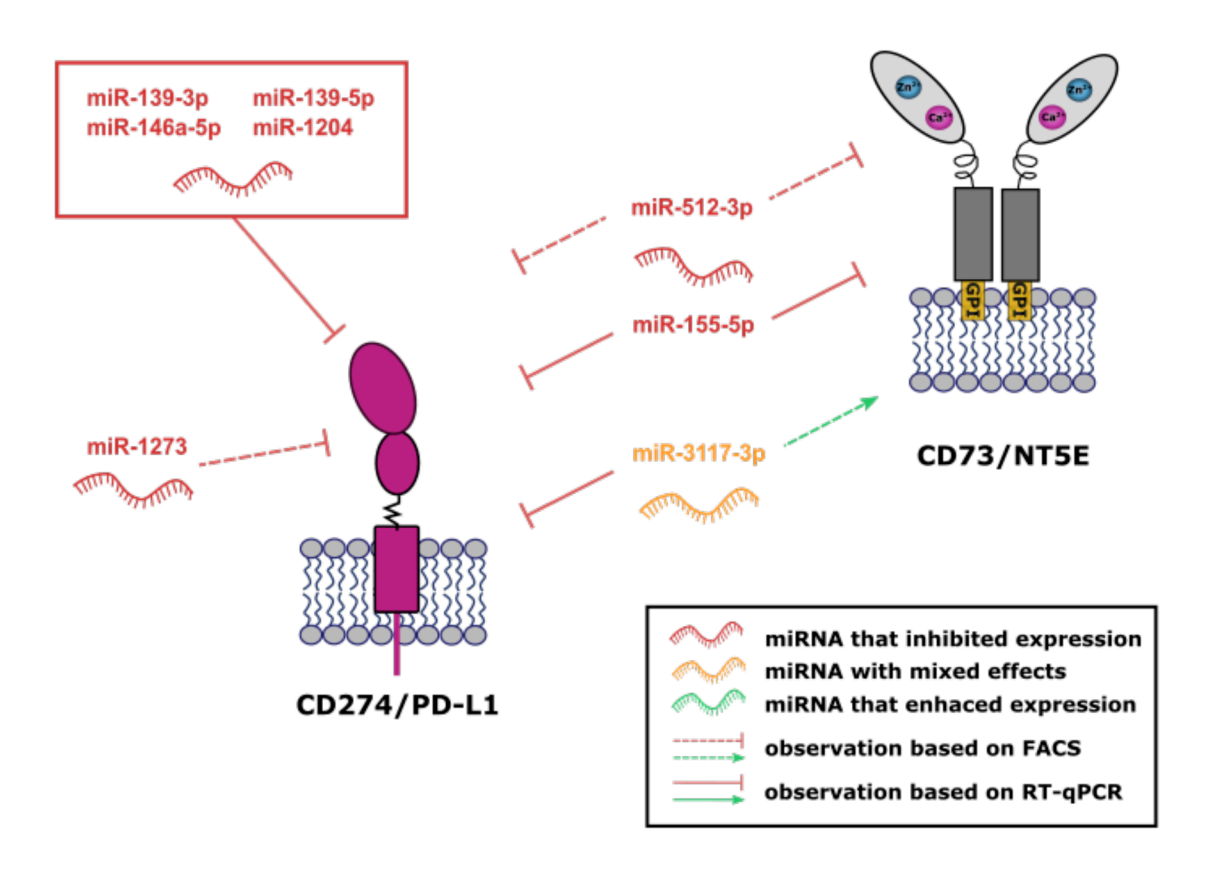


Figure 2: Zusammenfassung der miRNA Effekte in der Brustkrebslinie MDA-MB-231. In grün oder rot markiert sind mRNAs, die die Expression eines Immun-Checkpoint-Moleküls verstärkten oder hemmen. miRNAs mit gemischten Effekten sind in orange dargestellt. Beobachtungen, die nur auf der FACS-Analyse basieren sind mit gestrichelten Linien dargestellt, während RT-qPCR validierte intrazelluläre Effekte mit durchgehenden Linien dargestellt sind.

# 2. Introduction

# 2.1. microRNAs: small but powerful

#### 2.1.1. The function of microRNAs

The first microRNA (miRNA), lin-4, was discovered in Caenorhabditis elegans, where it was identified to regulate the expression of the protein lin-14 during the development of the round worm (R. C. Lee et al., 1993). This finding did not only shake the foundation of the central dogma of gene expression and regulation (Crick, 1956), but has also since irrevocably awarded microRNA with its great importance, hence revolutionizing the field of RNA research (Almeida et al., 2011; Orellana, 2015). Nowadays, miRNAs are defined as an abundant group of highly conserved, endogenous, small non-coding RNA molecules consisting of 19-22 nucleotides (nt) with the power of post-transcriptionally regulating the expression of genes (Hammond, 2015). Specifically, miRNAs possess a 2-8 nt long seed region that enables the binding of several different target mRNAs (Bartel, 2004, 2018). Their primary modus operandi is the targeting of a complementary sequence in the 3' untranslated region of a desired messenger RNA (mRNA) and the subsequent interference in the cell's translational machinery (Mayya & Duchaine, 2019). The exact outcome of this process is highly dependent on the degree of successful base-pairing between a miRs seed region and the mRNA transcript: Large-scale base-pairing triggers the recruitment of mRNA decay factors leading to target mRNA destabilization and degradation (Wilczynska & Bushell, 2015). The matchup of seed and mRNA sequences at a less extensive scale result in the blockage of mRNA translation (Farazi et al., 2008). Consequently, miRs are capable of regulating gene expression and play a crucial role in various biological processes such as cell differentiation, proliferation and apoptosis (Y. Huang et al., 2011).

## 2.1.2. Biogenesis of microRNAs

The biosynthesis of miRNAs commences with the transcription of deoxyribonucleic acid (DNA) in the nucleus. The origin of miRNA sequences can be of intragenic or intergenic nature. Currently, more than half of the identified miRNAs are intragenic, stemming from miRNA genes located within the genomic region of a protein encoding gene. Intragenic miRNAs are mainly processed from intronic and few extronic sequences of their host genes. Adjacently, intergenic miRNAs are independently transcribed from host genes through individual promoter and terminator units (Hinske et al., 2014; Monteys et al., 2010).

The processing of miRNA can be divided into the realms of canonical and non-canonical miRNA biogenesis (Figure 3, p. 6). In mammals the majority of miRNAs are transcribed canonically by RNA polymerase II/III resulting in long primary transcripts called pri-miRNAs (Borchert et al., 2006; Ha & Kim, 2014). Next, pri-mRNAs are further processed within the nucleus by a microprocessor protein

complex, consisting RNA binding protein DiGeorge Syndrome Critical Region 8 (DGCR8) and the RNAse III-type endonuclease Drosha (Denli et al., 2004). Specifically, DGCR8 recognizes N6-methylated GCAC motives within the hairpin loop of pri-miRNAs, while Drosha catalyzes the cleavage of the transcripts into pre-miRNAs with a characteristic 70 nucleotide (nt) long hairpin structure and 2 nt long 3'-overhangs (Alarcón et al., 2015; Roth et al., 2013).

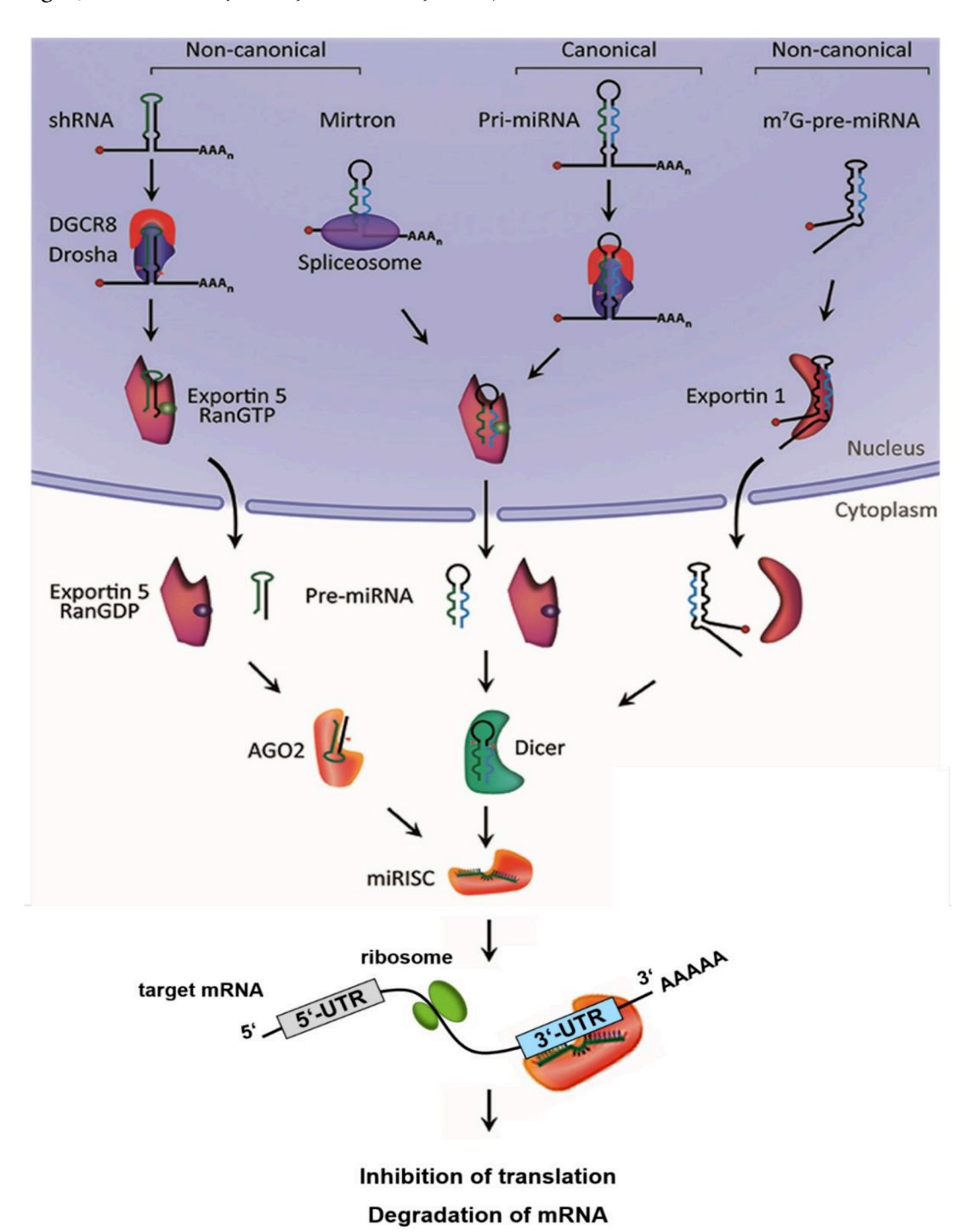


**Figure 3: Biogenesis of miRNAs through canonical and non-canonical pathways.** Mature miRNAs are incorporated into the miRNA-induced silencing complex (miRISC) targeting the 3'-UTR of mRNA transcripts, blocking translation or inducing mRNA degradation (adapted from O'Brien et al., 2018).

The resulting pre-miRNA molecule is exported to the cytosol by the Ran-GTP-dependent nuclear transporter Exportin 5 (XPO5) and further processed by the RNase III endonuclease Dicer (Roth et al., 2013). Thereby, Dicer cleaves the pre-miRNA, removing its terminal loop and creating an approximately 20 nt long mature miRNA/miRNA\* duplex (H. Zhang et al., 2004). The completion of miRNA biogenesis is achieved by the Argonaute protein family (Ago) facilitated binding of the pre-miRNA forming the miRNA-induced silencing complex (miRISC). Finally, RNA helicases unwind the miRNA duplex, which leads to the unloading and subsequent AGO2-mediated cleavage of the miRNA\* passenger strand. The vestigial guide strand remains bound in the miRISC complex as mature miRNA (Pong & Gullerova, 2018).

In contrast, non-canonical miRNA biogenesis is carried out in either Drosha/DGCR8-independent or Dicer-independent pathways. An example of Drosha/DGCR8-independent pre-miRNA processing are mirtrons, which transcribed within intronic sequences of protein encoding genes. In principle, mirtrons are spliced and debranched by the RNA lariat debranching enzyme. The resulting refolded hairpin pre-miRNA structures are further processed to mature miRNAs by Dicer, without the involvement of typical hairpin processing by Drosha (Westholm & Lai, 2011). Adjacently, endogenous short hairpin RNA (shRNAs) transcripts are processed in an Drosha-dependent matter in Dicer-independent biogenesis pathways. Notably, these short pre-miRNAs require AGO2-mediated miRNA maturation, as they lack sufficient length to be processed by Dicer (S. Yang et al., 2010).

#### 2.1.3. Cancer and microRNAs

Copious studies have established that the aberrrant biogenesis of miRs is linked to numerous molecular mechanisms in various diseases (Ardekani & Naeini, 2010). Explicitly, it has been discovered that miRNA dysregulation has a profound effect on cancer development, signaling and progression. Further effects on the hallmarks of cancer include the evasion of growth suppressors, resistance to cell death, initiation of tumor angiogenesis and cell invasion (Shah & Shah, 2020). The microRNA mismanagement in aberrant cells is promoted by the amplification, deletion, point mutation and abnormal methylation of miRNA genes, along with failing transcriptional controls and defects within the miRNA biogenesis machinery (Peng & Croce, 2016). Thereby, microRNAs can be dissected into two oversimplified classes of corruption: Severely overexpressed, cancer promoting oncomiRNAs and actively downregulated tumor suppressor miRs, that encourage the disease advancement through the creation of a pro-tumoral environment accompanied by immune cell evasion (Cho, 2007; M. Yi et al., 2020). In recent years, miRNA profiling and deep sequencing have embraced ill-willed miRNA expression and in return have elucidated dysregulation signatures as a tool for tumor classification, diagnosis and even prognosis of patient survival (Paranjape et al., 2009; Zhou et al., 2015). Moreover, it has been demonstrated that the

respective inhibition or stimulation of oncomiRNAs and tumor suppressor miRNAs leads to a significant reduction in cancer cell proliferation and metastasis, with the potential for complete cancer regression (Medina et al., 2010). The categoric duality and net function of individual miRNAs in the tumor microenvironment has been controversially discussed (Svoronos et al., 2016), sparking research in the field of miRNA drugs. Forthwith, two ideologies have formed: The employment of antagomiRs for the targeted interference with oncomiRs through complementary sequence binding. Adjacently, the use of tumor suppressive mimic miRs for the silencing of oncogenes (Ors-Kumoglu et al., 2019). Finally, the full potential of microRNAs as biomarkers, therapeutic drugs and targets is yet to be realized. New innovative large-scale and high-throughput screening methods for miRNA library characterization and better strategies for targeted-stable *in vivo* miRNA delivery must be generated in order to unleash the unequivocal power of RNA in modern medicine (Momin et al., 2021; Rupaimoole & Slack, 2017).

# 2.2. The role of immune checkpoint molecules

# 2.2.1. At the intersection of programmed cell death

The programmed cell death-protein 1 (PD-1), also known as CD297, is a co-inhibitory receptor expressed on the surface of antigen-stimulated T cells and B cells (Agata et al., 1996; Ishida et al., 1992). PD-1 is an important immune checkpoint molecule that plays a vital role in the upkeep of self-tolerance and limiting tissue damage through the surveillance of T-cell activity. Thereby, autoimmunity is prevented by the activation of apoptosis in self-reactive T cells, while cell death of regulatory T cells is inhibited (Fife & Pauken, 2011). The type 1 transmembrane protein belongs to the immunoglobulin (Ig) superfamily and consists of an extracellular N-terminal Ig-V like domain, a transmembrane domain and an intracellular tail. Thereby, the cytosolic unit contains two phosphorylation sites within an immunoreceptor tyrosine-based switch motif (ITSM) and an immunoreceptor tyrosine-based inhibitory motif (ITIM) (X. Zhang et al., 2004). PD-1 is bound by its two ligands, programed cell death-ligand 1 and 2 (PD-L1/2), which are referred to as CD274 and CD273 according to their cluster of differentiation. Under normal conditions PD-L1 is expressed on the surface of antigen presenting cells, T and B cells, as wells as non-hematopoietic cells such as endo- and epithelial cells. Structurally, the 40 kDA large ligand is made up of an extracellular N-terminal Ig-V and a C-terminal Ig-C like domain, as well as a transmembrane domain and a short intracellular segment that does not contain any canonical signaling motifs (Dong et al., 1999; Zheng et al., 2019). Its sister ligand, PD-L2, shares several homologous sequence motives with PD-L1 and is specific to macrophages, dendritic cells and mast cells. Under pathological conditions, both PD-L1 and PD-L2 are expressed by a wide array of cancer cells and tumor-associated stroma cells (Latchman et al., 2001; Sharpe et al., 2007). In the last two decades, studies have shown that the interaction between PD-1 and PD-L1/2 at tumor sites contributes to the

creation of a pro-tumoral environment through the inhibition of T cell activation and proliferation, leading to a state of T cell exhaustion (Okadome et al., 2020; Sun et al., 2018).

In detail, the binding of PD-L1s extracellular domains to PD-1 induces a conformational change within the receptor, which enables the phosphorylation of both ITSM and ITIM by Src family kinases. In return these phosphorylated tyrosine motives recruit SHP-1 and SHP-2 protein tyrosine phosphatases, which then dephosphorylate the co-stimulatory receptor CD28 (Figure 4). In addition, PD-1/PD-L1 binding induces the dephosphorylation of the T-cell receptor associated molecule Zeta-chain-associated protein kinase 70 (ZAP70), leading to the attenuation of T cell activating signals (Hui et al., 2017; Zak et al., 2015). The interaction of PD-1 and PD-L1 results in the overall reduction of cytokine production, T cell proliferation and survival, aiding cancer cells in immune evasion (Butte et al., 2007; Sheppard et al., 2004).

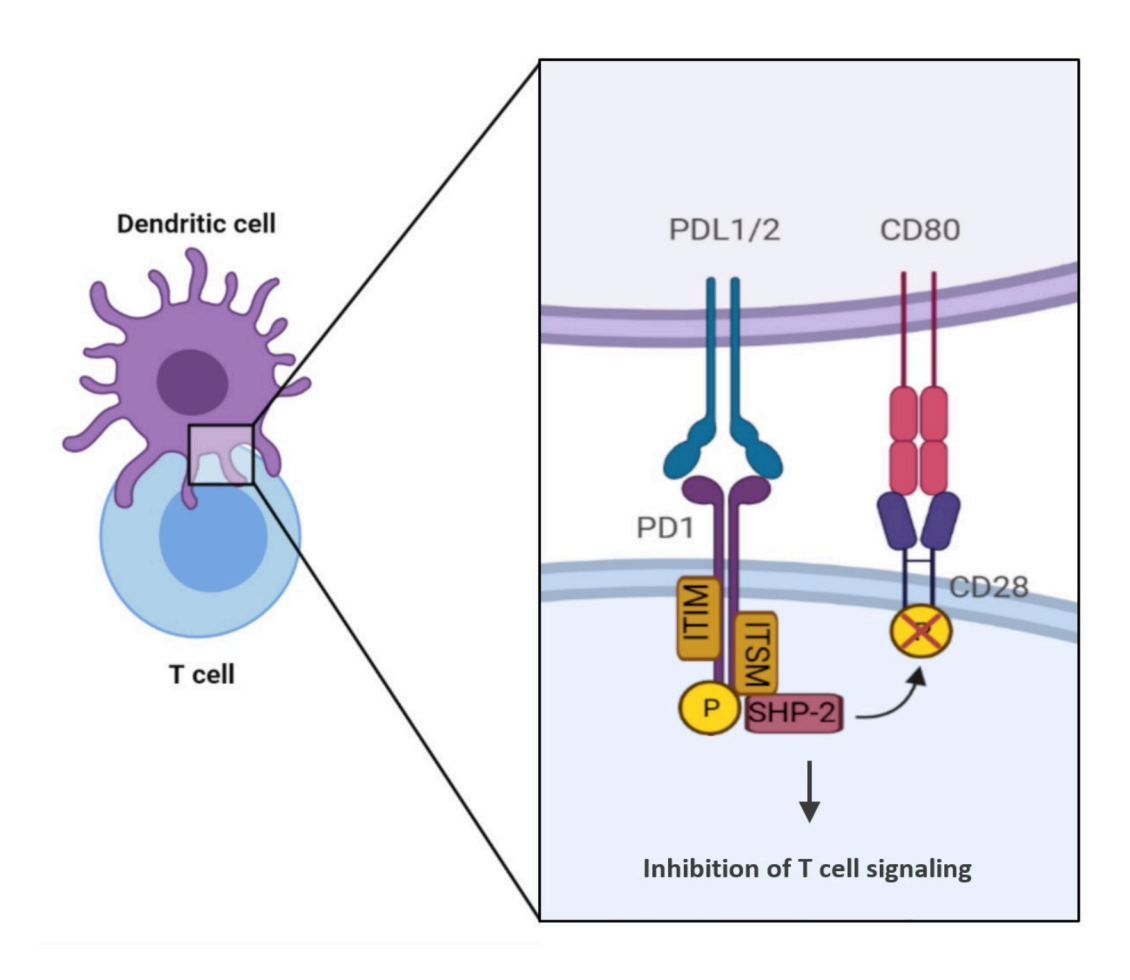


Figure 4: Structure and function of PD-1 and its ligand PD-L1. The ligation of PD-1 / PD-L1 induces the phosphorylation of the immunoreceptor tyrosine-based switch motif (ITSM) and the immunoreceptor tyrosine-based inhibitory motif (ITIM), recruiting SHP-2 protein tyrosine phosphatases for the dephosphorylation of the co-stimulatory receptor CD28. Overall, the binding of PD-1 to its ligand PD-L1 results in the inhibition of T cell signaling and survival (adapted from Farrukh et al., 2021).

Since, PD-1 overexpression plays a global role in a large number of malignancies, the PD-1-PD-L1 axis harbors great potential as a therapeutic target (Couzin-Frankel, 2013). Different approaches to this challenge have since been undertaken with the most notable strides in the field of antibody-based inhibitors: Numerous studies in patients have demonstrated that the blockage of PD-1 pathways through the application of engineered IgGs have a positive effect on tumor reduction, responsiveness and overall survival rate in an abundance of cancer; including but not limited to melanoma, non-small cell lung cancer, Hodgkin's lymphoma, bladder cancer, renal-, squamous- and Merkel cell carcinoma (Han et al., 2020). For instance, Han and colleagues have recently reported the complete remission of a patient with advanced metastatic gastric cancer through the admission of the PD-1 blocking fully human monoclonal antibody Nivolumab in combination with chemotherapy and palliative surgery (Dai et al., 2022). It has become ever so evident that therapeutically targeting PD-1-PD-L1 interactions in clinical illness is key to treating and potentially defeating so-called uncurable diseases.

#### 2.2.2. NT5E expression and the formation of immunosuppressive microenvironments

The enzyme ecto-5'-nucleotidase (NT5E), also referred to as CD73, is expressed on the cell surface of various cells types and plays an important role in the maintenance of immune homeostasis (D. Allard et al., 2017). Thereby, NT5E acts like an immunological switch by facilitating the transition between pro- and anti-inflammatory states, through nucleotide hydrolysis (Beavis et al., 2012). The ecto-enzyme consists of a dimeric C-terminal domain that harbors the substrate binding pocket and is anchored to the cell membrane through glycosylphosphatidyl inositol linkage, with no additional membrane-embedded elements. Whereas, the N-terminal domain coordinates the divalent catalytic co-factors Zn<sup>2+</sup> and Ca<sup>2+</sup>. Both segments are connected by a flexible  $\alpha$ -helix, that enables the change of enzyme conformation during substrate cleavage (Sträter, 2006). Functionally, NT5E cooperates with ectonucleoside triphosphate diphosphohydrolase 1 (ENTPD1) in the catabolization of extracellular adenosine triphosphate (ATP). Initially, ENTPD1 catalyzes the reversible two-step dephosphorylation of ATP into adenosine monophosphate (AMP) (Antonioli et al., 2013). Next, the generated AMP substrate is bound by NT5E and irreversibly hydrolyzed forming free adenosine (Figure 5, p. 11). Human regulatory T cells are widely known to express NT5E on their cell surface in order to sustain anti-inflammatory responses among surrounding effector T cells, macrophages, dendritic and natural killer cells. This process is crucial for the preservation of self-tolerance and hence the prevention of autoimmune diseases (Bettelli et al., 2006; Kalekar et al., 2016). The released adenosine acts on the G-coupled receptors A1, A2a, A2b and A3 in neighboring cells. Namely, the adenosine receptor A2a is expressed on T cells, natural killer cells and dendritic cells, where it is encoded by the ADORA2A gene and is associated with Ga proteins of the G<sub>s</sub> subtype (Fredholm et al., 2011). Upon adenosine stimulation, the receptor changes

conformation allowing the release of the activated  $G\alpha_s$  subunit from its  $G\beta\gamma$  dimers. While G protein  $G\beta\gamma$  subunits contribute to mitogen-activated protein kinase (MAPK) and phospholipase C (PLC) signaling, the  $G\alpha_s$  group initiates the cyclic AMP (cAMP) pathway (Carpenter & Lebon, 2017; Jacobson & Gao, 2006). Specifically, the activation of adenylyl cyclases results in the hydrolysis of intracellular ATP forming cAMP, which leads to the further activation of the protein kinase A (PKA). In effector T cells, PKA finally phosphorylates the C-terminal Scr kinase, thus inhibiting the Src family tyrosine kinases Lck and Fyn and blocking the completion of T cell receptor signaling (Mosenden & Taskén, 2011).

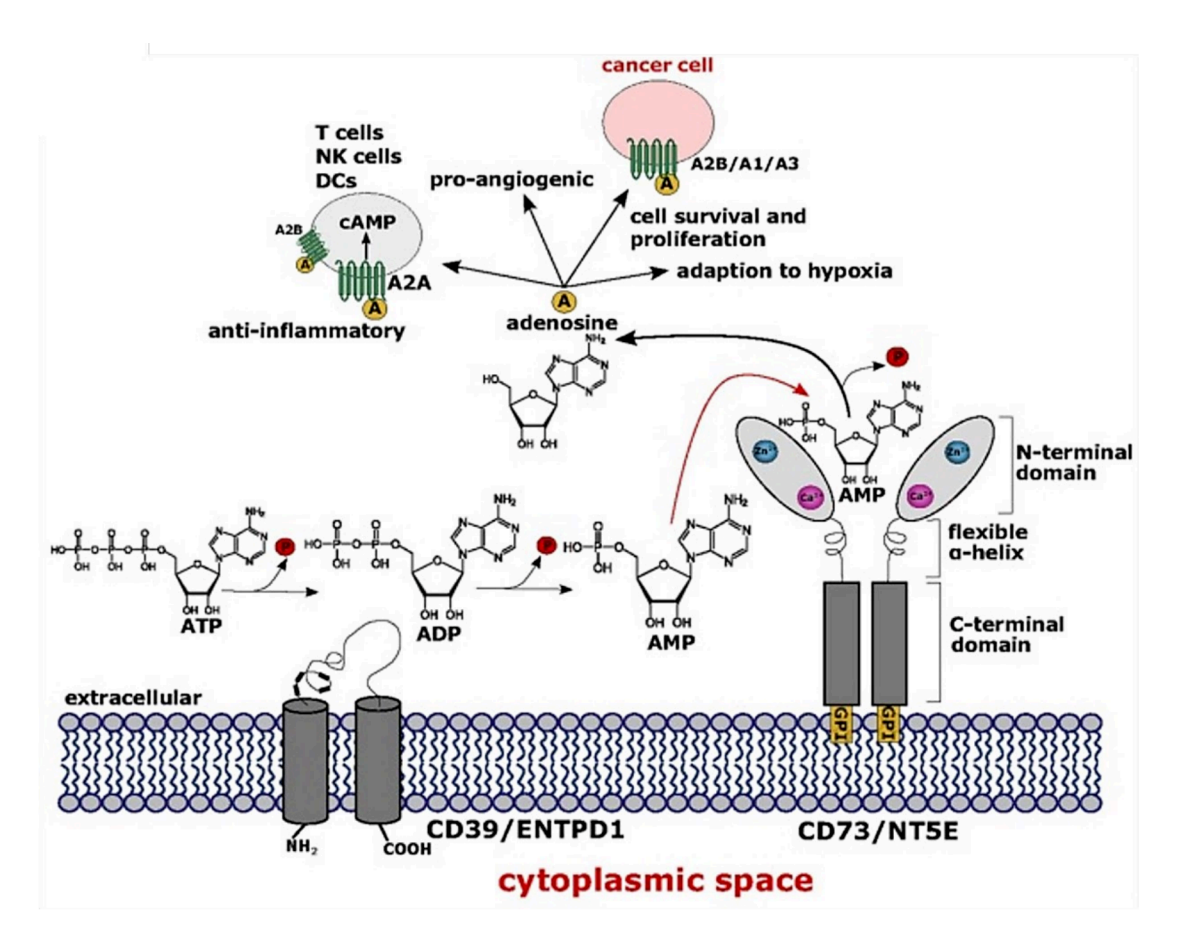


Figure 5: Structure and function of NT5E. The membrane bound enzymes ectonucleoside triphosphate diphosphohydrolase 1 (ENTPD1) and ecto-5'-nucleotidase (NT5E) cooperatively catabolize extracellular adenosine triphosphate (ATP) to free adenosine. In T cells, natural killer (NK) and dendritic cells (DCs) the produced adenosine is bound by the adenosine A2A receptor and induces anti-inflammatory effects. In cancer cells A2B receptors are stimulated, resulting in increased tumor cell proliferation and survival (Kordaß et al., 2018).

Under heathy conditions, NT5E expression is a safe guard protecting from overreactive immune responses, while in sickness infected and genetically aberrant cells strategically express the enzyme to further an anti-inflammatory state (Aandahl et al., 1998; Stagg et al., 2011). The aberrant expression of

NT5E by tumor cells has been reported in numerous cancer entities, including melanoma, glioblastoma, non-small cell lung cancer, breast, ovarian and prostate cancer. Thereby, cancer cells make use of the adenosine dependent blockage of T cell proliferation, activation and migration creating a tumor friendly environment. Additionally, adenosine-driven immune escape is facilitated by the suppression of inflammatory cytokine secretion in macrophages, as well as the accelerated conversion of tumor-reactive type 1 macrophages into tumor-tolerant type 2 macrophages (Antonioli et al., 2016; Haskó & Pacher, 2012; T. Jiang et al., 2018). In further synergy, cancer cells hijack the downstream cAMP pathway by expressing several adenosine receptors: Stimulation of A2B receptors in cancer cells results in tumor cell proliferation and survival. The additional expression of A1 and A3 receptors leads to tumor cell migration through Gi protein signaling (Ohta, 2016). As extracellular adenosine levels coincide with intracellular cAMP levels, which promote overall cancer cell aggressiveness, unresponsiveness, metastasis and angiogenesis, researcher have deemed NT5E as a promising therapeutic target (B. Allard et al., 2014; Stagg & Smyth, 2010).

Recent trends in cancer targeting are shifting their focus from therapeutic antibodies to small molecules: Müller and colleagues have reported the function of a potent NT5E inhibitor in various cell types. The small molecule  $\alpha,\beta$ -methylene-ADP (APCP) and its derivatives harbor great clinical potential, as they block the synthesis of adenosine by highly competing with the substrate AMP (Bhattarai et al., 2015). These results are especially promising considering reports stating that the application of small molecules in cancer therapy has several advantages over the treatment with traditional monoclonal antibodies. The significant size difference is a particular asset of small molecules, facilitating the movement across physiological borders and thus achieving greater exposure within the microenvironment of the tumor. Additionally, small molecules have better bioavailability upon oral application and thus are more easily administered to patients, compared to therapeutic antibody administration (Young et al., 2014). Concluding, the further exploration of cancer as a dynamic process is crucial for enhancing our knowledge on how and why cancer evolves. In future, the full scope of targets and adjacent treatments must be investigated while also considering innovative forms of therapeutic molecule delivery.

## 2.3. miRNA library for the regulation of PD-L1

The ongoing discovery of new miRNAs, function and targets produces an ever so increasing density of information, necessitating the collection of miRNA sequences and annotations in public databases (Alles et al., 2019). Currently, the reference repository miRBase (v22) contains 38589 entries across 271 organisms, including 1917 human miRNA hairpin precursors and 2656 mature miRNAs (Kozomara et al., 2019). The exploration of uncharacterized miRNA-mRNA interactions and the identification of

functionally active miRNAs in high-throughput screenings is yet to be concluded. The growing number of miRNAs constitute a challenge of great dimension not only for *in vivo* validation, but also for *in silico* bioinformatic prediction and analysis (Plotnikova et al., 2019). Previous works of the Eichmüller group utilized the MISSION Human miRNA mimics library V21 from Siga-Aldrich, containing 2754 individual miRNAs. The comprehensive FACS-based library screen elucidated novel miRNAs involved in the regulation of immune checkpoint molecule expression in human cancer cells. Specifically, miR-1285-5p and miR-3134 were identified as tumor suppressive miRNAs by binding to the 3'-UTR of NT5E and thus inhibiting the expression of this immunoregulatory enzyme (Kordaß, 2021; Kordaß et al., 2018). Following this investigation, a refined miRNA library was compiled of miRNAs downregulating surface expression levels of PD-L1 in the human breast cancer cell line MDA-MB-231. This preselected miRNA library was further utilized and examined in the following study (Table 1, p. 15).

## 2.4. Aim of this study

The rationale of this thesis was the identification and characterization of miRNAs regulating the aberrant immune checkpoint molecule expression in human tumor cells, with particular focus on the immunomodulatory ligand PD-L1. Therefore, a preselected human miRNA library was screened for miRNAs affecting PD-L1 expression in three different tumor entities and normal kidney cells upon transient transfection, aiming to elucidate multi-functional miRNA candidates. Unveiling universally applicable tumor-suppressive miRNAs inhibiting PD-L1, might provide new options to improve therapeutic cancer targeting.

# 3. Methods

All used chemicals, solutions and materials, as well as the vendors and their headquarters are listed in the appendix (Table 10-16).

#### 3.1. Cell culture

The described cell culture experiments were performed under sterile conditions within a laminar flow hood using four human cell lines of various tumor entities as well as healthy human kidney cells. The investigated cancer cell lines included the human epithelial breast adenocarcinoma cell line MDA-MB-231 (ATCC®: HTB-26, USA), the human metastatic melanoma cell line MaMel86b (Universitätsklinik Mannheim, Germany), the human non-small-cell lung carcinoma cell line CRL-5826 (ATCC®: NCI-H226, USA) and the human colorectal adenocarcinoma cell line HT-29 (ATCC®: HTB-38, USA). Additionally, the proximal tubular kidney cell line HK-2 (ATCC®: CRL-2190, USA) was cultivated. All cell lines were authenticated by genetic genotyping and continuous mycoplasma testing was performed to verify correct genetic lineage and sterile cell stocks. All solutions were warmed up to 37 °C prior to their usage and all incubation steps were carried out at 37 °C, 5 % CO<sub>2</sub> and 98 % humidity.

#### 3.1.1. Standard cell culture conditions

All cells were cultivated in Roswell Park Memorial Institute 1640 medium (RPMI 1640) supplemented with 10 % (v/v) fetal calf serum (FCS) and 1 % (v/v) penicillin-streptomycin antibiotics. The four cell lines were passaged twice weekly, following this procedure: The cells were briefly washed with 10 mL phosphate buffered saline (PBS). Next, the cells were detached using 3 mL of 0.25 % trypsin-EDTA and incubated at 37 °C for 5 min. The trypsinization reaction was stopped by the addition of 7 mL of culture medium.

The live cell concentration for cell seeding was determined by mixing 90  $\mu$ l cell suspension with 10  $\mu$ l 0.4 % trypan blue solution. Thereafter, 10  $\mu$ l of the created cell-trypan blue sample was pipetted onto a C-CHIP disposable hemocytometer. All living cells within the large 4x4 grid square divisions were counted and the cell titer was calculated according to Equation 1.

$$\frac{\text{Counted cells}}{4} * 10 = X * 10^4 \text{ cells/mL}$$
 Equation I

Lastly, 5\*10<sup>5</sup> cells were seeded into 15 mL of culture medium and cultivated in a new cell culture flask.

For the following experiments cells were seeded in antibiotic-free culture medium. For FACS and RT-qPCR experiments the fast-growing cell lines MDA-MB-231 and CRL-5826 and the slow-growing cell lines MaMel86b, HK-2 and HT-29 were seeded in 12-well plates at a cell density of  $1*10^5$  and respectively  $2*10^5$  cells per well. For the XTT assay and 3'UTR reporter assay all cells were seeded in 96-well plates at a density of  $1*10^4$  cells per well.

#### 3.2. miRNA Transfection

The transfection of microRNA into human cells was carried out through the generation of Lipofectamine<sup>™</sup> RNAiMAX (Thermo Fischer Scientific, USA) liposomes. All steps performed during transfection were carried out using RNase free filter-tips. To begin with, MDA-MB-231, CRL-5826, MaMel86b and HK-2 cells were seeded in 12-well plates to achieve 60-70 % confluency at the day of transfection. After 24 h, the appropriate cell growth and confluency was checked before commencing with the transfection of miRNAs in Table 1. Cells were transfected according to the manufacturers protocol with a final miRNA concentration of 50 nM per well. After transfection, cells were incubated at standard cell culture conditions for 24 h before the addition of 1 mL/ well culture medium. Finally, cells were harvested for RT-qPCR or FACS measurements 48 h or 72 h post transfection (p.t.).

Table 1: microRNA library and short reference names used for Lipofectamine™ transfection.

microRNAs	Referred to as	Sequence
miRIDIAN® microRNA Mimic:  1. hsa-miR-139-3p	miR-139-3p	UGGAGACGCGGCCCUGUUGGAGU
2. hsa-miR-139-5p	miR-139-3p	UCUACAGUGCACGUGUCUCCAGU
3. hsa-miR-146a-3p	miR-146a-3p	CCUCUGAAAUUCAGUUCUUCAG
4. hsa-miR-146a-5p	miR-146a-5p	UGAGAACUGAAUUCCAUGGGUU
5. hsa-miR-155-5p	miR-155-5p	UUAAUGCUAAUCGUGAUAGGGGUU
6. hsa-miR-374b-3p	miR-374b-3p	CUUAGCAGGUUGUAUUAUCAUU
7. hsa-miR-512-3p	miR-512-3p	AAGUGCUGUCAUAGCUGAGGUC
8. hsa-miR-1204	miR-1204	UCGUGGCCUGGUCUCCAUUAU
9. hsa-miR-1228-3p	miR-1228-3p	UCACACCUGCCUCGCCCCCC
10. hsa-miR-1273c	miR-1273c	GGCGACAAAACGAGACCCUGUC
11. hsa-miR-3117-3p	miR-3117-3p	AUAGGACUCAUAUAGUGCCAG
mirVana™ miRNA Mimic: Negative Control #1 (ath-miR-416)	Mimic Control-1	GGUUCGUACGUACACUGUUCA
ON-TARGETplus SMART pool Human CD274	PD-L1 siRNA pool	Composed of 4 individual siRANs
ON-TARGETplus SMART pool Human NT5E	NT5E siRNA pool	Composed of 4 individual siRANs

## 3.3. RT-qPCR

In order to prevent RNA degradation during the sample preparation for RT-qPCR, all steps were performed using RNaseZAP<sup>TM</sup> cleaned equipment and RNase free filter-tips.

#### 3.3.1. Harvest of cells for RT-qPCR

For RT-qPCR analysis, cells were harvested 48 h p.t. by removing the culture media and adding  $100\,\mu\text{l}/\text{ well }0.25\,\%$  trypsin-EDTA. The cells were detached at 37 °C for 5 min and resuspended in  $500\,\mu\text{l}$  antibiotic-free culture medium. Next, the cell suspension was centrifuged for 5 min at 3500 rcf and 4 °C. Ultimately, the cell pellets were resuspended in 1 mL QiAzol<sup>TM</sup> lysis reagent (Qiagen, Germany) and stored at -80 °C until further RNA isolation.

#### 3.3.2. Isolation of RNA

For the isolation of total RNA from frozen cell samples, the miRNeasy Mini Kit (Qiagen, Germany) was used according to the manufacturers protocol. The phenol/guanidine thiocyanate-based lysis of samples and the silica membrane-based purification of RNA enabled the analysis of intracellular miRNA and mRNA expression. Specifically, RNA was eluted in 40  $\mu$ l nuclease-free water and stored at -80 °C until further usage in cDNA synthesis.

#### 3.3.3. Quantification of RNA

The quantification of isolated RNA was carried out by fluorometric concentration measurements via the Qubit<sup>™</sup> 4 Fluorometer (Thermo Fisher Scientific, 2022). Therefore, the RNA samples, Qubit<sup>™</sup> microRNA standards and the working solution was pipetted into Qubit<sup>™</sup> Assay Tubes according to the instructions of the Qubit<sup>™</sup> microRNA Assay Kit (Thermo Fischer Scientific, USA). All assay tubes with respective compositions (Table 2) were vortexed for 3 s, incubated at RT for 2 min and measured by the microRNA program of the Qubit<sup>™</sup> 4 Fluorometer.

Table 2: Composition of assay tubes for Qubit™ 4 Fluorometer measurements.

Reagent volume	Qubit <sup>™</sup> standard	Sample
Working solution	190 μl	198 μl
Qubit <sup>TM</sup> Standards #1 and #2	$10~\mu\mathrm{l}$	-
Sample	-	$2\mu\mathrm{l}$
Total volume in assay tube	200 μl	200 μl

### 3.3.4. Synthesis of cDNA

For the synthesis of cDNA, 500 ng of isolated total RNA were reverse-transcribed using the High-Capacity cDNA Reverse Transcription Kit (Thermo Fischer Scientific, USA). The reaction was carried out with a Veriti<sup>TM</sup> 96 Well Thermal Cycler (Applied Biosystems, USA) according to the manufacturer's specifications (Table 3).

Table 3: cDNA Synthesis components and thermal conditions.

Reagent volume	Amount	Program		
for 1 reaction		Temperature [°C]	Time [min]	
RNA	10 μl (500 ng)			
10x RT Buffer	$2\mu\mathrm{l}$	65	10	
25x dNTP Mix (100 mM)	$0.8\mu\mathrm{l}$	Immediately on ice	5	
10x RT Random Primer	$2\mu\mathrm{l}$	50	60	
MultiScribe™ Reverse Transcriptase	$1~\mu \mathrm{l}$	85	5	
Nuclease-free water	$4.2~\mu\mathrm{l}$	4	$\infty$	
Total volume	$20~\mu l$			

For the subsequent usage in RT-qPCR, the synthesized cDNA samples were diluted in 1:4 PCR grade water and stored at -20 °C.

#### 3.3.5. RT-qPCR

The RT-qPCR reaction was carried out, in order to analyze the intracellular levels of specific mRNA targets. Therefore, individual master mixes for each target were prepared using the *Power* SYBR® Green PCR Master Mix (Applied Biosystems, USA). For the reaction,  $2 \mu l$  diluted cDNA sample and  $18 \mu L$  master mix were pipetted into a 96-well plate. Lastly, all RT-qPCRs were run on a QuantStudio<sup>TM</sup> 3 Real-Time PCR System using the QuantStudio<sup>TM</sup> Design and Analysis software version 1.5.2 (Applied Biosystem, 2022) according to the manufacturer's specifications (Table 4, p. 18).

Table 4: PowerSYBR® Green RT-qPCR components and program.

Reagent volume	Amount	Program		Melt curve	
for 1 reaction		Temperature [°C]	Time [s]	Temperature [°C]	Time [s]
cDNA	$2 \mu l$	50	120	95	15
	(1:4)				
Forward Primer (10 $\mu$ M)	$0.4\mu\mathrm{l}$	95	120	60	60
Reverse Primer (10 $\mu$ M)	$0.4\mu\mathrm{l}$	95	15*	95	1
PCR Master Mix	$10~\mu l$	60	60*		
Nuclease-free water	$7.2~\mu\mathrm{l}$	72	30		
Total volume 20 μl		*Repeat 40 cycles		Ramp rate at 1.6 °C/ s	

Glyceraldehyde-3-phophate dehydrogenase (GAPDH) and ribosomal protein 19 (RPL19) were selected as endogenous housekeeping genes as they lack a putative binding site for all transfected miRNAs. These housekeeping genes (HK) were used to normalize the measured samples for the genes of interest (GOI), PD-L1 and NT5E. The primer sequences of all targets are listed below (Table 5).

Table 5: Primer sequences for *Power*SYBR® Green RT-qPCR.

Primers	Purpose	Amplicon [nt]	Sequence
CD73_Pagnotta_fwd	Gene of interest	123	ATTGCAAAGTGGTTCAAAGTCA
CD73_Pagnotta_rs	NT5E	120	ACACTTGGCCAGTAAAATAGGG
CD274_fwd	Gene of interest	120	TGGCATTTGCTGAACGCATTT
CD274_rev	PD-L1	120	TGCAGCCAGGTCTAATTGTTTT
GAPDH_fwd	Housekeeping	238	GAGTCAACGGATTTGGTCGT
GAPDH_rs	gene	200	TTGATTTTGGAGGGATCTCG
RPL19_fwd	Housekeeping	198	GGCACATGGGCATAGGTAAG
RPL19_rs	gene	170	CCATGAGAATCCGCTTGTTT

#### 3.3.6. RT-qPCR analysis

For the quantification of selected mRNA targets within the measured samples, the mean Ct-values of the tree technical replicates was determined. The relative expression of the targets was calculated using the  $2^-\Delta\Delta Ct$ -method (Equation II-III, p. 19). Therefore, the  $\Delta Ct$ -value was determined by subtracting the mean Ct-value of the housekeeping gene from the mean Ct-value of the gene of interest.

Next, the  $\Delta Ct$ -value of the Mimic Control-1 sample was subtracted from the  $\Delta Ct$ -values of the other samples in the miRNA library, resulting in the  $\Delta \Delta Ct$ . Finally, the base two logarithm of the fold change was calculated for all samples using Equation IV and V.

$$\Delta Ct = Ct_{GOI} - Ct_{HK}$$
 Equation II

$$\Delta \Delta Ct = Ct_{miR} - Ct_{Mimic\ Control-1}$$
 Equation III

Fold change: 
$$FC = 2^{-\Delta \Delta Ct}$$
 Equation IV

$$log (FC) = log_2 (2^{-\Delta \Delta Ct})$$
 Equation V

### 3.4. Flow cytometry

Prior to FACS measurements the human cell lines MDA-MB-231, CRL-5826, MaMel86b, HK-2 and HT-29 were transfected using Lipofectamine™ RNAiMAX reagent.

#### 3.4.1. Harvest of cells for FACS

On the 72 h mark p.t., cells were prepared for FACS analysis by aspirating the culture media and adding  $100~\mu\text{l}/\text{ well TrypLE}^{\text{TM}}$ . In order to detach the cells, an incubation step at 37 °C for 7 min was carried out. The mild trypsinization reaction was stopped by the addition of  $100~\mu\text{l}$  FACS buffer (3 % FCS in PBS). Next, the cells were transferred into a round bottom 96-well plate and centrifuged for 5 min at 300~rcf. The supernatant was discarded and the cell pellets were washed and centrifuged twice with  $200~\mu\text{l}$  FACS buffer.

#### 3.4.2. Immunofluorescence staining and FACS measurement

For FACS staining cells were stained for Live/Dead using Pacific orange<sup>1</sup> at a 1:1000 dilution in FACS buffer. The dye reacts with free amines on the cell in- and exterior of compromised cell membranes, enabling the discrimination of live cells with intact cell membranes from dead cells by their difference in fluorescence intensity (Invitrogen, 2022). Further, the expression of NT5E and PD-L1 were visualized using R-Phycoerythrin (PE)- and Allophycocyanin (APC)-conjugated target specific antibodies at a 1:100 dilution in FACS buffer. The sample cells were resuspended and stained in  $100\,\mu l$  of the staining mixture. Additionally, untransfected cells were utilized as single-stained and isotype controls for both antibodies.

<sup>&</sup>lt;sup>1</sup> All used fluorescent dyes, antibodies and respective isotypes with short name references and pipetted volumes are listed in Table 6, p. 20.

All cells were stained for 1 h at 4 °C in the absence of light. After the incubation, the cells were centrifuged and washed twice with 200  $\mu$ l FACS buffer. Subsequently, cells were resuspended in 100  $\mu$ l FACS buffer and passed through cell-strainer caps of polystyrene round-bottom tubes.

Table 6: Fluorescent dyes and antibodies with short reference names used in this study.

Florescent dyes	Referred	Excitation	Volume per sample	
	to as	laser	in 100 $\mu$ l FACS buffer	
Yellow fluorescent reactive dye	Pacific	VL-510-50	$0.01~\mu l$	
	orange	VII 510 50	0.01 μ1	
Antibodies				
Anti-Hu CD274 (PD-L1, B7-H1)	APC	RL-670-14-A	$1~\mu \mathrm{l}$	
[0. 5 μg/ mL], REF. 17-5983-48	antibody	101-070-14-71	1 μ1	
PE anti-human CD73 (Ecto-5'-nucleotidase)	PE	BL-585-42-A	$1\mu\mathrm{l}$	
[400 $\mu$ g/ mL], Cat. 344044	antibody	DL 303 +2 11	1 μ1	
Isotype				
Mouse IgG1 kappa Isotype Control eFluor 660	APC	RL-670-14-A	$1~\mu \mathrm{l}$	
[0.2 mg/ mL], REF.50-4714-82	isotype	101-070-14-71	$1~\mu 1$	
Mouse IgG1 kappa Isotype Control PE	PE	BL-585-42-A	$1~\mu \mathrm{l}$	
[0.2 mg/ mL], REF. 12-4714-82	isotype	DL-303-72 <b>-</b> N	1 μι	

The prepared samples were analyzed by the BD FACSCanto<sup>™</sup> II Flow Cytometer using the BD FACSDiva<sup>™</sup> Software (BD Biosciences, 2022a). The untreated and unstained sample was used to adjust the forward scatter (FSC) and side scatter (SSC). Further, the single-stained controls were used to determine fluorescence channel spill-overs and facilitated compensation.

#### 3.4.3. Analysis of FACS data

Analysis of acquired FACS data was performed with FlowJo<sup>TM</sup> version 10.8.1 (BD Biosciences, 2022b). In first place, events were gated on single cells and live cells. Next, the isotype control sample was used to set gates for both NT5E and PD-L1 channels. The percentage of live cells and their median fluorescence intensity (MFI) were exported and subsequent initial data analysis was performed using Microsoft Excel version 2209 (Microsoft Cooperation, 2022).

#### 3.5. XTT Assay

In order to assess the effect of specific miRNAs on the cell viability of transfected human cells, a next-generation tetrazolium salt assay was conducted. The XTT assay is a colorimetric cell metabolic activity and proliferation assay that is based on the reduction of yellow 2,3-bis (2-methoxy-4-nitro-5-sulfophenyl)-5-[(phenylamino) carbonyl]-2H-tetrazolium hydroxide (XTT) to water-soluble orange XTT formazan salt shown in Figure 6 (Mosmann, 1983; Roehm et al., 1991). Specifically in metabolically active live cells, the mitochondrial reductase NAD(P)H-dependent cellular oxidoreductase converts the tetrazolium compound allowing the linkage of mitochondrial activity to the number of viable cells (Stockert et al., 2018).

Figure 6: XTT assay. The mitochondrial reduction of yellow XTT forms orange XTT formazan salt.

For the XTT assay, the XTT Cell Proliferation Assay (SERVA Electrophoresis GmbH, Germany) was used according to the manufacturers protocol. Therefore, MDA-MB-231 and MaMel86b cells were seeded in three separate 96-well plates at a cell density of  $1*10^4$  cells per well. After 24 h, the cells were transfected with a final miRNA concentration of 25 nM per well using Lipofectamine<sup>TM</sup> RNAiMAX (Thermo Fischer Scientific, USA). The XTT assay was conducted 24, 48 or 72 p.t. by directly pipetting  $50\,\mu$ L XTT detection solution into each well. The cells were further incubated at 37 °C for 60 min before absorbance measurements were carried out on a CLARIOstar<sup>®</sup> *Plus* microplate reader (BMG LABTECH GmbH, Germany). The absorbance (A) of the technical quintuplicates was normalized by subtracting the absorbance reading at 450 nm from the background absorbance at 630 nm (Equation VI).

$$A = A_{450 nm} - A_{630 nm}$$
 Equation VI

# 3.6. 3'-UTR reporter assay

In order to investigate the interaction of specific miRNAs with the 3'-UTR of PD-L1, a luciferase reporter assay was conducted. To begin with, MDA-MB-231, CRL-5826, MaMel86b and HK-2 cells were seeded in opaque flat-bottom 96-well plates at a cell density of  $1*10^4$  cells per well. After 24 h, 25 nM and  $100 \text{ ng pLS-PD-L1-3'-UTR plasmid}^2$  were transfected using the DharmaFECT Duo Transfection Reagent (Dharmacon<sup>TM</sup>, USA). The luciferase activity was measured 24 h p.t. with the LightSwitch<sup>TM</sup> Luciferase Assay Kit (Active Motif, Belgium). Therefore, the assay solution was freshly prepared protected from light by solving the lyophilized assay substrate in 1 mL substrate solvent and diluting it in 100 mL assay buffer. Next,  $100 \mu$ L assay solution was pipetted into each well and the cells were left to incubate for 30 min at RT in the dark. Finally, the luminescence was read out for 2 sec / well using the luminometer setting on a CLARIOstar<sup>®</sup> *Plus* microplate reader (BMG LABTECH GmbH, Germany).

#### 3.7. Statistical analysis

The results obtained by the performed experiments are presented as mean values with a standard error of the mean (SEM). If not stated otherwise, experiments were executed at least three individual times to establish the experimental error. For FACS and RT-qPCR experiments the fold changes of all samples and the Mimic Control-1 were calculated and  $\log_2$  transformed. The significance was assessed through a One-Sample T-Test using the GraphPad Prism 9.4.1 software (Dotmatics, 2022). The applied significances are shown below in Table 7.

Table 7: Applied significance levels.

P-value	Symbol	Wording
P > 0.05	ns	Not significant
$P \le 0.05$	*	Significant
$P \le 0.01$	**	Very significant
$P \le 0.001$	***	Highly significant
$P \le 0.0001$	****	Extremely significant

For the XTT- and 3'-UTR reporter assay experiments, the technical replicates of each sample were tested for significant outliers by performing the Grubb's test offered by GraphPad Prism (Dotmatics, 2023). Outliers with p values < 0.05 were excluded from the analysis. To determine sample significance, a Dunnett's Multiple Comparison Test was conducted applying the significance levels listed above.

22

<sup>&</sup>lt;sup>2</sup> The vector map of pLS-PD-L1-3'-UTR is shown in Supplementary Figure 1, p. 66.

# 4. Results

The aim of this study was the elucidation of miRNA-mediated post-transcriptional regulation of immune checkpoint molecule expression, with a particular focus on immunomodulatory ligand PD-L1. Therefore, a preselected miRNA library was screened for potential tumor-suppressive miRNAs that downregulated PD-L1 mRNA and protein levels in three tumor entities and in normal kidney cells. For the validation of the screening results, the effect of miRNAs on the cell viability was assessed, followed by the examination of molecular interactions between selected miRNA candidates and the 3'-UTR of the PD-L1 encoding mRNA. Furthermore, the miRNA library was investigated for miRNAs affecting the expression of the ectonucleotides NT5E, aiming to identify multi-functional miRNA candidates.

### 4.1. Comparison of immune checkpoint molecule expression profiles

The expression pattern of the immune modulating molecules PD-L1 and NT5E was determined in different types of human cells through flow cytometry, in order to identify suitable cells lines for the investigation of the miRNA library. Therefore, single live cell populations of the breast cancer cell line MDA-MB-231, the lung carcinoma cell line CRL-5826, the melanoma cell line MaMel86b, the colorectal adenocarcinoma cell line HT-29 and the proximal tubular kidney cell line HK-2 were selected through a gating strategy exemplified in Supplementary Figure 2:Supplementary Figure 2. For the comparison of relative target cell surface levels across all five cell lines, the mean fluorescence intensities of Mimic Control-1 samples were normalized to their respective isotype control (Supplementary Figure 3, p. 67). The resulting NT5E expression level for all examined cell lines is shown in Figure 7.

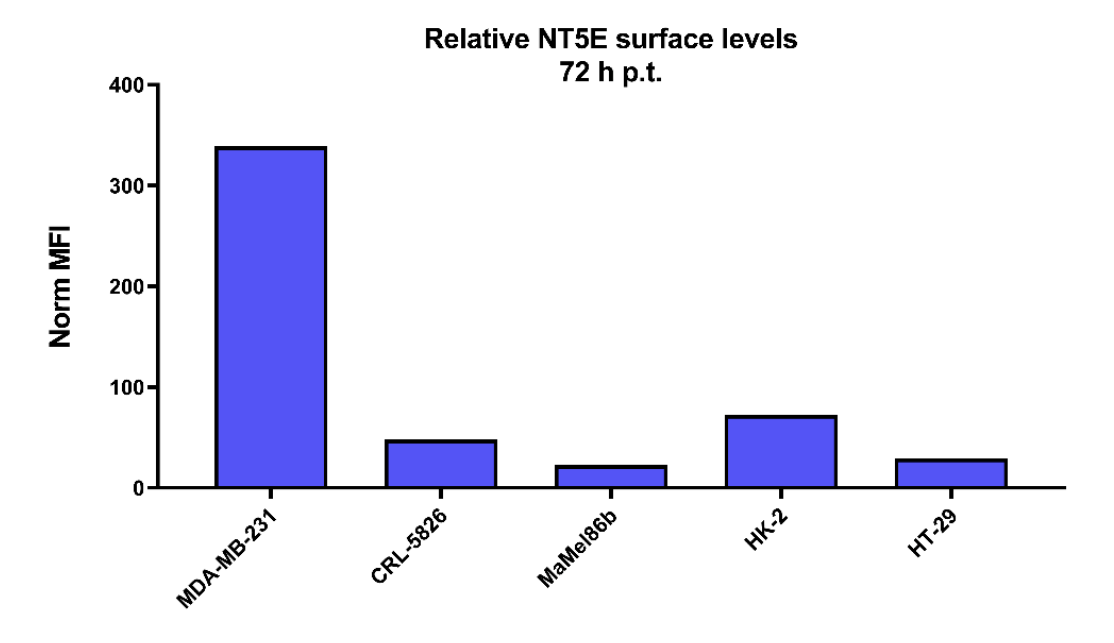


Figure 7: NT5E surface expression among human cell lines of different non-/tumor entities. Results show mean fluorescence intensities of Mimic Control-1 normalized to the isotype control of NT5E.

All investigated human cell lines exerted robust NT5E expression. Thereby, the highest relative NT5E surface level was found in the breast cancer cell line MDA-MB-231 with a normalized MFI of 340. Following, the proximal tubular HK-2 cells (Norm MFI: 73), the lung carcinoma CRL-5826 cells (Norm MFI: 49) and the colorectal carcinoma HT-29 cells (Norm MFI: 30) displayed a moderate expression of the surface enzyme NT5E. The lowest NT5E levels were detected in the skin cancer cell line MaMel86b (norm MFI: 23).

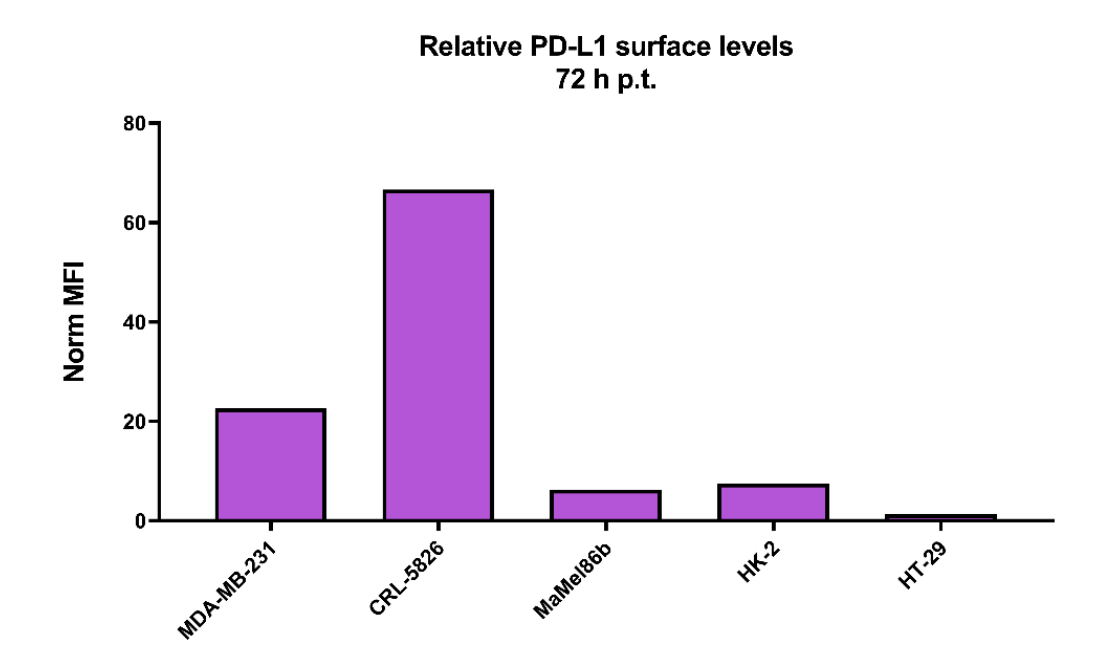


Figure 8: PD-L1 surface expression among human cell lines of different non-/tumor entities. Display of mean fluorescence intensities of Mimic Control-1 normalized to the isotype control of PD-L1.

The expression of the cell surface ligand PD-L1 could be found in four cell lines, expect for the colorectal carcinoma cell line HT-29 showing marginal PD-L1 levels (Figure 8). Overall, the highest expression of PD-L1 was observed in CRL-5826 cells (Norm MFI: 66). For the human tumor cells lines MDA-MB-231 (Norm MFI: 23), HK-2 (Norm MFI: 8) and MaMel86b (Norm MFI: 7) a moderate to low expression of PD-L1 was detected. The substantially lower and thus negligible target expression levels seen in HT-29 cells ruled out the further employment of the colorectal carcinoma in following experiments. Specifically, for HT-29 cells only 2.4 % of gated cell population were tested positive for PD-L1 expression (Supplementary Figure 4, p. 68).

## 4.2. Quantification of miRNA library transfection effects on PD-L1 and NT5E

In order to evaluate potential effects of the miRNA library on expression of the immune modulating molecules PD-L1 and NT5E, the relative surface levels of both targets were determined in human cell lines via flow cytometry. Accordingly, the investigated tumor cells MDA-MB-231, CRL-5826 and MaMel86b, as well as the normal kidney cell line HK-2 were transfected with the miRNA library, Mimic Control-1, NT5E and PD-L1 siRNA pools using 50 nM (705 ng) miRNA and Lipofectamine™ RNAiMAX. Treated cells were cultivated for 72 h p.t., consequently mean fluorescence intensities were detected through flow cytometric analysis (Exemplary histograms in Supplementary Figure 5, p. 69). The recorded results were normalized to Mimic Control-1 and Log2 transformed, enabling the comparison of miRNA library effects among both targets and all cell types.

The relative surface levels of PD-L1 and NT5E on the breast cancer cell line MDA-MB-231 are shown below in Figure 9. To begin with, the transfection of both siRNA pools resulted in an extremely significant downregulation of the respective targets, indicating the successful transfection of the investigated cells. For the surface ligand PD-L1, the introduction of seven miRNAs from the library induced a significant reduction in surface expression levels. The highest fold-change was observed in miR-3117-3p with a highly significant 1.6-fold decrease, followed by the less significant 0.8-fold decrease seen in miR-1273c. A moderate downregulation of relative PD-L1 levels was achieved by the transfection of miR-139-5p, miR-146a-5p, miR-155-5p and miR-512-3p ranging from a 0.2-fold to 0.55-fold decrease of the surface ligand. Though insignificant, both miR-139-3p and miR-146a-3p showed downregulation tendencies for PD-L1, while the transfection of miR-1204 and miR-1273c resulted in no effect. Finally, the untreated and mock samples were consistent with Mimic Control-1 levels.

The relative NT5E surface levels after 72 h of library transfection were significantly downregulated by two miRNAs (Figure 9B). Thereby, the introduction of miR-155-5p resulted in an extremely significant 1.1-fold decrease of the surface expression, similar to the very significant 0.7-fold change for miR-512-3p. In contrast the transfection of miR-1204 resulted in a significant 0.4-fold increase of NT5E levels. Further, an insignificant tendency for NT5E up- and downregulation could be observed in miR-139-3p, miR-146a-5p, miR-1204, miR-1228-3p and respectively for miR-139-5p, miR-374b-3p and miR-1273c. Lastly, the relative surface expression of NT5E in untreated and mock samples were similar to each other, yet significantly lower than NT5E levels detected in Mimic Control-1.

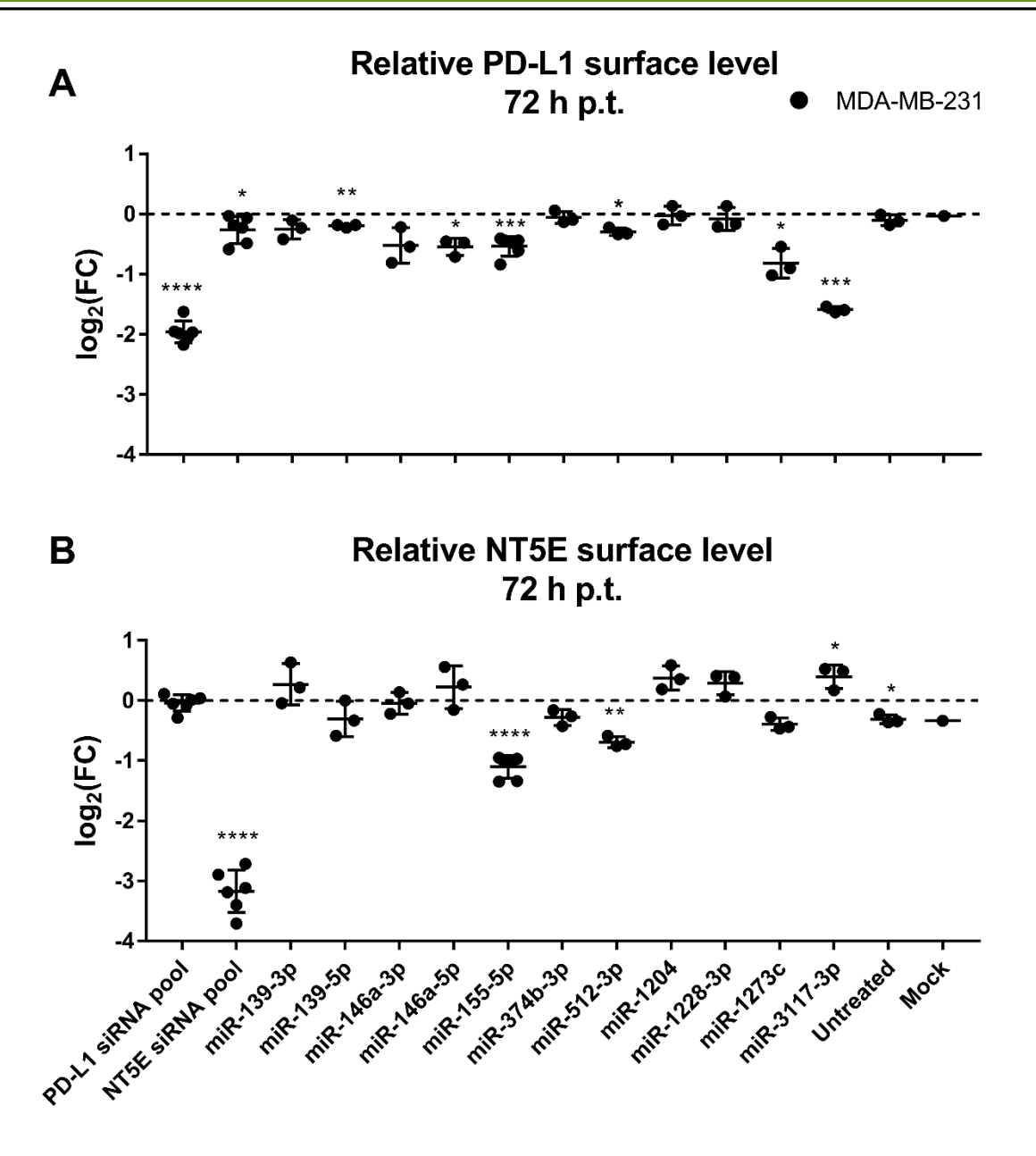


Figure 9: Log2 fold change of target MFIs for miRNA library transfection in MDA-MB-231. Results show the relative NT5E (A) and PD-L1 (B) surface levels 72 h post transfection. The graph displays mean values and SEM of >3 independent experiments in MDA-MB-231 cells. Fold changes were calculated compared to Mimic Control-1. Significances were assessed by One-sample T-Test (\* =  $P \le 0.05$ ; \*\*  $P \le 0.01$ ; \*\*\* =  $P \le 0.001$ ; \*\*\*\* =  $P \le 0.0001$ ).

The potential effect of the miRNA library on the relative surface levels of PD-L1 and NT5E was also investigated in the human non-small-cell lung carcinoma cell line CRL-5826 (Figure 10, p. 27). The transfection of the PD-L1 and NT5E siRNA pools resulted in a highly significant decrease of target levels, establishing the successful transfection of miRNA in the examined tumor cells. For PD-L1, an overall reduction of relative surface level expression was achieved by the introduction of the miRNA library,

with exception of the upregulatory tendency seen for miR-1204. It was found that seven miRNAs induced the reduction of target levels significantly. Precisely, miR-3117-3p and miR-1273c introduced a very significant 1.1-fold and 0.9-fold decrease of PD-L1. In contrast, the transfection of miR-139-3p, miR-146a-3p, miR-146a-5p, miR-155-5p, miR-374b-3p and miR-512-3p resulted in the less significant reduction of ligand levels ranging from a 0.1- to 0.4-fold decrease. Notably, the relative PD-L1 surface levels of the untreated and mock samples were downregulated 0.5-fold compared to PD-L1 levels in the Mimic Control-1 sample.

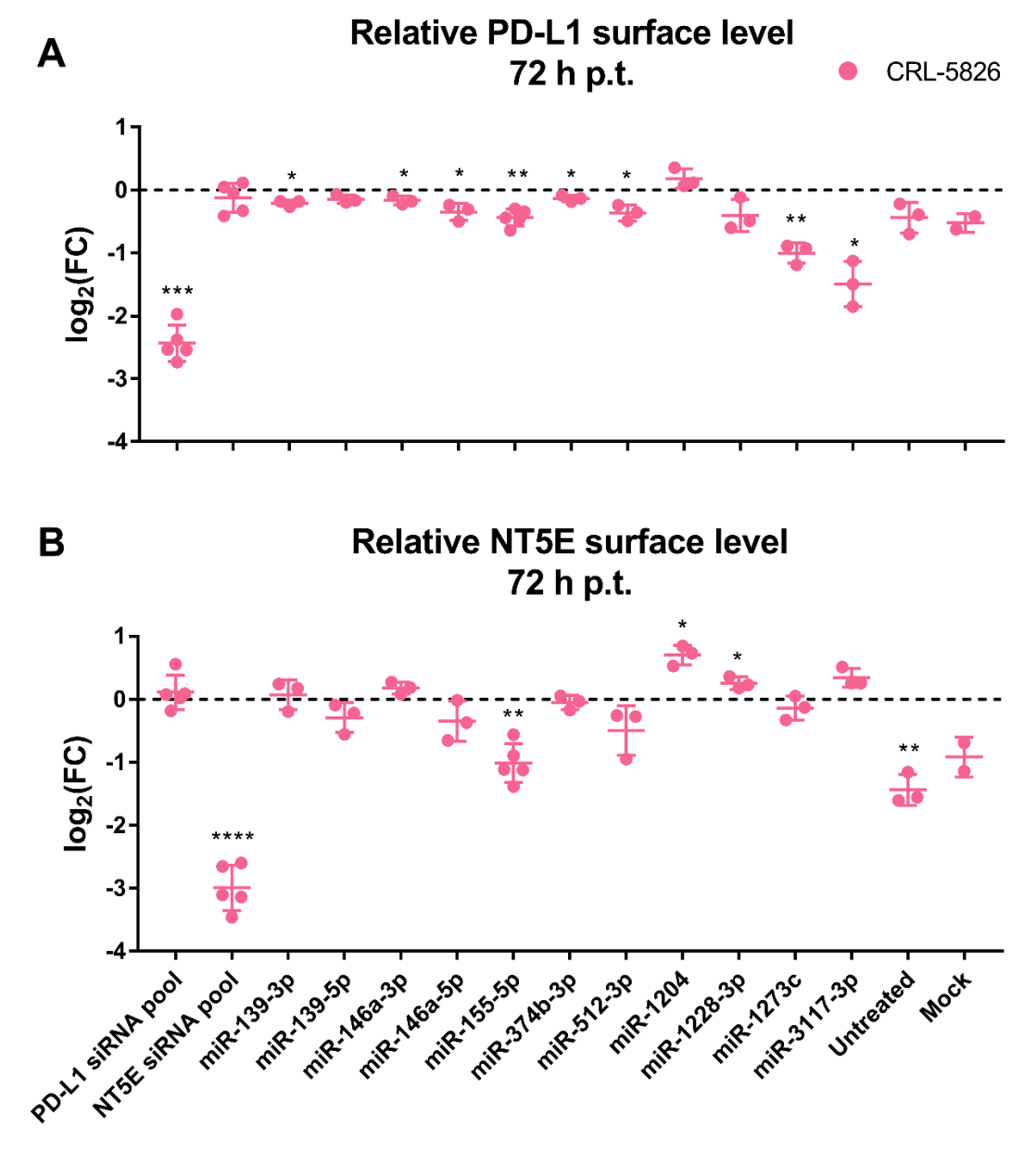


Figure 10: Log2 fold change of target MFIs after miRNA library transfection of CRL-5826 cells. Results show the relative NT5E (A) and PD-L1 (B) surface levels 72 h post transfection. The graph displays mean values and SEM of >3 independent experiments in CRL-5826 cells. Fold changes were calculated compared to Mimic Control-1. Significances were assessed by One-sample T-Test (\* =  $P \le 0.05$ ; \*\*  $P \le 0.01$ ; \*\*\*\* =  $P \le 0.001$ ; \*\*\*\* =  $P \le 0.0001$ ).

The relative NT5E surface levels after 72 h of library transfection were significantly downregulated by only one miRNA (Figure 10 B, p. 27). Precisely, the introduction of miR-155-5p resulted in a very significant single-fold decrease of the surface enzyme expression. Despite the moderate data spread, the transfection of miR-139-5p, miR-146a-5p, miR-512-3p and miR-1273c showed downregulation tendencies with an up to half-fold reduction in target cell expression. Contrastingly, the transfection of miR-1204, miR-1228-3p and miR-3117-3p resulted in a significant 0.7- to 0.35-fold increase of the surface expression levels of NT5E. Lastly, the relative NT5E surface levels of the untreated and mock treated samples very significantly downregulated compared to Mimic Control-1 levels.

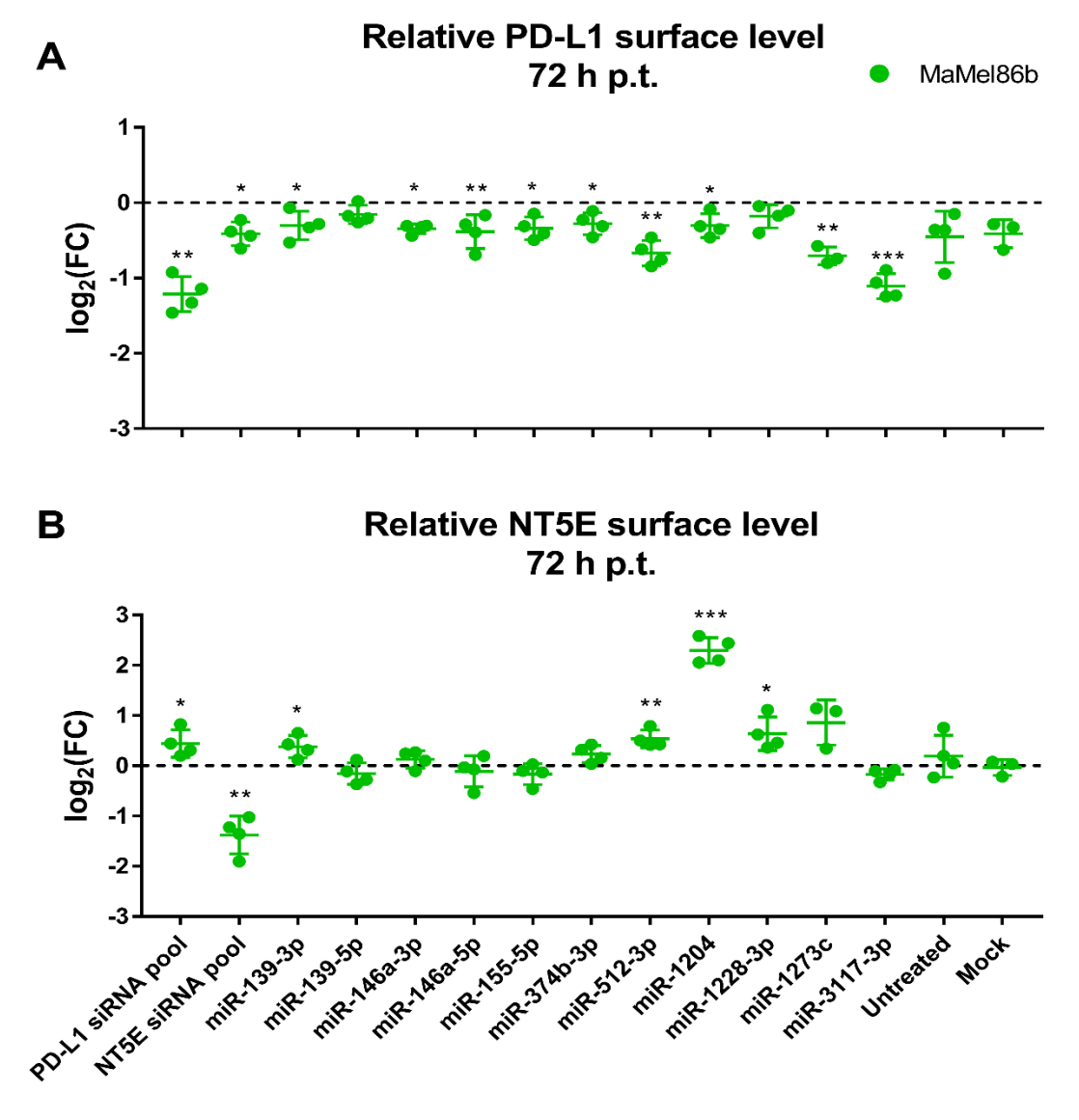


Figure 11: Log2 fold change of target MFIs for miRNA library transfection in MaMel86b. Results show the relative NT5E (A) and PD-L1 (B) surface levels 72 h post transfection. The graph displays mean values and SEM of 4 independent experiments in MaMel86b cells. Fold changes were calculated compared to Mimic Control-1. Significances were assessed by One-sample T-Test (\* =  $P \le 0.05$ ; \*\*  $P \le 0.01$ ; \*\*\* =  $P \le 0.001$ ).

The relative surface levels of PD-L1 and NT5E of the human metastatic melanoma cell line MaMel86b are displayed above in Figure 11. To begin with, the transfection of both siRNA pools resulted in the desired significant downregulation of both targets, verifying the successful transfection of the inspected cells. The introduction of all eleven miRNAs from the library the resulted in an overall reduced relative surface level of PD-L1. The highest fold-change was observed for miR-3117-3p with a highly significant 1.1-fold decrease, followed by the very significant 0.7-fold decrease seen in both miR-512-3p and miR-1273c. The miRNAs, miR-139-3p, miR-146a-3p, miR-146a-5p, miR-155-5p, miR-374b-3p and miR-1204 significantly downregulated moderate PD-L1 surface expression around -0.3-fold in MaMel86b cells. Additionally, similar relative PD-L1 surface levels were detected in the untreated and mock samples that were 0.4-fold reduced compared to Mimic Control-1 levels.

For the surface enzyme NT5E, the transfection of the miRNA library resulted in unchanged to upregulated target levels when folded to the Mimic Control-1 (Figure 11 B, p. 28). The highest fold-change was induced by miR-1204 with a highly significant 2.3-fold increase of surface NT5E expression. Furthermore, miR-139-3p, miR-512-3p, miR-1228-3p and miR-1273c upregulated target levels by 0.4- to 0.9-fold with varying levels of significance. Finally, the relative NT5E surface levels of the mock sample were consistent with levels detected in Mimic Control-1.

The effect of the miRNA library on the relative surface levels of PD-L1 and NT5E was investigated in the normal proximal tubular kidney cell line HK-2, to compare and contrast the potential miRNA effects on healthy and cancerous human cells (Figure 12, p. 30). Noticeably, the transfection of miRNAs in HK-2 cells resulted in a moderate fluctuation of data points compared to the investigated tumor entities described above (Figure 9-11). Despite the observed data spread, the reduction of PD-L1 and NT5E target levels stemming from the siRNA pools, proved the appropriate transfection of the kidney cells. The introduction of the miRNA library caused an overall decrease of the surface ligand expression. The four miRNAs, miR-512-3p, miR-1228-3p, miR-1273c and miR-3117-3p significantly reduced PD-L1 levels ranging from a 0.5- to 0.8-fold decrease of target levels. The relative surface levels detected in the untreated and mock sample were also significantly lower by 0.3-fold from the levels detected in Mimic Control-1.

For the surface enzyme NT5E, the introduction of two miRNAs from the library induced significant increase or reduction of detected target levels, respectively. The miRNAs, miR-1204 and miR-3117-3p upregulated NT5E levels by 0.8- and 0.3-fold, while miR-139-5p and miR-155-5p decreased the target levels to 0.3- and 0.9-fold. The remainder of the miRNA library left relative NT5E levels constant or downregulated compared to levels of the Mimic Control-1. Lastly, both the untreated and the mock

sample exerted significantly lowered relative NT5E surface levels by 0.5 and 0.35-fold, when compared to NT5E levels of the Mimic Control-1 sample.

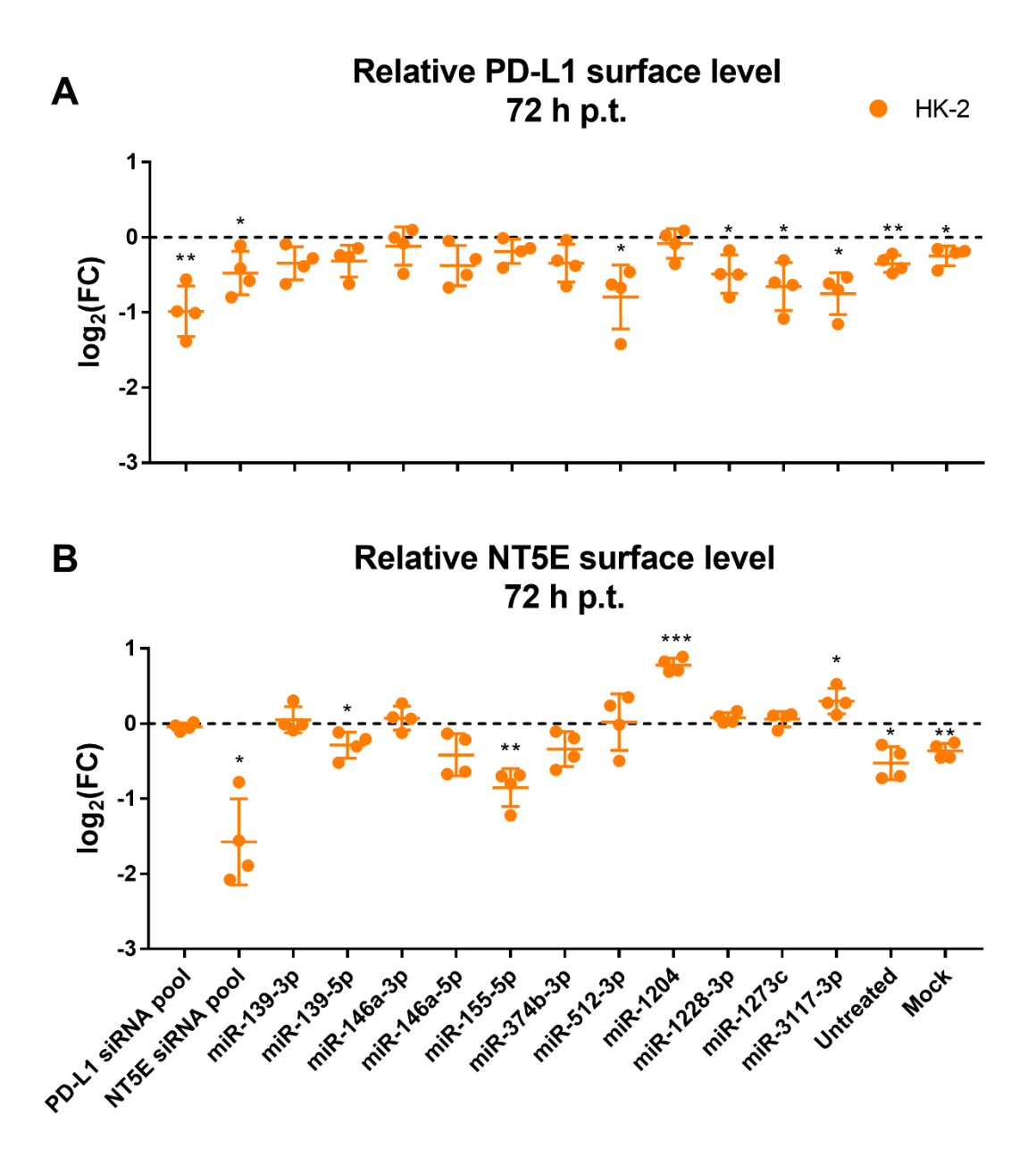


Figure 12: Log2 fold change of target MFIs for miRNA library transfection in HK-2. Results show the relative NT5E (A) and PD-L1 (B) surface levels 72 h post transfection. The graph displays mean values and SEM of 4 independent experiments in HK-2 cells. Fold changes were calculated compared to Mimic Control-1. Significances were assessed by One-sample T-Test (\* =  $P \le 0.05$ ; \*\*  $P \le 0.01$ ; \*\*\* =  $P \le 0.001$ ).

#### 4.3. Validation of selected miRNA candidates

In order to validate promising miRNA candidates based on the flow cytometric analysis of the miRNA library, the relative mRNA expression levels of PD-L1 and NT5E were determined in human cells through RT-qPCR. Therefore, MDA-MB-231, CRL-5826, MaMel86b and HK-2 cells were transfected with 50 nM miRNA and RNA was isolated two days post transfection. For intracellular target quantification, the housekeeping gene RPL19 was chosen for sample normalization, as the miRNAs were predicted to be ineffectual to its gene levels. The main focus of the validation was set on miRNAs that had significantly downregulated PD-L1 and NT5E surface expression in numerous cell lines. In total, four miRNAs fulfilled this criterion for PD-L1 downregulation, while one miRNA was elucidated for NT5E. The miRNAs of interest are listed in Table 8 with their target downregulation significance levels in the respective cell lines. Also included were the number of predicted binding sites within the 3'-UTR of the targets for the miRNA candidates. Notably, miR-155-5p downregulated both immunoregulatory molecules in several investigated cell lines.

Table 8: miRNAs of interest decreasing PD-L1 and NT5E surface expression in human cell lines.

PD-L1 inhibiting miRNAs							
iDNA	Dinding sites	Cell line significance					
miRNA Binding sites	MDA-MB-231	CRL-5826	MaMel86b	HK-2			
miR-155-5p	2	***	**	*			
miR-512-3p	1	*	*	**	*		
miR-1273c	1	*	**	**	*		
miR-3117-3p	3	***	*	***	*		

NT5E	inhibiting	g miRNAs

;DNA	Dinding sites	Cell line significance			
miRNA	Binding sites	MDA-MB-231	CRL-5826	MaMel86b	HK-2
miR-155-5p	2	***	**		*
miR-512-3p	1	**			

For the further investigation of the miRNAs, the potential effect of the miRNA library on the intracellular levels of the immune modulating target molecules was examined through RT-qPCR. The relative PD-L1 and NT5E mRNA expression levels in the investigated human cells are displayed below in Figure 13.

# Relative PD-L1 and NT5E mRNA expression 48 h p.t.

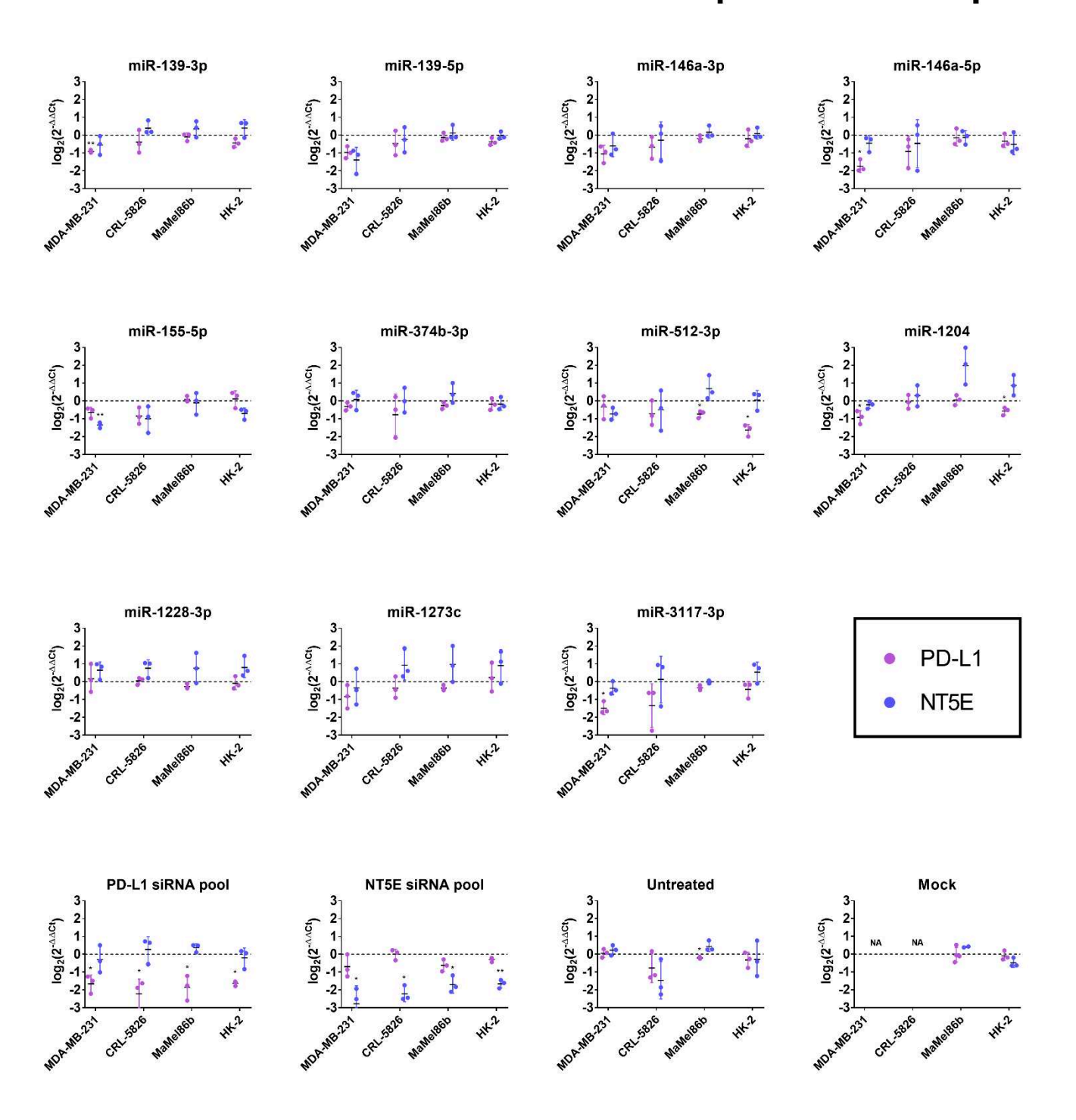


Figure 13: RT-qPCR examination of PD-L1 and NT5E mRNA levels for miRNA library transfection. The graph displays mean values and SEM of 3 independent experiments in MDA-MB-231, CRl-5826, MaMel86b and HK-2 cells. Samples were normalized on the housekeeping gene RPL19 and fold changes were calculated using Mimic Control-1. Significances were assessed by a One-sample T-Test (\* =  $P \le 0.05$ ; \*\*  $P \le 0.01$ ).

The transfection of PD-L1 and NT5E siRNA pools induced a significant decrease of intracellular target mRNA levels aligned with the effects seen in the flow cytometric analysis, confirming overall successful cell transfection. For the ligand PD-L1, mRNA transcript levels were very significantly decreased by five miRNAs in the breast cancer cell line: miR-139-3p, miR-139-5p and miR-1204 reduced mRNA target levels by a single-fold. The highest fold-change was observed for miR-146a-5p with a very significant 1.7-fold decrease, closely followed by the very significant 1.5-fold decrease seen in miR-3117-5p. Hereinafter, the observed significant decrease of extracellular protein ligand levels in flow cytometry for miR-139-5p, miR-146a-5p and miR-3117-3p were additionally verified on an intracellular mRNA level in MDA-MB-231 cells. Additionally, the FACs based miRNAs of interest miR-512-3p and miR-1273c exerted an insignificant downregulation tendency.

In the proximal tubular kidney cell line HK-2, PD-L1 mRNA expression was significantly reduced by miR-512-3p and miR-1204 by 1.6 and 0.6-fold. Moreover, a significant 0.6-fold reduction of ligand mRNA levels was also seen for miR-512-3p in the melanoma cell line MaMel86b. Again, the effects observed for the PD-L1 mRNA transcripts were reflected by significant changes in the PD-L1 protein levels of the respective cell lines. For CRL-5826 cells, acquired RT-qPCR data possessed broad fluctuations with only insignificant downregulation tendencies seen in miR-146a-5p, miR-155-5p, miR-512-3p and miR-3117-3p with an over 0.8-fold target reduction, slightly above the reduced level of the untreated sample and aligning with significant FACS data.

For the surface enzyme NT5E, only one miRNA significantly decreased mRNA transcript levels: In the breast cancer cells MDA-MB-231, miR-155-5p reduced intracellular NT5E levels by 1.35-fold. Though target downregulation tendencies could be observed for the miRNAs of interest: miR-512-3p, miR-1273c and miR-3117-3p. The greatest foldchange was seen for miR-139-5p at a 1.4-fold reduction in MDA-MB-231 cells. Strikingly, several miRNAs of the library enhanced NT5E mRNA levels by a moderate-fold. Though insignificant, miR-1228-3p increased target levels in all investigated cell lines, aligning with significant FACS data in lung adenocarcinoma and melanoma cells (See Table 9, p. 34). Further, it was found that miR-1273c raised NT5E expression levels by a single-fold in all cells, but MDA-MB-231. Further, miR-1204 elevated NT5E mRNA levels in MaMel86b and HK-2 cells by a maximum of two-fold. Also, miR-512-3p was observed increasing target levels by 0.7-fold in melanoma cells. These increased tendencies on the NT5E mRNA expression level were mostly consistent with significantly elevated relative surface protein expression levels of the target detected in flow cytometry.

Assessing the effects of the miRNA library on relative intra- and extracellular levels of PD-L1 and NT5E, it is apparent that miR-155-5p downregulates both targets in several cell lines. Adjacently, miR-512-3p, miR-1273c and miR-3117-3p compellingly reduce PD-L1 mRNA and protein levels significantly in all cell lines tested, whilst enhancing the expression of the enzyme NT5E in most human cell lines.

Table 9: miRNAs increasing NT5E surface expression in human cell lines.

NT5E enhancing miRNAs					
miRNA	Binding sites	Cell line significance			
		MDA-MB-231	CRL-5826	MaMel86b	HK-2
miR-512-3p	1	-	-	**	
miR-1204	0		*	***	*
miR-1228-3p	0		*	*	
miR-3117-3p	0	*			*

#### 4.4. Investigation of miRNA effects on cell viability

The potential effect of the miRNA library transfection on cell viability and proliferation was investigated through an XTT assay. Therefore, MDA-MB-231 and MaMel86b cells were seeded in 96-well plates and transfected with 25 nM miRNAs, PD-L1 or NT5E siRNA pools. The cell viability was quantified by detecting the enzymatic conversion of the reagent XTT. In living metabolically active cells the yellow tetrazolium salt is reduced to the orange product XTT formazan by mitochondrial reductases. The colorimetric assay was conducted 24, 48 or 72 h post miRNA transfection. The results for the breast cancer cell line MDA-MB-231 are shown below in Figure 14. Twenty-four hour after miRNA transfection the treated cells showed no difference overall to the range of cell viability detected for Mimic Control-1. At the 48 h timepoint miR-1228-3p significantly increased breast cancer cell numbers, while most miRNAs displayed fluctuating median values compared to the respective Mimic Control-1 samples of both experiments. Only 72 h p.t. some miRNAs induced greater impacts on cell viability above threshold: For the miRNA of interest miR-3117-3p a highly significant decrease in cell proliferation was recorded. Albeit significant reduction levels in absorbance were measured likewise for miR-139-5p, miR-146-3p, miR-1273c and the NT5E siRNA pool in one XTT assay, only insignificantly decreased cell viability tendencies were detected in repetition.

Moreover, an XTT assay was conducted examining cell viability and proliferation in the metastatic melanoma cell line MaMel86b. The data recorded for the 24, 48 and 72 h p.t. timepoints is displayed in Figure 15 (p. 36). The transfection of the miRNA library resulted in no significant effect after a 24 - 48 h

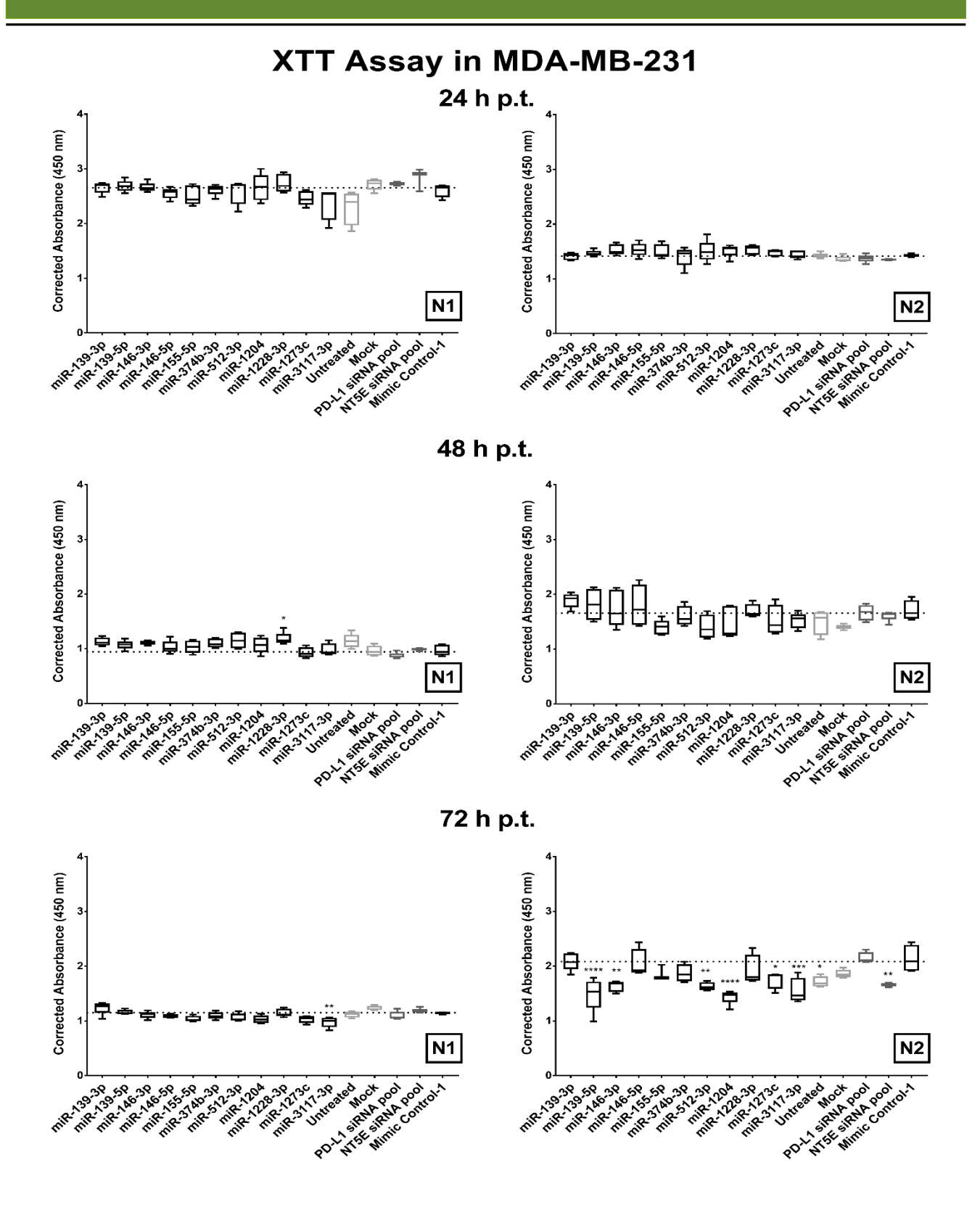


Figure 14: Effect of miRNAs on viability of transfected MDA-MB-231 cells 24-72 h post transfection. The box-and-whiskers plots display minimum, maximum and median values of two independent experiments (N1 and N2) with at least 4 technical replicates. All samples were compared to Mimic Control-1. Significance was assessed by one-way ANOVA using Dunnett's multiple comparison test (\* =  $P \le 0.05$ ; \*\*  $P \le 0.01$ ; \*\*\* =  $P \le 0.001$ ; \*\*\*\* =  $P \le 0.0001$ ).

miRNA treatment period. Notably, it was opted to compare samples of experiment N2 at 48 h p.t. to the mock sample via Dunnett's Multiple Comparison Test due to anomalies in the cell growth of Mimic Control-1. At the 72 h timepoint miR-139-3p and miR-512-3p significantly increased melanoma cell numbers, contradicting the results of the repetition measurements. Furthermore, the untreated and NT5E siRNA pool induced a very to extremely significant elevation of cell viability, that coincided with the tendency of increased absorbance measurements in experimental repetition.

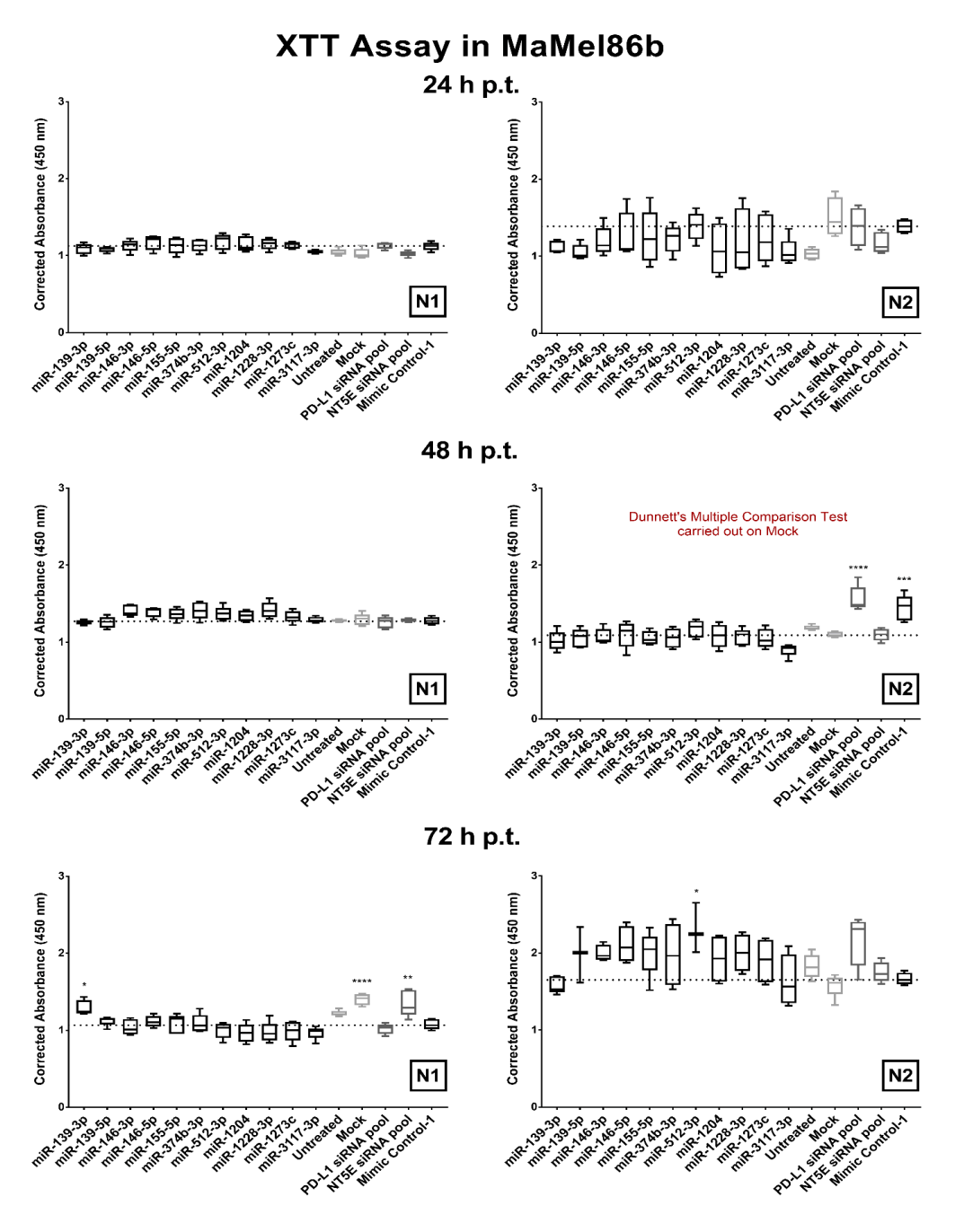


Figure 15: Effect of miRNAs on viability of transfected MaMel86b cells 24-72 h post transfection. The box-and-whiskers plots display minimum, maximum and median values of two independent experiments with at least 4 technical replicates. Most samples were compared to Mimic Control-1. Significance was assessed by one-way ANOVA using Dunnett's multiple comparison test (\* =  $P \le 0.05$ ; \*\*  $P \le 0.01$ ; \*\*\* =  $P \le 0.001$ ; \*\*\*\* =  $P \le 0.0001$ ).

#### 4.5. Validation of direct interactions between miRNAs and PD-L1

In order to further validate and characterize miRNAs of interest based on molecular interactions with their target gene, a 3'-UTR reporter assay was conducted for PD-L1. Specifically, the 3'-UTR sequence of the target is fused to a luciferase encoding gene, enabling the investigation of direct miRNA binding events. In principle, the formation of weak hydrogen bonds between miRNAs and complementary bases of the target mRNA transcript results in the physical blockage of translational enzymes. Hence, target protein levels decrease as gene translation cannot be fulfilled. The binding of miRNAs to the 3'-UTR of PD-L1 can be directly detected by a decrease of luciferase signals in the reporter assay. Therefore, MDA-MB-231, MaMel86b, HK-2 and CRL-5826 cells were seeded in 96-well plates and transfected with 25 nM miRNA and 100 ng pLS-PD-L1-3'-UTR plasmid. The interactions between miRNAs and the target were assessed 24 h p.t. through the measurement of emitted luciferase signals.

For the 3'-UTR luciferase reporter assay, three miRNAs of interest were selected for further molecular investigation based on the plasmids shortened PD-L1 3'-UTR fragment provided by Active Motive. Initially, target binding sites were predicted for the entire miRNA library using miRmap web (Vejnar & Blum, 2013) as depicted in Supplementary Figure 6 (p. 70). However, the provided plasmid only encoded a fourth of the full 3'-UTR of PD-L1, re-focusing investigation efforts onto miRNAs binding close to the 5' end of the full sequence. Hence, the potential binding effects of miRNA-139-3p, miR-512-3p and miR-1273c were solely investigated. Compiled flow cytometric and RT-qPCR analysis deemed the three selected candidates to be successful in the downregulation of PD-L1 expression levels. Following, the 3'-UTR reporter assay investigating miRNAs of interest in human breast, lung and skin cancer cells, as wells as normal kidney cells is displayed below in Figure 16. To begin with, luciferase signals detected for cells transfected by only the pLS-PD-L1-3'-UTR plasmid were overall similar to Mimic Control-1. Notably, a highly significant reduction of luciferase signals was detected in all investigated cell lines, but CRL-5826 cells. This verified the successful co-transfection of miRNAs and plasmid in the normal kidney, breast and skin cancer cell lines. Moving on, miR-1273c samples of all three cell lines exerted globally decreased levels of luciferase signals of varying significance. In both MDA-MB-231 and HK-2 cells the reduction induced by miR-1273c transfection was highly significant. These findings coincide with the significant downregulation of PD-L1 surface levels observed in flow cytometry data for all investigated cell lines. The most significant reduction in emitted visible light signals was recorded for miR-139-3p in both MBD-MB-231 and HK-2 cells. Similarly, the transfection of miR-512-5p lead to significantly lowered luciferase activity for both cell lines, while showing upregulated luciferase signaling tendencies in MaMel86b cells.

Brightfield microscopy imaging of the 3'-UTR reporter assay was carried out, qualitatively assessing cell growth and confluency of the DharmaFECT Duo co-transfected human cells (Supplementary Figure 7). For the breast cancer cell line MDA-MB-231, imaging revealed appropriate cell confluency of the untreated and pLS-PD-L1-3'-UTR plasmid transfected cells. For the metastatic melanoma and lung adenocarcinoma cell line qualitative brightfield microscopy showed cell confluences of over 70 %, while the proximal tubular kidney cell line HK-2 was the least confluent. For these three cell lines, a notable increase of dead cells, cell debris and dark gains in plasmid transfected cells was observed compared to untreated cells.

## PD-L1 3'-UTR reporter assay 24 h p.t.

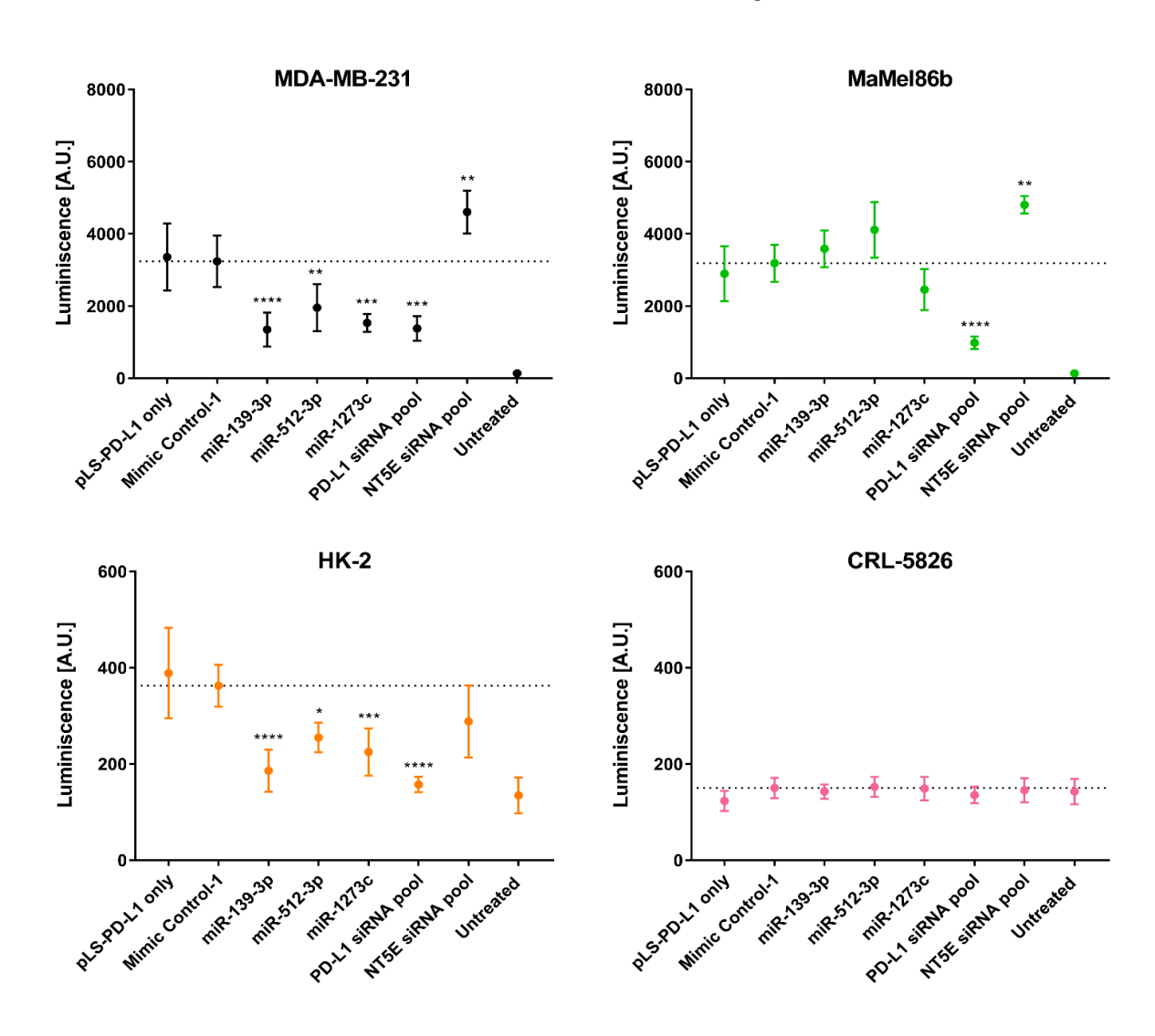


**Figure 16: PD-L1 3'-UTR reporter assay.** The graph displays mean values and SEM of at least 4 technical replicates in MDA-MB-231, MaMel86b, HK-2 and CRL-5826 cells. All samples were compared to Mimic Control-1. Significance was assessed by one-way ANOVA using Dunnett's multiple comparison test (\* =  $P \le 0.05$ ; \*\*  $P \le 0.01$ ; \*\*\* =  $P \le 0.001$ ; \*\*\*\* =  $P \le 0.0001$ ).

### 5. Discussion

The aim of this thesis was the investigation of miRNA-mediated aberrant immune checkpoint molecule expression in human cancer cells, with a particular focus on the immunomodulatory ligand PD-L1. Studies in various tumor entities have demonstrated that the interaction of PD-1 and PD-L1 promotes a pro-tumor environment by inhibiting T cell activation, proliferation and survival (Sun et al., 2018; Zheng et al., 2019). The development of antibody-based inhibitors targeting the PD-1/PD-L1 axis have significantly improved tumor responsiveness and the overall survival rate of cancer patients as shown in Supplementary Figure 8 (p. 72) (Han et al., 2020). Though high PD-L1 expression is deemed favorable for immunotherapy, it's also associated with tumor growth and progression resulting in poor patient prognosis (Yu et al., 2020). In breast, lung and prostate cancer, the risk of distant metastasis development and mortality from PD-L1-positive tumors is highly increased by induced immune escape factors, compared to PD-L1-negative patients (Mu et al., 2011; Petitprez et al., 2019; Qin et al., 2015; Y. Xu et al., 2021). Therefore, this study aimed to identify and characterize potential tumor suppressive miRNAs from a preselected library, that inhibit the expression of PD-L1. Additionally, the effect of the miRNA library on the immunomodulatory surface enzyme NT5E was investigated, aiming to find multi-functional miRNAs. The elucidation of novel inhibitory miRNAs and their targets generates further insights into the development of cancer and bears therapeutic potential for clinical application.

#### 5.1.1. miRNA-mediated inhibition of PD-L1 expression in breast cancer cells

The investigated miRNAs were preselected from a library of 2754 human miRNAs based on their potential to downregulate surface PD-L1 expression in the breast cancer cell line MDA-MB-231 (Kordaß, 2021). The presented flow cytometry and RT-qPCR data revealed a significant decrease of target ligand levels in 8 out of 11 miRNAs, of which miR-139-3p, miR-139-5p, miR-146a-5p, miR-155-5p and miR-1204-mediated downregulation were specific to the MDA-MB-231 cell line (Figure 17, p. 40). The comprehensive *in silico* prediction of miRNA-PD-L1 binding revealed that neither miR-139-5p, miR-146a-5p nor miR-1204 directly interacted with the target transcript (Vejnar & Blum, 2013). Thus, implicating that the significant change of PD-L1 levels is a result of indirect, binding site-independent downregulation effects in MDA-MB-231 cells, demonstrating the limitations of purely bioinformatic-based analysis. The tumor suppressive potential of miR-139-5p has been widely reported in various tumor entities: In colorectal cancer the overexpression of miR-139-5p inhibited not only the proliferation, migration and invasion of cancer cells *in vitro*, but also sensitized tumors to chemotherapy, while impairing tumor growth and metastasis *in vivo*. Further, it was identified that miR-139-5p directly targets and suppresses expression of multiple mediators in the oncogenic rat sarcoma virus (RAS) and wingless and Int-1 (Wnt) signaling pathways, like the nuclear phosphoprotein c-Jun of the activating

protein-1 transcription factor and the gene of beta-catenin (CTNNB1) (Du et al., 2020). Adjacently, in hepatocellular carcinoma, breast, prostate, thyroid and endometrial cancer the underexpression of miR-139-5p was associated with recurrent and metastatic disease leading to poor prognosis (J. H. Liu et al., 2018; Montero-Conde et al., 2020; B. Yang et al., 2019). Notably, studies in MDA-MB-231 cells and several hepatocellular carcinoma cell lines suggest that the oncogenic long noncoding RNA TTN antisense RNA 1 (TTN-AS1) directly interacts with miR-139-5p and decreases its expression, resulting in cancer cell proliferation, migration and invasion (Fang et al., 2020; X. Zhu et al., 2021). Although, miR-139-5p lacks PD-L1 binding sites, this investigation further validated reports of its tumor suppressive nature by the novel discovery of miR-139-5p-mediated downregulation of PD-L1 surface and mRNA expression levels through indirect effects.

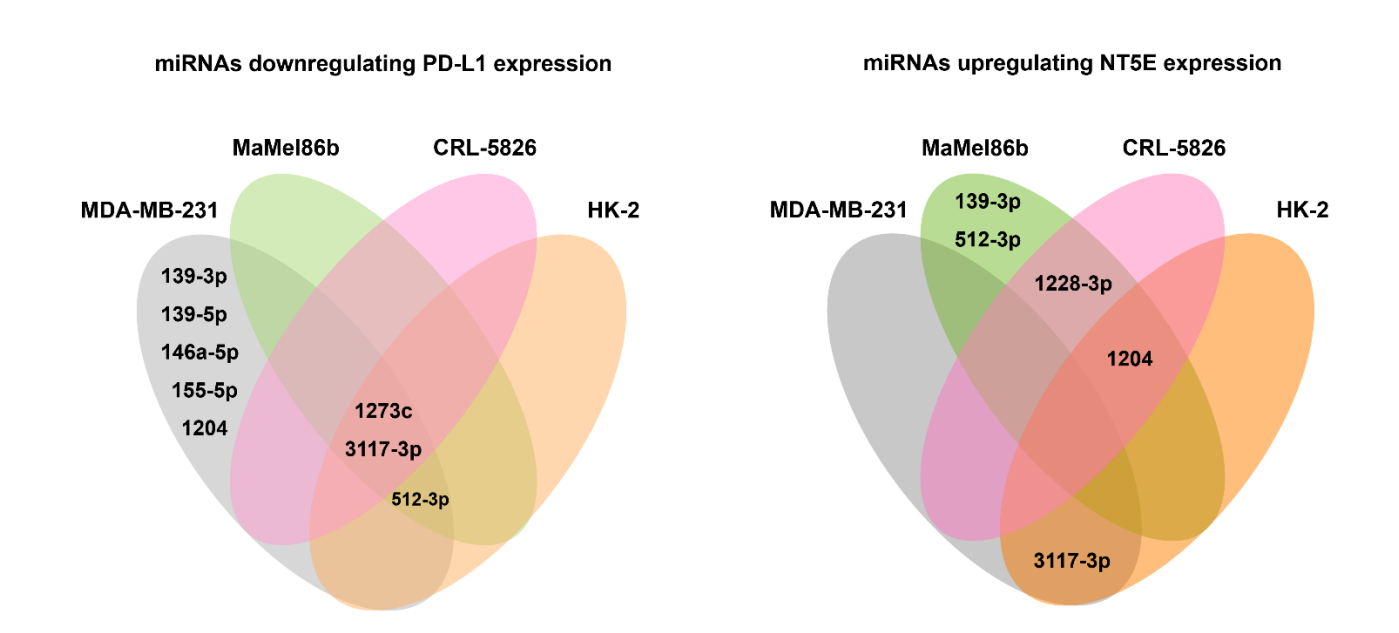


Figure 17: Venn diagram of miRNAs affecting mRNA and surface expression of PD-L1 and NT5E. Overlap of miRNAs significantly up- or downregulating immunomodulatory target molecules in MDA-MB-231, CRL-5826, MaMel86b and HK-2 cells.

Similar to miR-139-5p-induced effects, miR-146a-5p significantly downregulated PD-L1 expression levels in an indirect manner. Recent studies revealed that miR-146a-5p could act as a tumor suppressor and was downregulated in several types of cancerous tissues (Iacona & Lutz, 2019). In triple-negative breast cancer cells the introduction of exogenous miR-146a-5p inhibited cancer proliferation and migration by regulating the tumor-promoting Sry-related HMG box (SOX-5) transcription factor. Notably, miR-146a-5p overexpression repressed expression of unfavorable mesenchymal markers like fibronectin, vimentin and N-cadherin, which are commonly expressed by motile, invasive and aggressive cancer cells (F. Liu et al., 2016; Si et al., 2018). In the colorectal adenocarcinoma cell line HT-29, that

was ruled out for further investigation due to its marginal PD-L1 expression, the simultaneous overexpression of miR-146a-5p and miR-193a-5p also inhibited cancer cell proliferation and migration, while synergistically inducing apoptosis. Further, co-transfections resulted in the reduction of propylated extracellular signal-regulated kinase (pERK), which is a key component of dysregulated rapidly accelerated fibrosarcoma (RAF), mitogen-activated extracellular signal-regulated kinase (MEK), vascular endothelial growth factor (VEGF) and ERK signaling pathways in cancer cells (Noorolyai et al., 2021; Z. Zhang et al., 2009). This study supported previous findings on the tumor suppressive potential of miR-146a-5p.

In contrast, miR-1204 significantly downregulated only intracellular mRNA levels of PD-L1 in MDA-MB-231 cells through binding site-independent effects. Interestingly, numerous studies have characterized miR-1204 as a tumor-promoting oncomiRNA: In breast and ovarian cancer the intrinsic overexpression of miR-1204 is strongly correlated with disease progression, measured by increased cell proliferation, tumor size and aberrant glycolysis activity in cancer cells. Specifically, increased miR-1204 levels promoted the elevated expression of the glucose transporter 1 (GLUT-1), facilitating the uptake of glucose across mammalian plasma membranes (J. Xu et al., 2019; G. Yi et al., 2022). The increased uptake of glucose by cells is a typical hallmark of cancer, which fuels aerobic glycolysis in the cancer metabolism for the generation of new biomass (Carvalho et al., 2011). The oncogenic properties of miR-1204 are also reported in non-small-cell lung cancer (NSCLC), where miR-1204 decreased the expression of the transcription factor paired like homeodomain 1 gene (PITX1). Overall, high intrinsic miR-1204 and low PITX1 levels were highly correlated with increased NSCLC proliferation through reduced cell cycle arrest in vitro, as well as large tumor size, lymph node metastasis and poor patient prognosis (W. Jiang et al., 2019). Although miR-1204 was shown to downregulate PD-L1 in breast cancer cells as a potential tumor suppressive agent, miR-1204 very significantly upregulated the expression of the enzyme NT5E in other cell lines, supporting the studies of its oncogenic nature (Figure 17, p. 40).

#### 5.1.2. Effect of miRNA library on PD-L1 expression in human cell lines

The preselected miRNA library based on the inhibition of PD-L1 expression in breast cancer cells, was also examined for potential effects in the melanoma cell line MaMel86b, the lung carcinoma cell line CRL-5826 and the normal kidney cell line HK-2. Here the flow cytometric analysis revealed a global downregulation of target levels in only-Lipofectamine<sup>TM</sup> RNAiMAX-transfected mock cells compared to cells treated with Mimic Control-1. Notably, miR-ath-416 referred to as Mimic Control-1 was previously tested and chosen as a transfection control in MDA-MB-231 cells, because the miRNA does not possess functionality and thus didn't interfere with investigated target levels in breast cancer (Kordaß, 2021). Therefore, it was expected that mock and Mimic Control-1 levels were reliably similar in expressed target levels, enabling the fair folding of samples to the chosen control. This concept did not hold true for the

tested skin and lung cancer cell lines, as well as the healthy kidney cells. The observed difference in mock and Mimic Control-1 target levels, may stem from cell line specific intrinsic miRNA regulation: In theory, the overexpression of Mimic Control-1 floods the miRNA processing machinery of transfected cell with miR-ath-416. In the nucleus, the unfunctional miRNA is likely processed canonically, before being bound by Argonaute proteins to form the miRISC complex during miRNA maturation (O'Brien et al., 2018). Thereby, the influx of Mimic Control-1 occupies proteins and enzymes associated with of miRNA processing and thus temporarily blocks the processing of intrinsically expressed miRNAs. The tested CRL-5826, MaMel86b and HK-2 cells might express endogenous miRNAs that naturally downregulate the level of PD-L1 and NT5E expression, which could explain the lower levels of targets seen for the mock transfection. As a result, the induction of Mimic Control-1 processing could artificially upregulate the expression of PD-L1 and NT5E by obstructing intrinsic miRNA-mediated target regulation. This potential interference in expression patterns of the investigated cancer cells, necessitates the elucidation and employment of cell line specific transfection controls that better represent native target levels. As a consequence, the acquired flow cytometric data investigating the potential effect of the miRNA library transfection was additionally assessed considering respective mock levels in the heathy kidney cells, as well as breast and lung tumor cell lines. For PD-L1, the reevaluation of surface and mRNA levels revealed 2 miRNA candidates that significantly downregulated target levels across all four cell lines: miR-1273c and miR-3117-5p. Further miR-512-5p was identified to significantly inhibit target ligand levels in the three cell lines MDA-MB-231, MaMel86b and HK-2. While PD-L1 expression seems to be regulated by cell line specific factors, the discovery of globally applicable PD-L1-suppressing miRNAs bears large-scale therapeutic potential for a variety of cancers including metastases.

#### 5.1.3. miRNA library and the regulation of NT5E

Further investigation of transfection effects of the miRNA library in all four human cell lines was conducted, focusing on the immune modulatory molecule NT5E. Numerous studies have linked the aberrant expression of this enzyme with the promotion of an anti-inflammatory and pro-tumoral microenvironment. Specifically, NT5E-catalyzed adenosine inhibits secretion of proinflammatory cytokines, as well as proliferation, activation and migration of T cells, while accelerating the conversion of tumor-reactive type 1 macrophages into tumor-tolerant type 2 macrophages and increasing cancer cell proliferation and migration by facilitating cAMP production (Antonioli et al., 2016; Haskó & Pacher, 2012; T. Jiang et al., 2018). The presented flow cytometric and RT-qPCR data revealed a significant decrease of target levels for the candidate miR-155-5p in breast and lung cancer cells. Additionally, it was found that miR-512-3p downregulated NT5E only in the MDA-MB-231 breast cancer cell line. The bioinformatic analysis of both contenders revealed direct miRNA binding sites within the 3'-UTR of the enzyme NT5E, proofing the observed decrease of target levels through direct biding events. Notably,

previous work in the Eichmüller group has validated both of the predicted binding sites of miR-155-5p in the mRNA transcript of NT5E (Kordaß, 2021). Additionally, reports by Yee et al. studied the interaction of miR-155-5p and PD-L1, resulting in the downregulation of the ligand at the protein level. They also validated predicted bindings sites and reported that PD-L1 possess two conserved miR-155-binding sites in mice and humans (Yee et al., 2017). In accordance with observed PD-L1 downregulation tendencies seen in CRL-5826 cells, a study in the lung adenocarcinoma cell lines A549 and H1659, likewise suggested that miR-155-5p overexpression suppresses the overall expression level of the target ligand (J. Huang et al., 2020). Altogether, these reports support the mutual downregulation effects of miR-155-5p in both investigated targets, thus characterizing miR-155-5p as a novel and potentially multi-functional tumor suppressive miRNA. Interestingly, miR-155-5p overexpression in this study decreased the surface level expression of both NT5E and PD-L1, but only downregulated intracellular mRNA levels for the surface enzyme. This may suggest that miR-155-5p binds tightly to its two target sites in NT5E inducing the degradation of the mRNA transcript, while the miRNA only blocks the translation of PD-L1 unaltering its mRNA levels. Though miR-155-5p-mediated targeting of NT5E and PD-L1 has been reported, the exact mechanism of inhibition has yet to be elucidated (Kordaß, 2021). Remarkably, further studies examined mir-155-5p-mediated gene regulation in macrophages, CD4+ T cells, dendritic cells and B cells. It was discovered that miR-155-5p was a key regulator in the polarization of macrophages into the tumor-reactive M1 state (Genard et al., 2017; Hsin et al., 2018). This may suggest, that the exogenous expression of miR-155-5p in tumor tissues could act upon tumor-associated macrophages in a direct and indirect manner. Thereby, directly targeting the negative inhibitor suppressor of cytokine signaling 1 (SOCS1), which is known to block the generation of immunosuppressive signals acting upon Toll-like receptors on the surface of macrophages (N. Wang et al., 2014). An indirect effect on macrophage states could be associated with the miR-155-5p-mediated NT5E downregulation in cancer cells, resulting in lowered extracellular adenosine levels within the tumor. In return, decreased cAMP levels would be available for the conversion of beneficial M1 macrophages into tumor-tolerant type 2 macrophages (Polumuri et al., 2021). All in all, miR-155-5p demonstrated a multi-functional-tumor-suppressive potential in the investigated breast and lung cancer cell lines, by decreasing the expression level of the immunomodulatory molecules NT5E and PD-L1.

Additionally, the investigation of NT5E surface and mRNA levels revealed a significant increase of target levels in 5 out of 11 miRNA candidates, of which miR-139-3p and miR-512-3p-mediated upregulation were specific to the melanoma cell line MaMel86b. Further, miR-1204 universally increased NT5E levels in all investigated cell lines but MDA-MB-231, miR-3117-5p-induced elevated target levels in breast cancer and healthy human cells, and NT5E levels were observed to be increased in miR-1228-3p transfected melanoma and lung cancer cell lines (summarized in Figure 17, p. 40). A study in NSCLC

deemed upregulated miR-1228-3p levels as a biomarker for poor prognosis. It was computed that low miR-1228-3p expression was significantly associated with prolonged overall survival time based on the analysis of data retrieved from 50 lung cancer patients (Xue et al., 2020). Furthermore, a recent study in hepatocellular carcinoma investigated the effect of cancer-associated fibroblast-derived extracellular vesicles (EVs), filled with miR-1228-3p on the tumor cells. It was observed that the introduction of miR-1228-3p-EVs in hepatocellular carcinoma cells promoted tumor progression and chemoresistance. Specifically, it was elucidated that miR-1228-3p directly targets the protein placenta associated 8 (PLAC8), which is a pivotal regulator of tumor evolution in mammalian cells (Cabreira-Cagliari et al., 2018). The miR-1228-3p-mediated repression of PLAC8 lead to the activation of the phosphatidylinositol 3-kinase/protein kinase B (PI3K/AKT) pathway, which induce hepatocellular carcinoma cell proliferation, migration and invasion (Y. Zhang et al., 2023). The reported oncogenic nature of miR-1228-3p was supported by findings of our study here through the observation of significantly increased NT5E surface levels in melanoma and lung cancer cell lines, as well as significantly increased cell proliferation levels after at 48 h in an XTT assay conducted with the breast cancer cell line MDA-MB-231.

#### 5.1.4. Investigation of miRNA library induced cell viability effects

In order to further investigate and characterize miRNA candidates of the preselected library an XTT assay was conducted to assess cancer cell viability and proliferation of miRNA transfected MDA-MB-231 and MaMel86b cells. In both cells lines no significant changes in viability or proliferation was detected after 24 h, indicating that the transfection of miRNA library did not affect cancer cell proliferation within a single day. This finding enabled the untainted investigation of miRNA-PD-L1 interactions through the conduction of a PD-L1 3'-UTR reporter assay in cancer cells. Further, the overall assessment of the strongly fluctuating absorbance levels detected in the melanoma cell line MaMel86b, concluded that the XTT assay did not produce meaningful data. In contrast, the XTT assay conducted in the breast cancer cell line MDA-MB-231 showed significantly downregulated levels of cell viability and proliferation through reduced absorbance reading for the miRNA candidates: miR-139-5p, 146-3p, miR-512-3p, miR-1204, miR-1273c and miR-3117-3p compared to the Mimic Control-1. Thereby, the repetition of the XTT assay deemed the observed downregulation of cell proliferation reliable in only miR-3117-3p. This finding supports the observed significant downregulation effects in the surface level expression of the ligand PD-L1 in all four cell lines. The robust downregulation of mRNA and surface levels seen in the breast cancer cells, likely stems from the two predicted miRNA biding sites with in the 3'-UTR of PD-L1. While these assessments categorize miR-3117-3p as a potential globally applicable tumor-suppressing miRNA candidate, the investigation of the miRNA transfection effects on the surface enzyme NT5E revealed the duality of miR-3117-3p functionality. Here, miR-3117-3p significantly elevated the surface expression levels of the target NT5E in the breast cancer cell line and in healthy kidney cells, despite the lack of a predicted target binding site. To date, there are few reports on the investigation of miR-3117-3p function: A study on childhood acute lymphoblastic leukemia risk, identified the miR-3117-3p-mediated targeting of eight genes of the MAPK signaling pathway. Specifically, miR-3117-3p promoted the expression of the oncogene RAS (Gutierrez-Camino et al., 2018). It has been proven that the aberrant activation of the RAS/RAF/MAPK pathway is a major oncogenic event that is responsible for tumorigenesis and related angiogenesis in a wide array of human cancers (Masliah-Planchon et al., 2016; Molina & Adjei, 2006). Furthermore, miR-3117-3p has been linked to high risk factors for the development of cardiovascular diseases. The expression of miR-3117-3p was significantly correlated with arterial hypertension, hyperlipidemia, diabetes, smoking status, obesity and chronic lung disease in a cohort study of 191 individual patients with coronary artery disease (Neiburga et al., 2021). The function of miR-3117-3p must be further investigated and characterized in order to assess its potential as a tumor promoting or inhibiting miRNA.

#### 5.1.5. Validation of direct interactions between miRNAs and the 3'-UTR of PD-L1

In order to gain an in-depth understanding of the mode-of-action in the suppression of PD-L1 mediated by miR-1273c, miR-139-3p and miR-512-3p a PD-L1-3'-UTR luciferase reporter assay was carried out. For all three miRNA candidates at least one binding site within the 3'-UTR of the PD-L1 transcript was predicted. It was hypothesized that PD-L1 inhibiting miRNAs exert their suppressive function through direct binding of the target mRNA, resulting in the blockage of PD-L1 protein translation and the degradation of PD-L1 mRNA. Hence, the conduction of the reporter assay aimed to validate significant observations for the downregulation of the immunomodulatory ligand PD-L1 by assessing molecular interactions of the miRNAs and the target 3'-UTR sequence. The reporter assay was carried out in all four investigated human cell lines to gauge for cell line specific effects, which might falsify obtained results on miRNA binding. For the lung cancer cell line CRL-5826, detected luciferase signals were consistently low in all samples. This may stem from a cell line specific aversion to the co-transfection of the miRNA and pLS-PD-L1 plasmid using the DharmaFECT Duo Transfection Reagent or the ineffective translation of the luciferase enzyme. Hence the data acquired in lung cancer cells was deemed insubstantial. In contrast, luciferase signals of reporter assays conducted in MDA-MB-231, MaMel86b and HK-2 cells were substantially higher. The luciferase signals of the proximal tubular kidney cells were likely lower due a decreased number of viable cells post transfection compared to the breast and skin cancer cells. Regardless, the 3'-UTR reporter assay conducted in HK-2 cells was successful considering the extremely significant downregulation of luminescence levels seen in the PD-L1 siRNA pool sample, similarly observed in MDA-MB-231 and MaMel86b cells. This verified the expected decrease of luminescence levels associated with direct miRNA-PD-L1-3'-UTR binding, forming the basis for the

assessment of miRNA candiate-PD-L1-3'-UTR interactions. For miR-1273c, a global downregulation of luminesce was observed in all three cell lines, with a decreased tendency in detected luminescence levels in MaMel86b cells and a highly significant decrease in MDA-MB-231 and HK-2 cells. Both miR-139-3p and miR-512-3p transfections produced a very significant downregulation of luminescence intensity in the breast cancer and normal kidney cell lines compared to Mimic Control-1. These observations proved direct binding events for all three investigated miRNA candidates in more than one cell line. The observed miR-1273c-mediated decrease of PD-L1 expression in all investigated human cell lines is supported by the verification of direct miRNA-target interactions at the precited binding site. Interestingly, the cell line-wide decrease in expression of the ligand PD-L1 was only observed for surface protein levels, indicating that miR-1273c merely blocks protein translation without inducing mRNA degradation. To date there are only few published investigations of miR-1273c in the context of cancer: A study in renal cell carcinoma reported on the miR-1273c mediated induction of the tumor suppressor Von Hippel-Lindau (VHL) through direct binding to the gene's promoter sequence. Further functional studies revealed that the transfection of miR-1273c inhibited cell proliferation and induced apoptosis of cancer cells in a dose dependent manner (C. W. Lee et al., 2014). In accordance, the study presented here identified miR-1273c as a universally applicable tumor suppressive miRNA candidate with therapeutic potential capable of downregulating the expression of PD-L1 through direct binding to the targets 3'-UTR in various human tumor cell lines.

For miR-139-3p in silico binding site predictions revealed the presence of 2 potential targeting sites, which are located close to the 5' or 3' end of the PD-L1 3'-UTR sequence. The current study investigated only the molecular interaction between miR-139-3p and its 5' targeting site, revealing extremely significant binding events between the miRNA candidate and the PD-L1 transcript. Despite the observed downregulation of luminescence signals in the PD-L1-3'-UTR luciferase reporter assay, miR-139-3p only significantly downregulated PD-L1 mRNA levels in the breast cancer cell line. In contrast, miR-139-3p upregulated the surface expression of the enzyme NT5E in MaMel86b cells via presumed cell line specific indirect effects, as the miRNA candidate lacks NT5E targeting sites. Nevertheless, the tumor suppressive nature of miR-139-3p has been widely reported in literature studying a wide array of cancer types: A study on head and neck squamous cell carcinoma reported low miR-139-3p expression levels in tumor tissue. Remarkably, it was shown that miR-139-3p overexpression effectively inhibited the proliferation, migration and invasion of laryngeal squamous cell carcinoma cells, further inducing cell cycle arrest and cancer cell apoptosis both in vitro and in vivo. Thereby, miR-139-3p directly targeted the Ras-related protein RAB5A, that is a key regulator of vesicular transport, membrane trafficking, and signaling pathways by mediating early endocytosis (Ma et al., 2020; Yuan & Song, 2020). Serval studies in acute myeloid leukemia, hepatocellular carcinoma, childhood hepatoblastoma, gastric, cervical and breast cancer report of significant tumor suppressive effects mediated by miR-139-3p, with a wide array of validated targets including the NIN1/RPNI2 binding protein 1 homolog (NOB1), Kinesin Family Member 18B (KIF18B), Wnt Family Member 5A (Wnt5A) and another Ras-related protein RAB1A (P. Huang et al., 2016; Ke et al., 2022; Stavast et al., 2022; Wu et al., 2023; W. Zhang et al., 2019; Y. Zhu et al., 2019). The extensively studied inhibitory effect of miR-139-3p on various cancer types was mostly validated by findings in the study presented here, in regard to the breast cancer cell line MDA-MB-231.

The miRNA candidate miR-512-3p possesses one predicted binding site for the immune modulatory molecules PD-L1 and NT5E. This study validated the direct binding of miR-512-3p to its target site in the ligand PD-L1, supporting the observed downregulation of surface target levels in MDA-MB-231, MaMel86b and HK-2 cells by miR-512-3p. Furthermore, flow cytometry revealed the miR-512-5p-mediated decrease of NT5E protein levels in breast cancer cells, adjacent to the increase of NT5E surface expression measured in the melanoma cell line. Notably, the exogenous overexpression of miR-512-3p did not affect target mRNA levels, suggesting the sole interference of the miRNA candidate with the translation apparatus. Recent studies in breast cancer reported of the tumor suppressive potential of miR-512-3p. The overexpression of miR-512-3p in MDA-MB-231 and MCF-7 cells resulted in a significant inhibition of breast cancer cell growth. Specifically, Duan et al. reported of enhanced chemosensitivity and decreased metastatic potential and reduced tumor growth as a result of exogenous miR-512-3p induction. Further it was elucidated that miR-512-3p directly targets and downregulates the anti-apoptotic oncogenic protein Livin (Duan et al., 2020). Mohamadzade et al. showed the miR-512-3p-driven downregulation of the human epidermal growth factor receptor 2 and 3 (HER2 and HER3), which are receptor tyrosine kinases responsible for cell growth and epithelial cell survival. The overexpression of HER2 is associated with aggressive tumor growth and poor prognosis in breast, lung, bladder, ovarian, endometrial, gastric, colorectal and head and neck cancers (Iqbal & Iqbal, 2014). Further, miR-512-3p overexpression also led to the downregulation of the PI3K/AKT pathway by acting upon genes encoding for phosphatidylinositol 3-kinase regulatory subunit beta (PIK3R2) and RAC-alpha serine/threonine-protein kinase (AKT1) (Mohamadzade et al., 2021). In healthy cells the PI3K/AKT signaling pathway is a key regulator of cell growth, metabolism, mobility and survival, while in cancer cells pathway dysregulation is associated with the inhibition of apoptosis and stimulation of cell proliferation in many human cancers (Rascio et al., 2021). Additionally, Mohamadzade et al. reported the decreased viability of miR-512-3p transfected MDA-MB-232 cells, which this current study could significantly validate. All in all, miR-512-3p is a potent inhibitor of tumorigenesis with a substantial list of targets. This study identified and validated miR-512-3p as a novel miRNA-targeting the immunomodulatory ligand PD-L1.

#### 5.1.6. miRNA candidates and impervious PD-L1 and NT5E levels

Finally, both miR-146a-3p and miR-374b-3p lack predicted binding sites for the investigated immune modulators PD-L1 and NT5E. This was reflected in insignificant transfection effects on the target molecules. For miR-146a-3p marginal downregulation tendencies seen in flow cytometric analyses support reports of tumor suppressive effects seen with this miRNA in bladder cancer. Xiang *et al.* uncovered the miR-146a-3p-driven inhibition of the pituitary tumor-transforming gene 1- oncogene (PTTG1), resulting in the decreased migration, invasion, metastasis formation and growth, as well as the induction of cell cycle arrest in bladder cancer cells (Xiang et al., 2017). Currently, there are less than a dozen studies investigating miR-374b-3p. A recent study on clear cell renal cell carcinoma (ccRCC) suggested that the downregulation of miR-374b-3p in ccRCC cells promoted proliferation and tumor angiogenesis (Ou et al., 2022). In return, this may imply that miR-374b-3p overexpression could inhibit ccRCC progression. Both miR-146a-3p and miR-374b-3p function and effects in the context of cancer are yet to be fully investigated.

### 6. Conclusion

This thesis investigated the effect of a preselected miRNA library on the aberrant immune checkpoint molecule expression in three human tumor entities. In particular, the miRNA-mediated downregulation of the immunomodulatory ligand PD-L1 was assessed. The overexpression of PD-L1 and its receptor PD-1 plays a key role in an increasing number of malignancies, by inhibiting T cell activation, proliferation and survival (Kuol et al., 2018). To date, targeting of the PD-1-PD-L1 axis harbors great therapeutic potential in the treatment of tumors by reversing cancer cell-driven immune escape (M. Zhang et al., 2017). Furthermore, this study examined the malignant expression of the immunoregulatory enzyme NT5E. The increased catalysis of extracellular adenosine in the tumor tissue is strongly associated with the promotion of an anti-inflammatory state by inhibiting cytokine secretion and T cell stimulation, while encouraging the generation of tumor-tolerant type 2 macrophages (Antonioli et al., 2016). The dysregulation of both PD-L1 and NT5E in cancer is linked to aggressive tumor growth and progression resulting in poor prognosis (T. Jiang et al., 2018; Yu et al., 2020). Notably, recent studies have reported that employment of common photon and carbon ion irradiation-based radiotherapy for solid tumors further elevated PD-L1 and NT5E expression levels in vivo (Hartmann et al., 2020; Schröter et al., 2020). This finding further necessitates the elucidation of novel therapeutic approaches that effectively target the immense oncogenic potential of PD-L1 and NT5E overexpression. The recent development of large-scale miRNA profiling and deep sequencing have revealed the significance of miRNA-mediated cancer regulation, revolutionizing research in the field of miRNA drugs (Ors-Kumoglu et al., 2019; Paranjape et al., 2009). In accordance, this current study aimed to identify and characterize novel tumor suppressive miRNAs for the therapeutically-valuable downregulation of the immunomodulatory ligand PD-L1 in human cancer cells.

The comprehensive investigation of the miRNA library through flow cytometric and RT-qPCR-based analysis validated the PD-L1 suppressive potential of miR-139-3p, miR-139-5p, miR-146a-5p, miR-155-5p and miR-1204 specific to the breast cancer cell line MDA-MB-231. Further examinations identified the global miRNA-mediated downregulation of target ligand levels in several tumor entities by miR-3117-3p, miR-1273c and miR-512-3p. The highly significant miR-3117-3p-driven decrease of PD-L1 surface levels in all investigated cell lines is likely linked to the presence of three predicted target binding sites within the 3'-UTR of PD-L1. The interaction of miR-3117-3p and PD-L1 resulted in an overall decrease of target protein and mRNA levels, indicating the miRNA-mediated blockage of translation and the initiation of mRNA transcript degradation. In accordance, miR-3117-3p significantly reduced cell proliferation, yet upregulated NT5E levels through binding site-independent effects in breast cancer cells. Furthermore, the molecular interaction of three miRNA candidates with the 3'-UTR of the PD-L1 mRNA transcript was validated in a luciferase reporter assay: Direct binding events between miR-1273c and the PD-L1 transcript supported the observed decrease of PD-L1 protein levels in all

miR-1273c-transfected cell lines. Seemly miR-1273c only interferes with protein translation by lose target binding, without inducing full mRNA degradation. In contrast, the endogenous introduction of miR-139-3p resulted in the decrease of PD-L1 mRNA levels, which was supported by the validation of one of its two bindings sites within the 3'-UTR of PD-L1. For miR-512-3p the computational prediction of binding sites revealed a single binding site in both PD-L1 and NT5E. This study validated the direct binding of miR-512-3p to PD-L1 in both breast cancer and normal kidney cells, resulting in a decrease of PD-L1 surface levels in several investigated cell lines. Interestingly, miR-512-3p acted as a multi-functional tumor suppressor by downregulating both PD-L1 and NT5E expression in breast cancer cells, while elevating NT5E enzyme levels in the melanoma cell line. Furthermore, this study was able to characterize miR-155-5p as another potential multi-functional tumor suppressive miRNA candidate, based on the simultaneous downregulation of both PD-L1 and NT5E surface levels. Notably, binding site predictions revealed the presence of respectively two binding sites in the investigated targets.

In conclusion, this study helped to gain more insight into the regulation of miRNA-mediated PD-L1 regulation in different human tumor entities. Serval novel tumor-suppressive miRNA candidates were validated and characterized for the immune checkpoint molecule PD-L1. Especially, miR-3117-3p and miR-1273c were identified as potent inhibitors of the target ligand in all examined cell lines. Moreover, the investigation elucidated miR-512-3p and miR-155-5p as potentially multi-functional miRNA candidates for the downregulation of the surface molecules PD-L1 and NT5E via predicted binding sites in both targets. The presented examination of the preselected miRNA library necessitates the further elucidation of the molecular mode-of-action for miR-3117-3p and miR-155-5p in the context of PD-L1 transcript targeting. The elucidation of novel inhibitory miRNAs and their targets generates further insights into the development of cancer and bears large therapeutic potential for clinical application. In particular, the presented discovery of PD-L1 inhibiting miRNAs could be implemented as a new tool in combined radiation therapy to mitigate PD-L1 enhancing side effects. Though small in size, microRNAs certainly have the capability to revolutionize traditional medicine by changing the course and fate of to-date-uncurable diseases.

#### 6.1. Outlook

Future investigations of the miRNA library should examine miRNA-mediated effects on other immunomodulatory targets in an extended spectrum of human tumor entities. In particular, the interaction of miR-374b-3p and miR-512-3p with the receptor PD-1 should be elucidated, as predicted target bindings sites give rise to potential regulatory effects. Additionally, the predicted binding of miR-155-5p to the immune checkpoint molecule cytotoxic T-lymphocyte-associated protein 4 (CTLA4)

should be investigated as a novel target. In tumor tissue the dysregulation of the receptor CTLA4 is strongly associated with the generation of an immunosuppressive state, promoting the act of immune escape (Buchbinder & Desai, 2016). Recent developments in immunotherapy demonstrate that the employment of anti-CTLA4 antibodies significantly improves the overall survival rate of patients, by reactivating suppressed T cell activity and proliferation, as well as by reducing regulatory T cell-mediated immunosuppression at the tumor site (Seidel et al., 2018). The targeting of the immune checkpoint molecules PD-1 and CTLA4 by novel miRNA therapeutics harbors great tumor suppressive potential by re-activating intrinsic immune responses in cancer patients.

The discovery of potential miRNA therapeutics calls for the investigation of potent candidates in context of traditional cancer therapies *in vivo*. Recent developments of next-generation combinatorial treatments report of increased therapeutical efficacy through the employment of miRNAs (Seo et al., 2019). Therefore, another point of great concern that needs to be better addressed by future research is the application of miRNA-based therapies in the body. State of the art investigations, employ modified lipid nano particles (LNPs) as vehicles of intracellular miRNA delivery. Conveniently LNPs are molecules of low immunogenicity, as they consist of endogenous lipids that can easily be recycled by the transfected cells (Hydbring & Du, 2019). A recent study on hepatocellular carcinoma, successfully co-delivered the interfering RNA anti-miR-27a and the kinase inhibitor Sorafenib in liver tumor bearing mice. Remarkably, the employment of an antibody-tagged cationic pH-responsive LNP system unlocked the synergistic anticancer effects of both molecules, resulting a significant suppression of the tumor burden (Z. Wang et al., 2019). Though promising, LNP technologies need further refining as currently a major hurdle in LNP-mediated miRNA transport is the topic of endosomal escape. It has been reported that effectively only less than two percent of the administered nucleic acids escape the endosome and reach the cytosol where they can unleash their therapeutic potential (Maugeri et al., 2019). Therefore, other methods of microRNA transmission like viral vectors and polymer-based nanoparticles should also be explored, in order to determine an ideal transfection strategy for the intracellular delivery of therapeutic mircoRNAs (Paunovska et al., 2022). A study by Cui et al., developed novel polymeric nanoparticles for the delivery of the chemotherapy drug Paclitaxel (PTX) together with miR-7 for the treatment of ovarian cancer. The commonly used first-line chemotherapeutic drug PTX is known to induce the epidermal growth factor receptor (EGFR)/ ERK pathway resulting in tumor cell proliferation, survival, invasion and drug resistance. Remarkably, the nanoparticle-facilitated controlled release of miRNA and drugs in this study enhanced the efficacy of the chemotherapeutic treatment by inhibiting the PTX-induced side effects through miR-7 intervention. Thereby, decreasing the half-maximal inhibitory concentration of PTX and thus aiding the mitigation of cytotoxicity events in vivo (Cui et al., 2018). Concluding, future research must further characterize mircoRNAs and respective targets involved in sickness and health, while further improving and developing methods of effective intracellular nucleic acid delivery.

## 7. Bibliography

- Aandahl, E. M., Aukrust, P., Skålhegg, B. S., Müller, F., Fr⊘land, S. S., Hansson, V., & Taskén, K. (1998).

  Protein kinase A type I antagonist restores immune responses of T cells from HIV-infected patients. *The FASEB Journal*, 12(10), 855–862. https://doi.org/10.1096/fasebj.12.10.855
- Active Motif. (2023). *LightSwitch*<sup>TM</sup> *Luciferase Assay System Overview* https://switchgeargenomics.com/resources/science-technology#lspromoter
- Agata, Y., Kawasaki, A., Nishimura, H., Ishida, Y., Tsubata, T., Yagita, H., & Honjo, T. (1996). Expression of the PD-1 antigen on the surface of stimulated mouse T and B lymphocytes. *International Immunology*, 8(5), 765–772. https://doi.org/10.1093/intimm/8.5.765
- Alarcón, C. R., Lee, H., Goodarzi, H., Halberg, N., & Tavazoie, S. F. (2015). N6-methyladenosine marks primary microRNAs for processing. *Nature*, *519*(7544), 482–485. https://doi.org/10.1038/nature14281
- Allard, B., Turcotte, M., Spring, K., Pommey, S., Royal, I., & Stagg, J. (2014). Anti-CD73 therapy impairs tumor angiogenesis. *International Journal of Cancer*, 134(6), 1466–1473. https://doi.org/10.1002/ijc.28456
- Allard, D., Turcotte, M., & Stagg, J. (2017). Targeting A2 adenosine receptors in cancer. *Immunology & Cell Biology*, 95(4), 333–339. https://doi.org/10.1038/icb.2017.8
- Alles, J., Fehlmann, T., Fischer, U., Backes, C., Galata, V., Minet, M., Hart, M., Abu-Halima, M., Grässer, F. A., Grässer, G., Lenhof, H.-P., Keller, A., & Meese, E. (2019). An estimate of the total number of true human miRNAs. *Nucleic Acids Research*, *47*(7), 3353–3364. https://doi.org/10.1093/nar/gkz097
- Almeida, M. I., Reis, R. M., & Calin, G. A. (2011). MicroRNA history: Discovery, recent applications, and next frontiers. In *Mutation Research Fundamental and Molecular Mechanisms of Mutagenesis* (Vol. 717, Issues 1–2, pp. 1–8). Elsevier. https://doi.org/10.1016/j.mrfmmm.2011.03.009
- Antonioli, L., Pacher, P., Vizi, E. S., & Haskó, G. (2013). CD39 and CD73 in immunity and inflammation. In *Trends in Molecular Medicine* (Vol. 19, Issue 6, pp. 355–367). Trends Mol Med. https://doi.org/10.1016/j.molmed.2013.03.005
- Antonioli, L., Yegutkin, G. G., Pacher, P., Blandizzi, C., & Haskó, G. (2016). Anti-CD73 in Cancer Immunotherapy: Awakening New Opportunities. In *Trends in Cancer* (Vol. 2, Issue 2, pp. 95–109). Cell Press. https://doi.org/10.1016/j.trecan.2016.01.003
- Applied Biosystem. (2022). *QuantStudio 3 and 5 Real-Time PCR System Software*. https://www.thermofisher.com/de/de/home/global/forms/life-science/quantstudio-3-5-software.html

- Ardekani, A. M., & Naeini, M. M. (2010). The role of microRNAs in human diseases. In *Avicenna Journal* of Medical Biotechnology (Vol. 2, Issue 4, pp. 161–179). Avicenna Research Institute. /pmc/articles/PMC3558168/
- Bartel, D. P. (2004). MicroRNAs: Genomics, Biogenesis, Mechanism, and Function. In *Cell* (Vol. 116, Issue 2, pp. 281–297). Cell Press. https://doi.org/10.1016/S0092-8674(04)00045-5
- Bartel, D. P. (2018). Metazoan MicroRNAs. In *Cell* (Vol. 173, Issue 1, pp. 20–51). Cell Press. https://doi.org/10.1016/j.cell.2018.03.006
- BD Biosciences. (2022a). *BD FACSDiva<sup>TM</sup> Software* . https://www.bdbiosciences.com/eneu/products/software/instrument-software/bd-facsdiva-software
- BD Biosciences. (2022b). FlowJo<sup>TM</sup> v10.8.1. https://www.flowjo.com/solutions/flowjo/downloads
- Beavis, P. A., Stagg, J., Darcy, P. K., & Smyth, M. J. (2012). CD73: A potent suppressor of antitumor immune responses. In *Trends in Immunology* (Vol. 33, Issue 5, pp. 231–237). Trends Immunol. https://doi.org/10.1016/j.it.2012.02.009
- Bettelli, E., Carrier, Y., Gao, W., Korn, T., Strom, T. B., Oukka, M., Weiner, H. L., & Kuchroo, V. K. (2006). Reciprocal developmental pathways for the generation of pathogenic effector TH17 and regulatory T cells. *Nature*, *441* (7090), 235–238. https://doi.org/10.1038/nature04753
- Bhattarai, S., Freundlieb, M., Pippel, J., Meyer, A., Abdelrahman, A., Fiene, A., Lee, S. Y., Zimmermann, H., Yegutkin, G. G., Sträter, N., El-Tayeb, A., & Müller, C. E. (2015). α,β-Methylene-ADP (AOPCP) Derivatives and Analogues: Development of Potent and Selective ecto-5′-Nucleotidase (CD73) Inhibitors. *Journal of Medicinal Chemistry*, 58(15), 6248–6263. https://doi.org/10.1021/acs.jmedchem.5b00802
- Borchert, G. M., Lanier, W., & Davidson, B. L. (2006). RNA polymerase III transcribes human microRNAs. *Nature Structural and Molecular Biology*, *13*(12), 1097–1101. https://doi.org/10.1038/nsmb1167
- Buchbinder, E. I., & Desai, A. (2016). CTLA-4 and PD-1 Pathways. *American Journal of Clinical Oncology*, 39(1), 98–106. https://doi.org/10.1097/COC.0000000000000039
- Butte, M. J., Keir, M. E., Phamduy, T. B., Sharpe, A. H., & Freeman, G. J. (2007). Programmed Death-1 Ligand 1 Interacts Specifically with the B7-1 Costimulatory Molecule to Inhibit T Cell Responses. *Immunity*, *27*(1), 111–122. https://doi.org/10.1016/j.immuni.2007.05.016
- Cabreira-Cagliari, C., Dias, N. D. C., Bohn, B., Fagundes, D. G. D. S., Margis-Pinheiro, M., Bodanese-Zanettini, M. H., & Cagliari, A. (2018). Revising the PLAC8 gene family: From a central role in differentiation, proliferation, and apoptosis in mammals to a multifunctional role in plants. *Genome*, 61(12), 857–865. https://doi.org/10.1139/gen-2018-0035
- Carpenter, B., & Lebon, G. (2017). Human Adenosine A2A Receptor: Molecular Mechanism of Ligand Binding and Activation. *Frontiers in Pharmacology*, 8(DEC), 898. https://doi.org/10.3389/fphar.2017.00898

- Carvalho, K. C., Cunha, I. W., Rocha, R. M., Ayala, F. R., Cajaíba, M. M., Begnami, M. D., Vilela, R. S., Paiva, G. R., Andrade, R. G., & Soares, F. A. (2011). GLUT1 expression in malignant tumors and its use as an immunodiagnostic marker. *Clinics*, 66(6), 965–972. https://doi.org/10.1590/S1807-59322011000600008
- Cho, W. C. S. (2007). OncomiRs: The discovery and progress of microRNAs in cancers. In *Molecular Cancer* (Vol. 6, Issue 1, p. 60). BioMed Central. https://doi.org/10.1186/1476-4598-6-60
- Couzin-Frankel, J. (2013). Breakthrough of the year 2013. Cancer immunotherapy. In *Science* (Vol. 342, Issue 6165, pp. 1432–1433). Science. https://doi.org/10.1126/science.342.6165.1432
- Crick, F. (1956). *Ideas on Protein Synthesis*. The Biological Replication of Macromolecules Symposium. https://profiles.nlm.nih.gov/spotlight/sc/catalog/nlm:nlmuid-101584582X65-doc
- Cui, X., Sun, Y., Shen, M., Song, K., Yin, X., Di, W., & Duan, Y. (2018). Enhanced Chemotherapeutic Efficacy of Paclitaxel Nanoparticles Co-delivered with MicroRNA-7 by Inhibiting Paclitaxel-Induced EGFR/ERK pathway Activation for Ovarian Cancer Therapy. ACS Applied Materials and Interfaces, 10(9), 7821–7831. https://doi.org/10.1021/acsami.7b19183
- Dai, P., Rao, X., Zhang, X., Qiu, E., Wu, G., Lin, Y., Li, S., Li, Z., Cai, Z., & Han, S. (2022). Case Report: Complete Remission of a Patient With Metastatic Gastric Cancer Treated With Nivolumab Combined With Chemotherapy After Palliative Surgery. *Frontiers in Immunology*, 13, 2819. https://doi.org/10.3389/fimmu.2022.908558
- Denli, A. M., Tops, B. B. J., Plasterk, R. H. A., Ketting, R. F., & Hannon, G. J. (2004). Processing of primary microRNAs by the Microprocessor complex. *Nature*, *432*(7014), 231–235. https://doi.org/10.1038/nature03049
- Dong, H., Zhu, G., Tamada, K., & Chen, L. (1999). B7-H1, a third member of the B7 family, co-stimulates T-cell proliferation and interleukin-10 secretion. *Nature Medicine*, *5*(12), 1365–1369. https://doi.org/10.1038/70932
- Dotmatics. (2022). *GraphPad Prism*. https://www.graphpad.com/scientific-software/prism/
- Dotmatics. (2023). *Grubb's Test: Outlier calculator*. https://www.graphpad.com/quickcalcs/grubbs1/
- Du, F., Cao, T., Xie, H., Li, T., Sun, L., Liu, H., Guo, H., Wang, X., Liu, Q., Kim, T., Franklin, J. L., Graves-Deal, R., Han, W., Tian, Z., Ge, M., Nie, Y., Fan, D., Coffey, R. J., Lu, Y., & Zhao, X. (2020). KRAS mutation-responsive miR-139-5p inhibits colorectal cancer progression and is repressed by wnt signaling. *Theranostics*, 10(16), 7335–7350. https://doi.org/10.7150/thno.45971
- Duan, W. J., Bi, P. D., Ma, Y., Liu, N. Q., & Zhen, X. (2020). MiR-512-3p regulates malignant tumor behavior and multi-drug resistance in breast cancer cells via targeting Livin. *Neoplasma*, *67*(1), 102–110. https://doi.org/10.4149/neo 2019 190106N18
- Fang, J., Huang, C., Ke, J., Li, J., Zhang, W., Xue, H., & Chen, J. (2020). lncRNA TTN-AS1 facilitates proliferation, invasion, and epithelial-mesenchymal transition of breast cancer cells by regulating

- miR-139-5p/ZEB1 axis. *Journal of Cellular Biochemistry*, *121*(12), 4772–4784. https://doi.org/10.1002/jcb.29700
- Farazi, T. A., Juranek, S. A., & Tuschl, T. (2008). The growing catalog of small RNAs and their association with distinct Argonaute/Piwi family members. In *Development* (Vol. 135, Issue 7, pp. 1201–1214). The Company of Biologists. https://doi.org/10.1242/dev.005629
- Farrukh, H., El-Sayes, N., & Mossman, K. (2021). *Molecular Sciences Mechanisms of PD-L1 Regulation in Malignant and Virus-Infected Cells*. https://doi.org/10.3390/ijms22094893
- Fife, B. T., & Pauken, K. E. (2011). The role of the PD-1 pathway in autoimmunity and peripheral tolerance. *Annals of the New York Academy of Sciences*, 1217(1), 45–59. https://doi.org/10.1111/j.1749-6632.2010.05919.x
- Fredholm, B. B., IJzerman, A. P., Jacobson, K. A., Linden, J., & Müller, C. E. (2011). International union of basic and clinical pharmacology. LXXXI. Nomenclature and classification of adenosine receptors
   An update. In *Pharmacological Reviews* (Vol. 63, Issue 1, pp. 1–34). Pharmacol Rev. https://doi.org/10.1124/pr.110.003285
- Genard, G., Lucas, S., & Michiels, C. (2017). Reprogramming of tumor-associated macrophages with anticancer therapies: Radiotherapy versus chemo- and immunotherapies. In *Frontiers in Immunology* (Vol. 8, Issue JUL, p. 828). Frontiers Media S.A. https://doi.org/10.3389/fimmu.2017.00828
- Gutierrez-Camino, A., Martin-Guerrero, I., Dolzan, V., Jazbec, J., Carbone-Bañeres, A., de Andoin, N. G., Sastre, A., Astigarraga, I., Navajas, A., & Garcia-Orad, A. (2018). Involvement of SNPs in miR-3117 and miR-3689d2 in childhood acute lymphoblastic leukemia risk. *Oncotarget*, *9*(33), 22907–22914. https://doi.org/10.18632/oncotarget.25144
- Győrffy, B. (2021). Survival analysis across the entire transcriptome identifies biomarkers with the highest prognostic power in breast cancer. *Computational and Structural Biotechnology Journal*, *19*, 4101–4109. https://doi.org/10.1016/j.csbj.2021.07.014
- Győrffy, B., Surowiak, P., Budczies, J., & Lánczky, A. (2013). Online Survival Analysis Software to Assess the Prognostic Value of Biomarkers Using Transcriptomic Data in Non-Small-Cell Lung Cancer. *PLoS ONE*, 8(12), e82241. https://doi.org/10.1371/journal.pone.0082241
- Ha, M., & Kim, V. N. (2014). Regulation of microRNA biogenesis. In *Nature Reviews Molecular Cell Biology* (Vol. 15, Issue 8, pp. 509–524). Nature Publishing Group. https://doi.org/10.1038/nrm3838
- Hammond, S. M. (2015). An overview of microRNAs. *Advanced Drug Delivery Reviews*, 87, 3–14. https://doi.org/10.1016/j.addr.2015.05.001
- Han, Y., Liu, D., & Li, L. (2020). PD-1/PD-L1 pathway: current researches in cancer. *American Journal of Cancer Research*, 10(3), 727–742. http://www.ncbi.nlm.nih.gov/pubmed/32266087

- Hartmann, L., Schröter, P., Osen, W., Baumann, D., Offringa, R., Moustafa, M., Will, R., Debus, J., Brons, S., Rieken, S., & Eichmüller, S. B. (2020). Photon versus carbon ion irradiation: immunomodulatory effects exerted on murine tumor cell lines. *Scientific Reports*, 10(1), 1–13. https://doi.org/10.1038/s41598-020-78577-8
- Haskó, G., & Pacher, P. (2012). Regulation of macrophage function by adenosine. *Arteriosclerosis, Thrombosis, and Vascular Biology*, 32(4), 865–869. https://doi.org/10.1161/ATVBAHA.111.226852
- Hinske, L. C., França, G. S., Torres, H. A. M., Ohara, D. T., Lopes-Ramos, C. M., Heyn, J., Reis, L. F. L., Ohno-Machado, L., Kreth, S., & Galante, P. A. F. (2014). miRIAD—integrating microRNA inter- and intragenic data. *Database*, *2014*, 99. https://doi.org/10.1093/database/bau099
- Hsin, J. P., Lu, Y., Loeb, G. B., Leslie, C. S., & Rudensky, A. Y. (2018). The effect of cellular context on miR-155-mediated gene regulation in four major immune cell types. *Nature Immunology*, *19*(10), 1137–1145. https://doi.org/10.1038/s41590-018-0208-x
- Huang, J., Weng, Q., Shi, Y., Mao, W., Zhao, Z., Wu, R., Ren, J., Fang, S., Lu, C., Du, Y., & Ji, J. (2020).
   MicroRNA-155-5p suppresses PD-L1 expression in lung adenocarcinoma. *FEBS Open Bio*, 10(6), 1065–1071. https://doi.org/10.1002/2211-5463.12853
- Huang, P., Xi, J., & Liu, S. (2016). MiR-139-3p induces cell apoptosis and inhibits metastasis of cervical cancer by targeting NOB1. *Biomedicine and Pharmacotherapy*, 83, 850–856. https://doi.org/10.1016/j.biopha.2016.07.050
- Huang, Y., Shen, X. J., Zou, Q., Wang, S. P., Tang, S. M., & Zhang, G. Z. (2011). Biological functions of microRNAs: A review. *Journal of Physiology and Biochemistry*, 67(1), 129–139. https://doi.org/10.1007/s13105-010-0050-6
- Hui, E., Cheung, J., Zhu, J., Su, X., Taylor, M. J., Wallweber, H. A., Sasmal, D. K., Huang, J., Kim, J. M., Mellman, I., & Vale, R. D. (2017). T cell costimulatory receptor CD28 is a primary target for PD-1–mediated inhibition. *Science*, *355*(6332), 1428–1433. https://doi.org/10.1126/science.aaf1292
- Hydbring, P., & Du, J. (2019). Nanoparticle interaction with immune cells for nanoparticle-mediated (anticancer) immunotherapy. In *Theranostic Bionanomaterials* (pp. 55–73). Elsevier. https://doi.org/10.1016/B978-0-12-815341-3.00003-1
- Iacona, J. R., & Lutz, C. S. (2019). miR-146a-5p: Expression, regulation, and functions in cancer. *WIREs RNA*, 10(4), e1533. https://doi.org/10.1002/wrna.1533
- $\label{eq:lower_lower} Invitrogen. \qquad (2022). \quad \textit{LIVE/DEAD}^{\text{TM}} \quad \textit{Fixable} \quad \textit{Yellow} \quad \textit{Dead} \quad \textit{Cell} \quad \textit{Stain} \quad \textit{Kit.} \\ \text{https://www.thermofisher.com/order/catalog/product/de/en/L34959}$
- Iqbal, N., & Iqbal, N. (2014). Human Epidermal Growth Factor Receptor 2 (HER2) in Cancers: Overexpression and Therapeutic Implications. *Molecular Biology International*, 2014, 1–9. https://doi.org/10.1155/2014/852748

- Ishida, Y., Agata, Y., Shibahara, K., & Honjo, T. (1992). Induced expression of PD-1, a novel member of the immunoglobulin gene superfamily, upon programmed cell death. *EMBO Journal*, *11*(11), 3887–3895. https://doi.org/10.1002/j.1460-2075.1992.tb05481.x
- Jacobson, K. A., & Gao, Z. G. (2006). Adenosine receptors as therapeutic targets. In *Nature Reviews Drug Discovery* (Vol. 5, Issue 3, pp. 247–264). Nature Publishing Group. https://doi.org/10.1038/nrd1983
- Jiang, T., Xu, X., Qiao, M., Li, X., Zhao, C., Zhou, F., Gao, G., Wu, F., Chen, X., Su, C., Ren, S., Zhai, C., & Zhou, C. (2018). Comprehensive evaluation of NT5E/CD73 expression and its prognostic significance in distinct types of cancers. *BMC Cancer*, 18(1), 267. https://doi.org/10.1186/s12885-018-4073-7
- Jiang, W., He, Y., Shi, Y., Guo, Z., Yang, S., Wei, K., Pan, C., Xia, Y., & Chen, Y. (2019). MicroRNA-1204 promotes cell proliferation by regulating PITX1 in non-small-cell lung cancer. *Cell Biology International*, 43(3), 253–264. https://doi.org/10.1002/cbin.11083
- Kalekar, L. A., Schmiel, S. E., Nandiwada, S. L., Lam, W. Y., Barsness, L. O., Zhang, N., Stritesky, G. L.,
  Malhotra, D., Pauken, K. E., Linehan, J. L., O'Sullivan, M. G., Fife, B. T., Hogquist, K. A., Jenkins,
  M. K., & Mueller, D. L. (2016). CD4+ T cell anergy prevents autoimmunity and generates regulatory
  T cell precursors. *Nature Immunology*, 17(3), 304–314. https://doi.org/10.1038/ni.3331
- Ke, H., Wu, S., Zhang, Y., & Zhang, G. (2022). miR-139-3p/Kinesin family member 18B axis suppresses malignant progression of gastric cancer. *Bioengineered*, 13(2), 4528–4536. https://doi.org/10.1080/21655979.2022.2033466
- Kordaß, T. (2021). Controlling the immune suppressors: miRNAs regulating NT5E, ENTPD1 and CD274 Under Supervision of.
- Kordaß, T., Osen, W., & Eichmüller, S. B. (2018). Controlling the immune suppressor: Transcription factors and MicroRNAs regulating CD73/NT5E. In *Frontiers in Immunology* (Vol. 9, Issue APR, p. 813). Frontiers Media S.A. https://doi.org/10.3389/fimmu.2018.00813
- Kozomara, A., Birgaoanu, M., & Griffiths-Jones, S. (2019). MiRBase: From microRNA sequences to function. *Nucleic Acids Research*, 47(D1), D155–D162. https://doi.org/10.1093/nar/gky1141
- Kuol, N., Stojanovska, L., Nurgali, K., & Apostolopoulos, V. (2018). PD-1/PD-L1 in disease. In Immunotherapy (Vol. 10, Issue 2, pp. 149–161). Future Medicine Ltd. https://doi.org/10.2217/imt-2017-0120
- Latchman, Y., Wood, C. R., Chernova, T., Chaudhary, D., Borde, M., Chernova, I., Iwai, Y., Long, A. J.,
  Brown, J. A., Nunes, R., Greenfield, E. A., Bourque, K., Boussiotis, V. A., Carter, L. L., Carreno, B.
  M., Malenkovich, N., Nishimura, H., Okazaki, T., Honjo, T., ... Freeman, G. J. (2001). PD-L2 is a second ligand for PD-1 and inhibits T cell activation. *Nature Immunology*, 2(3), 261–268. https://doi.org/10.1038/85330

**57** 

- Lee, C. W., Kang, M. R., Yun, J., Oh, S. J., & Kang, J. S. (2014). Abstract 4387: Up-regulation of VHL by miR-1273C inhibits renal cell carcinoma. *Cancer Research*, 74(19\_Supplement), 4387–4387. https://doi.org/10.1158/1538-7445.am2014-4387
- Lee, R. C., Feinbaum, R. L., & Ambrost, V. (1993). The C. elegans Heterochronic Gene lin-4 Encodes Small RNAs with Antisense Complementarity to &II-14. In *Cell* (Vol. 75).
- Liu, F., Gu, L. N., Shan, B. E., Geng, C. Z., & Sang, M. X. (2016). Biomarkers for EMT and MET in breast cancer: An update (review). In *Oncology Letters* (Vol. 12, Issue 6, pp. 4869–4876). Spandidos Publications. https://doi.org/10.3892/ol.2016.5369
- Liu, J. H., Li, C. Y., Jiang, Y., Wan, Y. C., Zhou, S. L., & Cheng, W. J. (2018). Tumor-Suppressor role of miR-139-5p in endometrial cancer. *Cancer Cell International*, 18(1). https://doi.org/10.1186/s12935-018-0545-8
- Ma, Y., Gong, Z., Wang, H., Liang, Y., Huang, X., & Yu, G. (2020). Anti-cancer effect of miR-139-3p on laryngeal squamous cell carcinoma by targeting rab5a: In vitro and in vivo studies. *Pathology Research and Practice*, *216*(11). https://doi.org/10.1016/j.prp.2020.153194
- Masliah-Planchon, J., Garinet, S., & Pasmant, E. (2016). RAS-MAPK pathway epigenetic activation in cancer: MiRNAs in action. *Oncotarget*, 7(25), 38892–38907. https://doi.org/10.18632/oncotarget.6476
- Maugeri, M., Nawaz, M., Papadimitriou, A., Angerfors, A., Camponeschi, A., Na, M., Hölttä, M., Skantze, P., Johansson, S., Sundqvist, M., Lindquist, J., Kjellman, T., Mårtensson, I. L., Jin, T., Sunnerhagen, P., Östman, S., Lindfors, L., & Valadi, H. (2019). Linkage between endosomal escape of LNP-mRNA and loading into EVs for transport to other cells. *Nature Communications*, *10*(1), 1–15. https://doi.org/10.1038/s41467-019-12275-6
- Mayya, V. K., & Duchaine, T. F. (2019). Ciphers and executioners: How 3'-Untranslated Regions Determine the Fate of Messenger RNAs. In *Frontiers in Genetics* (Vol. 10, p. 6). Frontiers Media S.A. https://doi.org/10.3389/fgene.2019.00006
- Medina, P. P., Nolde, M., & Slack, F. J. (2010). OncomiR addiction in an in vivo model of microRNA-21-induced pre-B-cell lymphoma. *Nature*, *467*(7311), 86–90. https://doi.org/10.1038/nature09284
- Microsoft Cooperation. (2022). *Microsoft Excel Spreadsheet Software*. https://www.microsoft.com/en-us/microsoft-365/excel
- Mohamadzade, Z., Mahjoubi, F., & Soltani, B. M. (2021). Introduction of hsa-miR-512-3p as a new regulator of HER2 signaling pathway in breast cancer. *Breast Cancer Research and Treatment*, 185(1), 95–106. https://doi.org/10.1007/s10549-020-05937-3
- Molina, J. R., & Adjei, A. A. (2006). The Ras/Raf/MAPK Pathway. *Journal of Thoracic Oncology*, *1*(1), 7–9. https://doi.org/10.1016/s1556-0864(15)31506-9

- Momin, M. Y., Gaddam, R. R., Kravitz, M., Gupta, A., & Vikram, A. (2021). The challenges and opportunities in the development of microrna therapeutics: A multidisciplinary viewpoint. In *Cells* (Vol. 10, Issue 11). MDPI. https://doi.org/10.3390/cells10113097
- Montero-Conde, C., Graña-Castro, O., Martín-Serrano, G., Martínez-Montes, Á. M., Zarzuela, E., Muñoz, J., Torres-Perez, R., Pita, G., Cordero-Barreal, A., Leandro-García, L. J., Letón, R., López de Silanes, I., Guadalix, S., Pérez-Barrios, A., Hawkins, F., Guerrero-Álvarez, A., Álvarez-Escolá, C., Regojo-Zapata, R. M., Calsina, B., ... Robledo, M. (2020). Hsa-miR-139-5p is a prognostic thyroid cancer marker involved in HNRNPF-mediated alternative splicing. *International Journal of Cancer*, 146(2), 521–530. https://doi.org/10.1002/ijc.32622
- Monteys, A. M., Spengler, R. M., Wan, J., Tecedor, L., Lennox, K. A., Xing, Y., & Davidson, B. L. (2010). Structure and activity of putative intronic miRNA promoters. *RNA*, *16*(3), 495–505. https://doi.org/10.1261/rna.1731910
- Mosenden, R., & Taskén, K. (2011). Cyclic AMP-mediated immune regulation Overview of mechanisms of action in T cells. In *Cellular Signalling* (Vol. 23, Issue 6, pp. 1009–1016). Cell Signal. https://doi.org/10.1016/j.cellsig.2010.11.018
- Mosmann, T. (1983). Rapid colorimetric assay for cellular growth and survival: Application to proliferation and cytotoxicity assays. *Journal of Immunological Methods*, 65(1–2), 55–63. https://doi.org/10.1016/0022-1759(83)90303-4
- Mu, C. Y., Huang, J. A., Chen, Y., Chen, C., & Zhang, X. G. (2011). High expression of PD-L1 in lung cancer may contribute to poor prognosis and tumor cells immune escape through suppressing tumor infiltrating dendritic cells maturation. *Medical Oncology*, 28(3), 682–688. https://doi.org/10.1007/s12032-010-9515-2
- Neiburga, K. D., Vilne, B., Bauer, S., Bongiovanni, D., Ziegler, T., Lachmann, M., Wengert, S., Hawe, J. S., Güldener, U., Westerlund, A. M., Li, L., Pang, S., Yang, C., Saar, K., Huebner, N., Maegdefessel, L., Lange, R., Krane, M., Schunkert, H., & von Scheidt, M. (2021). Vascular tissue specific mirna profiles reveal novel correlations with risk factors in coronary artery disease. *Biomolecules*, *11*(11), 1683. https://doi.org/10.3390/biom11111683
- Noorolyai, S., Baghbani, E., Shanehbandi, D., Shahgoli, V. K., Kojabad, A. B., Mansoori, B., Hajiasgharzadeh, K., Mokhtarzadeh, A., & Baradaran, B. (2021). miR-146a-5pandmiR-193a-5p synergistically inhibited the proliferation of human colorectal cancer cells (HT-29 cell line) through ERK signaling pathway. *Advanced Pharmaceutical Bulletin*, 11(4), 755–764. https://doi.org/10.34172/APB.2021.085
- O'Brien, J., Hayder, H., Zayed, Y., & Peng, C. (2018). Overview of microRNA biogenesis, mechanisms of actions, and circulation. *Frontiers in Endocrinology*, 9(AUG). https://doi.org/10.3389/fendo.2018.00402

- Ohta, A. (2016). A metabolic immune checkpoint: Adenosine in Tumor Microenvironment. In *Frontiers in Immunology* (Vol. 7, Issue MAR, p. 109). Frontiers Media S.A. https://doi.org/10.3389/fimmu.2016.00109
- Okadome, K., Baba, Y., Nomoto, D., Yagi, T., Kalikawe, R., Harada, K., Hiyoshi, Y., Nagai, Y., Ishimoto, T., Iwatsuki, M., Iwagami, S., Miyamoto, Y., Yoshida, N., Watanabe, M., Komohara, Y., Shono, T., Sasaki, Y., & Baba, H. (2020). Prognostic and clinical impact of PD-L2 and PD-L1 expression in a cohort of 437 oesophageal cancers. *British Journal of Cancer*, 122(10), 1535–1543. https://doi.org/10.1038/s41416-020-0811-0
- Orellana, E. (2015). MicroRNAs in Cancer: A Historical Perspective on the Path from Discovery to Therapy. *Cancers*, 7(3), 1388–1405. https://doi.org/10.3390/cancers7030842
- Ors-Kumoglu, G., Gulce-Iz, S., & Biray-Avci, C. (2019). Therapeutic microRNAs in human cancer. In *Cytotechnology* (Vol. 71, Issue 1, pp. 411–425). Springer Netherlands. https://doi.org/10.1007/s10616-018-0291-8
- Ou, Y., Dai, X., Chen, X., Chen, Y., Wu, S., Zhou, Q., Yang, C., & Jiang, H. (2022). Circ-AFAP1 promote clear cell renal cell carcinoma growth and angiogenesis by the Circ-AFAP1/miR-374b-3p/VEGFA signaling axis. *Cell Death Discovery*, 8(1). https://doi.org/10.1038/s41420-022-00865-1
- Paranjape, T., Slack, F. J., & Weidhaas, J. B. (2009). MicroRNAs: Tools for cancer diagnostics. In *Gut* (Vol. 58, Issue 11, pp. 1546–1554). NIH Public Access. https://doi.org/10.1136/gut.2009.179531
- Paunovska, K., Loughrey, D., & Dahlman, J. E. (2022). Drug delivery systems for RNA therapeutics. In *Nature Reviews Genetics* (Vol. 23, Issue 5, pp. 265–280). Nature Research. https://doi.org/10.1038/s41576-021-00439-4
- Peng, Y., & Croce, C. M. (2016). The role of microRNAs in human cancer. In *Signal Transduction and Targeted Therapy* (Vol. 1, Issue 1, pp. 1–9). Springer Nature. https://doi.org/10.1038/sigtrans.2015.4
- Petitprez, F., Fossati, N., Vano, Y., Freschi, M., Becht, E., Lucianò, R., Calderaro, J., Guédet, T., Lacroix, L., Rancoita, P. M. V., Montorsi, F., Fridman, W. H., Sautès-Fridman, C., Briganti, A., Doglioni, C., & Bellone, M. (2019). PD-L1 Expression and CD8 + T-cell Infiltrate are Associated with Clinical Progression in Patients with Node-positive Prostate Cancer. *European Urology Focus*, *5*(2), 192–196. https://doi.org/10.1016/j.euf.2017.05.013
- Plotnikova, O., Baranova, A., & Skoblov, M. (2019). Comprehensive Analysis of Human microRNA–mRNA Interactome. *Frontiers in Genetics*, *10*, 933. https://doi.org/10.3389/fgene.2019.00933
- Polumuri, S., Perkins, D. J., & Vogel, S. N. (2021). cAMP levels regulate macrophage alternative activation marker expression. *Innate Immunity*, *27*(2), 133–142. https://doi.org/10.1177/1753425920975082

- Pong, S. K., & Gullerova, M. (2018). Noncanonical functions of microRNA pathway enzymes Drosha, DGCR8, Dicer and Ago proteins. *FEBS Letters*, *592*(17), 2973–2986. https://doi.org/10.1002/1873-3468.13196
- Qin, T., Zeng, Y. D., Qin, G., Xu, F., Lu, J. Bin, Fang, W. F., Xue, C., Zhan, J. H., Zhang, X. K., Zheng, Q. F., Peng, R. J., Yuan, Z. Y., Zhang, L., & Wang, S. Sen. (2015). High PD-L1 expression was associated with poor prognosis in 870 Chinese patients with breast cancer. *Oncotarget*, *6*(32), 33972–33981. https://doi.org/10.18632/oncotarget.5583
- Rascio, F., Spadaccino, F., Rocchetti, M. T., Castellano, G., Stallone, G., Netti, G. S., & Ranieri, E. (2021). The pathogenic role of PI3K/AKT pathway in cancer onset and drug resistance: an updated review. In *Cancers* (Vol. 13, Issue 16). MDPI. https://doi.org/10.3390/cancers13163949
- Roehm, N. W., Rodgers, G. H., Hatfield, S. M., & Glasebrook, A. L. (1991). An improved colorimetric assay for cell proliferation and viability utilizing the tetrazolium salt XTT. *Journal of Immunological Methods*, *142*(2), 257–265. https://doi.org/10.1016/0022-1759(91)90114-U
- Roth, B. M., Ishimaru, D., & Hennig, M. (2013). The core microprocessor component DiGeorge syndrome critical region 8 (DGCR8) is a nonspecific RNA-binding protein. *Journal of Biological Chemistry*, 288(37), 26785–26799. https://doi.org/10.1074/jbc.M112.446880
- Rupaimoole, R., & Slack, F. J. (2017). MicroRNA therapeutics: Towards a new era for the management of cancer and other diseases. In *Nature Reviews Drug Discovery* (Vol. 16, Issue 3, pp. 203–221). Nature Publishing Group. https://doi.org/10.1038/nrd.2016.246
- Schröter, P., Hartmann, L., Osen, W., Baumann, D., Offringa, R., Eisel, D., Debus, J., Eichmüller, S. B., & Rieken, S. (2020). Radiation-induced alterations in immunogenicity of a murine pancreatic ductal adenocarcinoma cell line. *Scientific Reports*, *10*(1). https://doi.org/10.1038/s41598-020-57456-2
- Seidel, J. A., Otsuka, A., & Kabashima, K. (2018). Anti-PD-1 and anti-CTLA-4 therapies in cancer: Mechanisms of action, efficacy, and limitations. In *Frontiers in Oncology* (Vol. 8, Issue MAR, p. 86). Frontiers Media S.A. https://doi.org/10.3389/fonc.2018.00086
- Seo, H. A., Moeng, S., Sim, S., Kuh, H. J., Choi, S. Y., & Park, J. K. (2019). MicroRNA-Based Combinatorial Cancer Therapy: Effects of MicroRNAs on the Efficacy of Anti-Cancer Therapies. *Cells*, *9*(1), 29. https://doi.org/10.3390/cells9010029
- Shah, V., & Shah, J. (2020). Recent trends in targeting miRNAs for cancer therapy. *Journal of Pharmacy* and *Pharmacology*, 72(12), 1732–1749. https://doi.org/10.1111/jphp.13351
- Sharpe, A. H., Wherry, E. J., Ahmed, R., & Freeman, G. J. (2007). The function of programmed cell death 1 and its ligands in regulating autoimmunity and infection. In *Nature Immunology* (Vol. 8, Issue 3, pp. 239–245). Nature Publishing Group. https://doi.org/10.1038/ni1443

- Sheppard, K. A., Fitz, L. J., Lee, J. M., Benander, C., George, J. A., Wooters, J., Qiu, Y., Jussif, J. M., Carter, L. L., Wood, C. R., & Chaudhary, D. (2004). PD-1 inhibits T-cell receptor induced phosphorylation of the ZAP70/CD3ζ signalosome and downstream signaling to PKCθ. *FEBS Letters*, 574(1–3), 37–41. https://doi.org/10.1016/j.febslet.2004.07.083
- Si, C., Yu, Q., & Yao, Y. (2018). Effect of miR-146a-5p on proliferation and metastasis of triple-negative breast cancer via regulation of SOX5. *Experimental and Therapeutic Medicine*, *15*(5), 4515–4521. https://doi.org/10.3892/etm.2018.5945
- Stagg, J., Divisekera, U., Duret, H., Sparwasser, T., Teng, M. W. L., Darcy, P. K., & Smyth, M. J. (2011). CD73-deficient mice have increased antitumor immunity and are resistant to experimental metastasis. *Cancer Research*, 71(8), 2892–2900. https://doi.org/10.1158/0008-5472.CAN-10-4246
- Stagg, J., & Smyth, M. J. (2010). Extracellular adenosine triphosphate and adenosine in cancer. In *Oncogene* (Vol. 29, Issue 39, pp. 5346–5358). Nature Publishing Group. https://doi.org/10.1038/onc.2010.292
- Stavast, C. J., van Zuijen, I., Karkoulia, E., Özçelik, A., van Hoven-Beijen, A., Leon, L. G., Voerman, J. S. A., Janssen, G. M. C., van Veelen, P. A., Burocziova, M., Brouwer, R. W. W., van IJcken, W. F. J., Maas, A., Bindels, E. M., van der Velden, V. H. J., Schliehe, C., Katsikis, P. D., Alberich-Jorda, M., & Erkeland, S. J. (2022). The tumor suppressor MIR139 is silenced by POLR2M to promote AML oncogenesis. *Leukemia*, *36*(3), 687–700. https://doi.org/10.1038/s41375-021-01461-5
- Stockert, J. C., Horobin, R. W., Colombo, L. L., & Blázquez-Castro, A. (2018). Tetrazolium salts and formazan products in Cell Biology: Viability assessment, fluorescence imaging, and labeling perspectives. *Acta Histochemica*, 120(3), 159–167. https://doi.org/10.1016/j.acthis.2018.02.005
- Sträter, N. (2006). Ecto-5'-nucleotidase: Structure function relationships. *Purinergic Signalling*, *2*(2), 343–350. https://doi.org/10.1007/s11302-006-9000-8
- Sun, C., Mezzadra, R., & Schumacher, T. N. (2018). Regulation and Function of the PD-L1 Checkpoint.

  In *Immunity* (Vol. 48, Issue 3, pp. 434–452). Cell Press. https://doi.org/10.1016/j.immuni.2018.03.014
- Svoronos, A. A., Engelman, D. M., & Slack, F. J. (2016). OncomiR or tumor suppressor? The duplicity of MicroRNAs in cancer. In *Cancer Research* (Vol. 76, Issue 13, pp. 3666–3670). American Association for Cancer Research Inc. https://doi.org/10.1158/0008-5472.CAN-16-0359
- Thermo Fisher Scientific. (2022). *Qubit 4 Fluorometer*. https://www.thermofisher.com/de/de/home/industrial/spectroscopy-elemental-isotopeanalysis/molecular-spectroscopy/fluorometers/qubit/models/qubit-4.html
- Vejnar, C. E., & Blum, M. (2013). *miRmap web: comprehensive microRNA target prediction online*. Nucleic Acids Research. https://doi.org/10.1093/nar

- Wang, N., Liang, H., & Zen, K. (2014). Molecular mechanisms that influence the macrophage M1-M2 polarization balance. In *Frontiers in Immunology* (Vol. 5, Issue NOV). Frontiers Media S.A. https://doi.org/10.3389/fimmu.2014.00614
- Wang, Z., Zhao, K., Zhang, Y., Duan, X., & Zhao, Y. (2019). Anti-GPC3 Antibody Tagged Cationic Switchable Lipid-Based Nanoparticles for the Co-Delivery of Anti-miRNA27a And Sorafenib in Liver Cancers. *Pharmaceutical Research*, *36*(10). https://doi.org/10.1007/s11095-019-2669-5
- Westholm, J. O., & Lai, E. C. (2011). Mirtrons: MicroRNA biogenesis via splicing. *Biochimie*, 93(11), 1897–1904. https://doi.org/10.1016/j.biochi.2011.06.017
- Wilczynska, A., & Bushell, M. (2015). The complexity of miRNA-mediated repression. In *Cell Death and Differentiation* (Vol. 22, Issue 1, pp. 22–33). Nature Publishing Group. https://doi.org/10.1038/cdd.2014.112
- Wu, Z., Chen, S., Zuo, T., Fu, J., Gong, J., Liu, D., & Wang, B. (2023). miR-139-3p/Wnt5A Axis Inhibits Metastasis in Hepatoblastoma. *Molecular Biotechnology*, 1–8. https://doi.org/10.1007/s12033-023-00714-1
- Xiang, W., Wu, X., Huang, C., Wang, M., Zhao, X., Luo, G., Li, Y., Jiang, G., Xiao, X., & Zeng, F. (2017). PTTG1 regulated by miR-146-3p promotes bladder cancer migration, invasion, metastasis and growth. *Oncotarget*, 8(1), 664–678. https://doi.org/10.18632/oncotarget.13507
- Xu, J., Gu, X., Yang, X., & Meng, Y. (2019). MiR-1204 promotes ovarian squamous cell carcinoma growth by increasing glucose uptake. *Bioscience, Biotechnology, and Biochemistry*, 83(1), 123–128. https://doi.org/10.1080/09168451.2018.1527208
- Xu, Y., Song, G., Xie, S., Jiang, W., Chen, X., Chu, M., Hu, X., & Wang, Z. wei. (2021). The roles of PD-1/PD-L1 in the prognosis and immunotherapy of prostate cancer. In *Molecular Therapy* (Vol. 29, Issue 6, pp. 1958–1969). Cell Press. https://doi.org/10.1016/j.ymthe.2021.04.029
- Xue, W. X., Zhang, M. Y., Rui Li, Liu, X., Yin, Y. H., & Qu, Y. Q. (2020). Serum miR-1228-3p and miR-181a-5p as Noninvasive Biomarkers for Non-Small Cell Lung Cancer Diagnosis and Prognosis. *BioMed Research International*, 2020. https://doi.org/10.1155/2020/9601876
- Yang, B., Zhang, W., Sun, D., Wei, X., Ding, Y., Ma, Y., & Wang, Z. (2019). Downregulation of miR-139-5p promotes prostate cancer progression through regulation of SOX5. *Biomedicine and Pharmacotherapy*, 109, 2128–2135. https://doi.org/10.1016/j.biopha.2018.09.029
- Yang, S., Maurin, T., Robine, N., Rasmussen, K. D., Jeffrey, K. L., Chandwani, R., Papapetrou, E. P., Sadelain, M., O'Carroll, D., & Lai, E. C. (2010). Conserved vertebrate mir-451 provides a platform for Dicer-independent, Ago2-mediated microRNA biogenesis. *Proceedings of the National Academy of Sciences of the United States of America*, 107(34), 15163–15168. https://doi.org/10.1073/pnas.1006432107

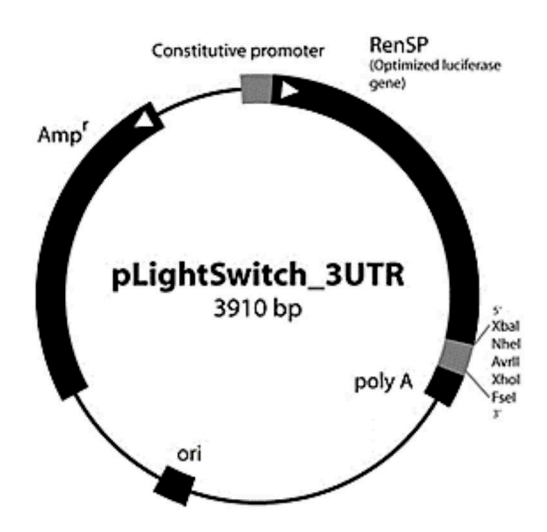
- Yee, D., Shah, K. M., Coles, M. C., Sharp, T. V., & Lagos, D. (2017). MicroRNA-155 induction via TNF-α and IFN-γ suppresses expression of programmed death ligand-1 (PD-L1) in human primary cells.

  \*\*Journal of Biological Chemistry, 292(50), 20683–20693. https://doi.org/10.1074/jbc.M117.809053
- Yi, G., Wang, D., Han, J., Jia, L., Liu, X., & He, J. (2022). circKLHL24 Blocks Breast Cancer Development by Regulating the miR-1204/ALX4 Network. *Cancer Biotherapy and Radiopharmaceuticals*, *37*(8), 684–696. https://doi.org/10.1089/cbr.2020.3992
- Yi, M., Xu, L., Jiao, Y., Luo, S., Li, A., & Wu, K. (2020). The role of cancer-derived microRNAs in cancer immune escape. In *Journal of Hematology and Oncology* (Vol. 13, Issue 1, pp. 1–14). BioMed Central Ltd. https://doi.org/10.1186/s13045-020-00848-8
- Young, A., Mittal, D., Stagg, J., & Smyth, M. J. (2014). Targeting cancer-derived adenosine: New therapeutic approaches. In *Cancer Discovery* (Vol. 4, Issue 8, pp. 879–888). American Association for Cancer Research Inc. https://doi.org/10.1158/2159-8290.CD-14-0341
- Yu, W., Hua, Y., Qiu, H., Hao, J., Zou, K., Li, Z., Hu, S., Guo, P., Chen, M., Sui, S., Xiong, Y., Li, F., Lu, J., Guo, W., Luo, G., & Deng, W. (2020). PD-L1 promotes tumor growth and progression by activating WIP and β-catenin signaling pathways and predicts poor prognosis in lung cancer. *Cell Death and Disease*, 11(7), 1–16. https://doi.org/10.1038/s41419-020-2701-z
- Yuan, W., & Song, C. (2020). The Emerging Role of Rab5 in Membrane Receptor Trafficking and Signaling Pathways. In *Biochemistry Research International* (Vol. 2020). Hindawi Limited. https://doi.org/10.1155/2020/4186308
- Zak, K. M., Kitel, R., Przetocka, S., Golik, P., Guzik, K., Musielak, B., Dömling, A., Dubin, G., & Holak, T.
  A. (2015). Structure of the Complex of Human Programmed Death 1, PD-1, and Its Ligand PD-L1.
  Structure, 23(12), 2341–2348. https://doi.org/10.1016/j.str.2015.09.010
- Zhang, H., Kolb, F. A., Jaskiewicz, L., Westhof, E., & Filipowicz, W. (2004). Single processing center models for human Dicer and bacterial RNase III. *Cell*, 118(1), 57–68. https://doi.org/10.1016/j.cell.2004.06.017
- Zhang, M., Sun, H., Zhao, S., Wang, Y., Pu, H., & Zhang, Q. (2017). Expression of PD-L1 and prognosis in breast cancer: A metaanalysis. *Oncotarget*, 8(19), 31347–31354. https://doi.org/10.18632/oncotarget.15532
- Zhang, W., Xu, J., Wang, K., Tang, X., & He, J. (2019). MIR-139-3p suppresses the invasion and migration properties of breast cancer cells by targeting RAB1A. *Oncology Reports*, 42(5), 1699–1708. https://doi.org/10.3892/or.2019.7297
- Zhang, X., Schwartz, J. C. D., Guo, X., Bhatia, S., Cao, E., Chen, L., Zhang, Z. Y., Edidin, M. A., Nathenson, S. G., & Almo, S. C. (2004). Structural and functional analysis of the costimulatory

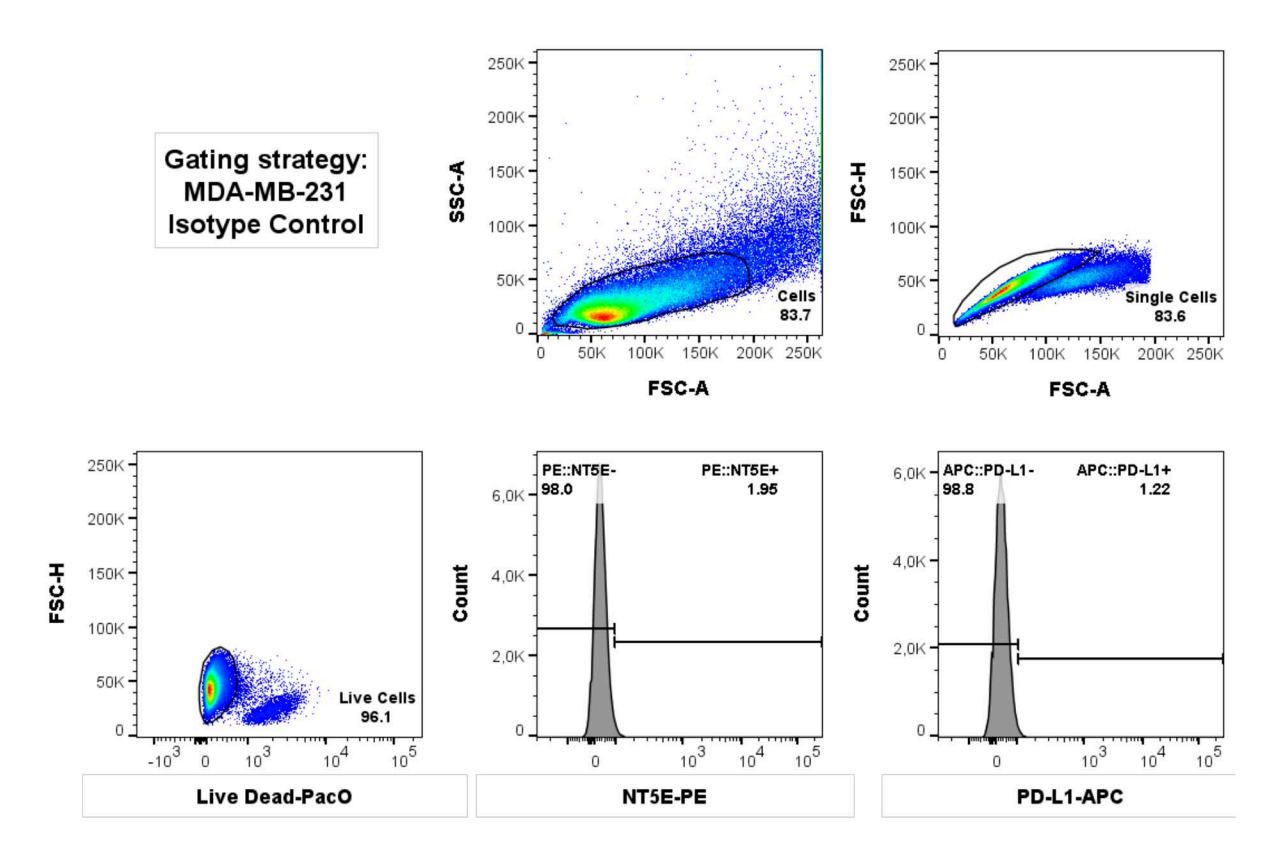
- receptor programmed death-1. *Immunity*, 20(3), 337–347. https://doi.org/10.1016/S1074-7613(04)00051-2
- Zhang, Y., Pan, Q., & Shao, Z. (2023). Extracellular vesicles derived from cancer-associated fibroblasts carry tumor-promotive microRNA-1228-3p to enhance the resistance of hepatocellular carcinoma cells to sorafenib. *Human Cell*, 36(1), 296–311. https://doi.org/10.1007/s13577-022-00800-7
- Zhang, Z., Zhou, X., Shen, H., & Wang, D. (2009). Phosphorylated ERK is a potential predictor of sensitivity to sorafenib when treating hepatocellular carcinoma: Evidence from an in vitro study. *BMC Medicine*, 7(1), 41. https://doi.org/10.1186/1741-7015-7-41
- Zheng, Y., Fang, Y. C., & Li, J. (2019). PD-L1 expression levels on tumor cells affect their immunosuppressive activity. *Oncology Letters*, 18(5), 5399–5407. https://doi.org/10.3892/ol.2019.10903
- Zhou, X., Ji, G., Chen, H., Jin, W., Yin, C., & Zhang, G. (2015). Clinical role of circulating miR-223 as a novel biomarker in early diagnosis of cancer patients. *International Journal of Clinical and Experimental Medicine*, 8(9), 16890–16898. www.ijcem.com/
- Zhu, X., Jiang, S., Wu, Z., Liu, T., Zhang, W., Wu, L., Xu, L., & Shao, M. (2021). Long non-coding RNA TTN antisense RNA 1 facilitates hepatocellular carcinoma progression via regulating miR-139-5p/SPOCK1 axis. *Bioengineered*, 12(1), 578–588. https://doi.org/10.1080/21655979.2021.1882133
- Zhu, Y., Zhou, C., & He, Q. (2019). High miR-139-3p expression predicts a better prognosis for hepatocellular carcinoma: a pooled analysis. *Journal of International Medical Research*, *47*(1), 383–390. https://doi.org/10.1177/0300060518802727

## 8. Appendix

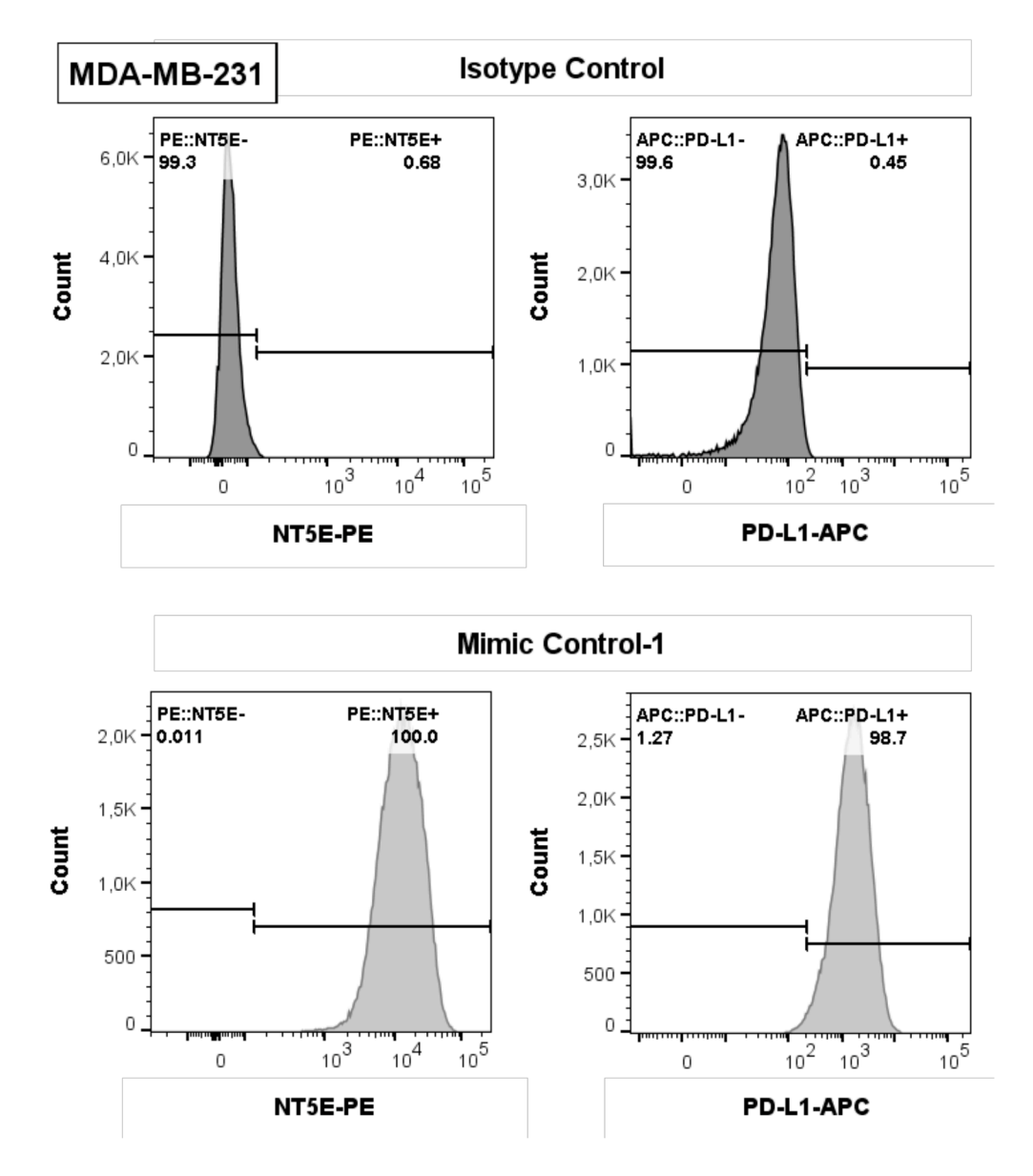
#### 8.1. Supplementary figures



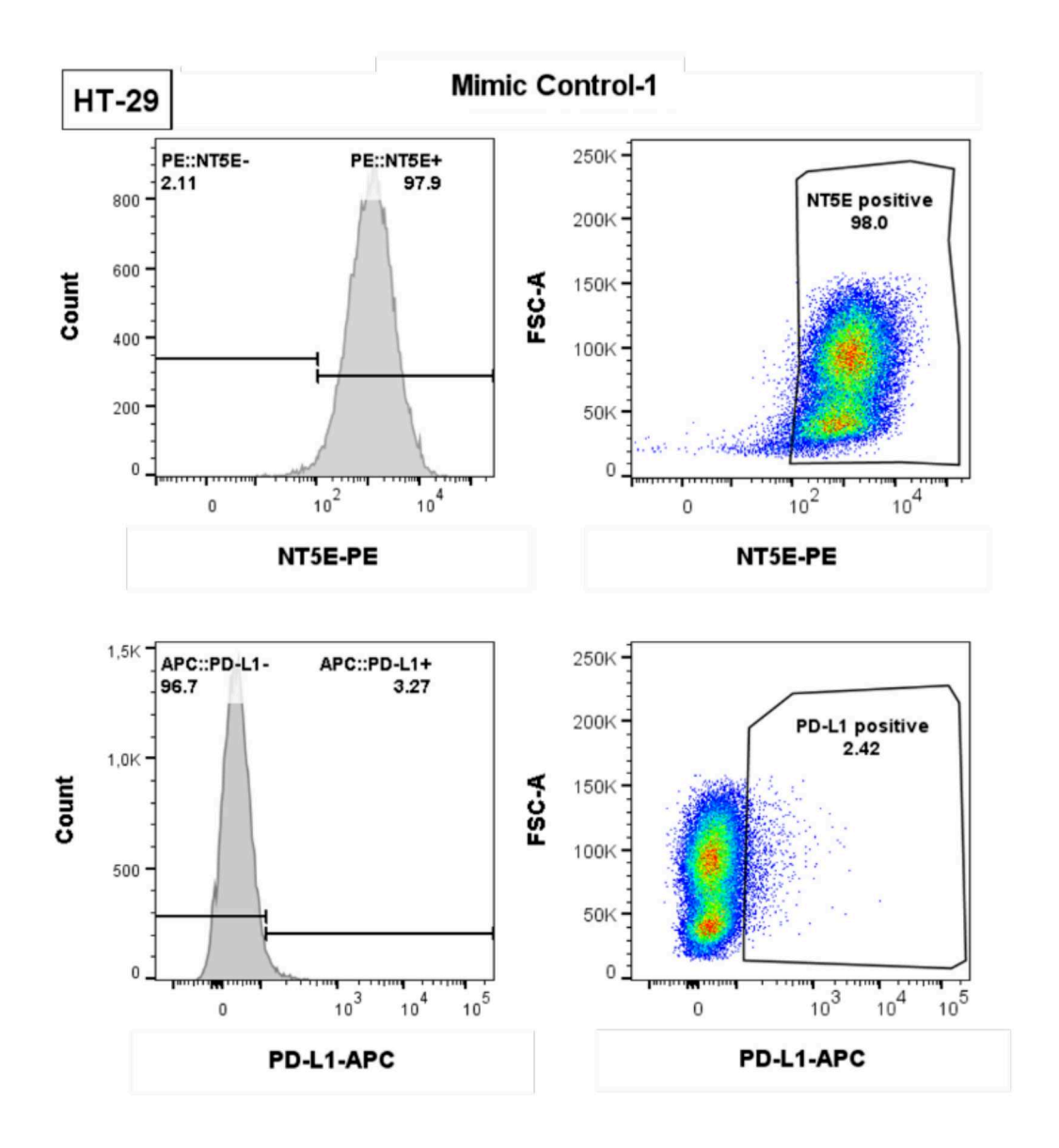
**Supplementary Figure 1: Vector map of pLS-PD-L1-3'-UTR plasmid.** The human PD-L1 3'-UTR sequence is fused to the gene encoding renilla firefly luciferase (Active Motif, 2023).



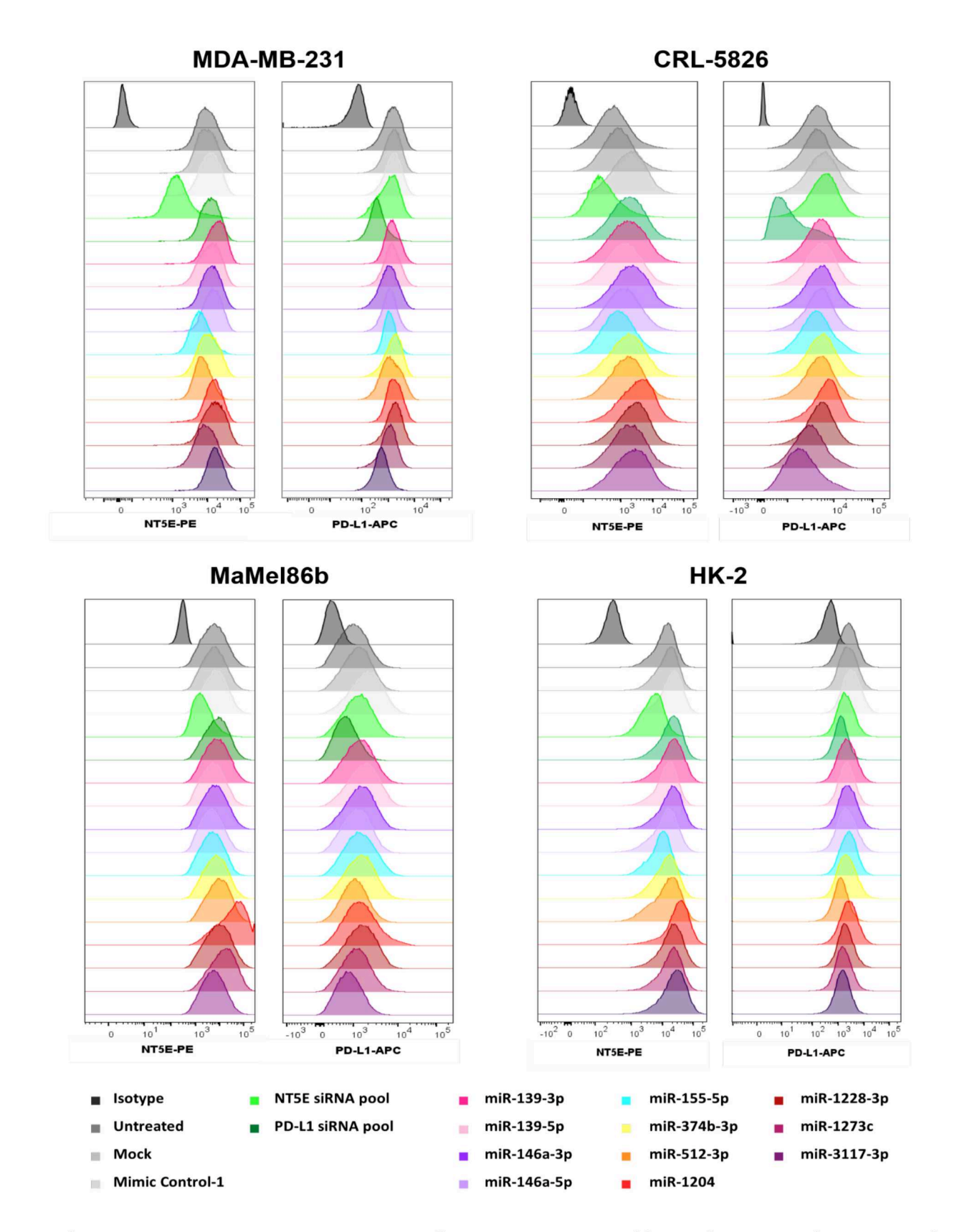
**Supplementary Figure 2: Representative gating strategy on isotype control.** Investigated human cell lines were selected for cells, single and live cells with gates for the targets PE::NT5E and APC::PD-L1.



Supplementary Figure 3: Representative results showing surface expression of NT5E and PD-L1 for Mimic Control-1. For all investigated human cell lines positive target signals were gated on the isotype control and further applied onto remaining samples.



Supplementary Figure 4: Surface expression of NT5E (top) and PD-L1 (bottom) on HT-29 cells. Display of Mimic Control-1 histogram and dot plot with respective gates for NT5E and PD-L1.



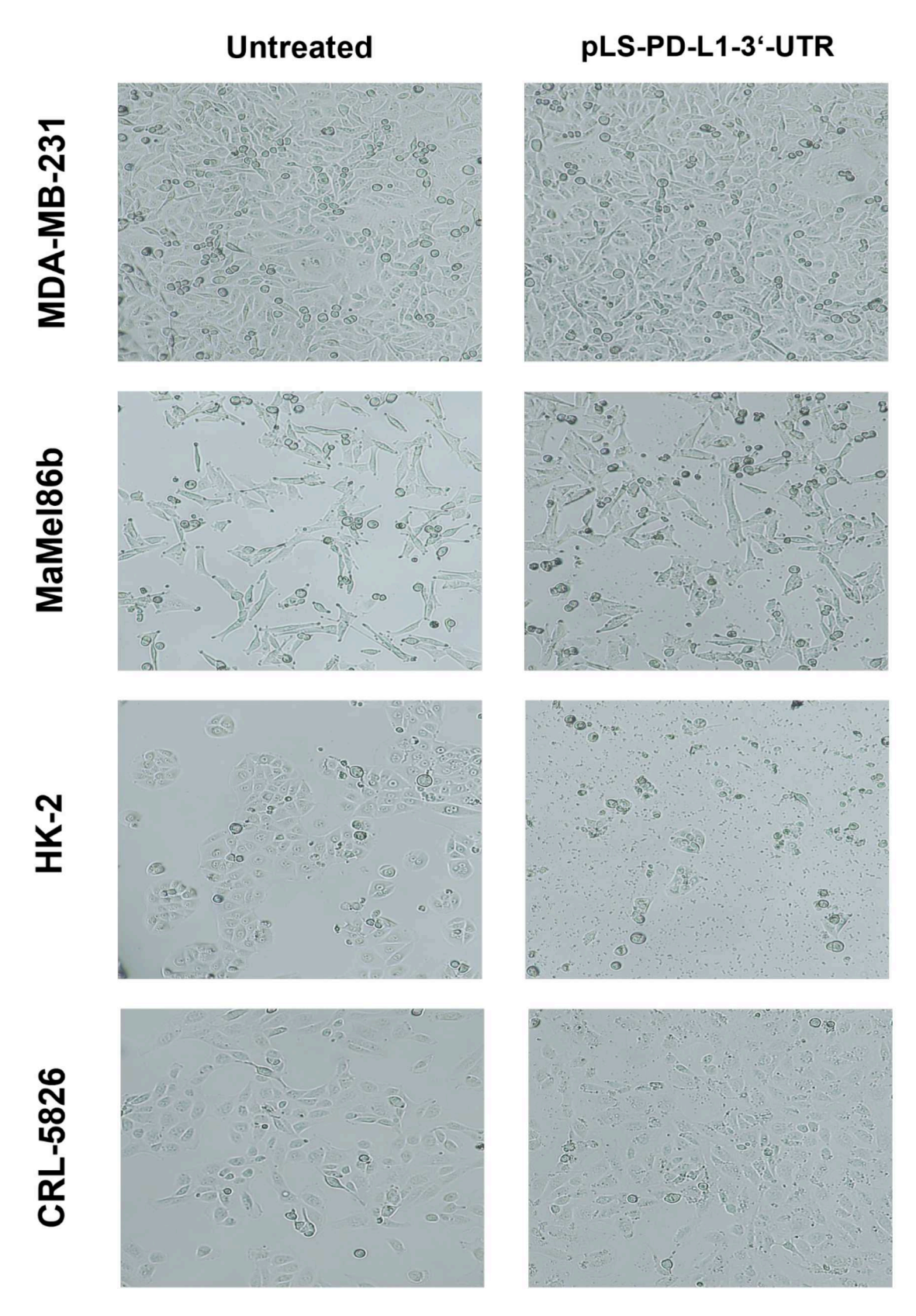
Supplementary Figure 5: Representative flow cytometric profiling of NT5E and PD-L1 surface expression on investigated human cells. Display of histograms of a single miRNA library transfection experiment for MDA-MB-231, CRL-5826, MaMel86b and HK-2 cells.

#### PD-L1 3'-UTR Sequence

5'-UCCAGCAUUGGAACUUCUGAUCUUCAAGCAGGGAUUCUCAACCUGUGGUUUAGGGGUUCAUCGGGGCUGAGCGUGAC AAGAGGAAGGAAUGGGCCCGUGGGAUGCAGGCAAUGUGGGACUUAAAAGGCCCA<mark>AGCACU</mark>GAAAAUGGAACCUGGCGAAA CUCAUCGACGCCUGUGACAGGGAGAAAGGAUACUUCUGAACAAGGAGCCUCCAAGCAAAUCAUCCAUUGCUCAUCCUAGG AAGACGGGUUGAGAAUCCCUAAUUUGAGGGUCAGUUCCUGCAGAAGUGCCCUUUGCCUCCACUCAAUGCCUCAAUUUGUU GGUCUUCUUGUCAUGUGAGUGUGGUUGUGAAUGAUUUCUUUUGAAGAUAUAUUGUAGUAGAUGUUACAAUU<mark>UUGUCGC</mark>CA AACUAAACUUGCUGCUUAAUGAUUUGCUCACAUCUAGUAAAACAUGGAGUAUUUGUAAGGUGCUUG**GUCUCC**UCUAUAAC GUUGACCUAAUCUUAUUCUCAGACCUCAAGUGUCUGUGCAGUAUCUGUUCCAUUUAAAUAUCAGCUUUACAAUUAUGUGG UAGCCUACACACAUAAUCUCAUUUCAUCGCUGUAACCACCCUGUUGUGAUAACCACUAUUAUUUUACCCAUCGUACAGCU ACAAUUUACAGCUAUAUUUUACUUUAAGCAAUUCUUUUAUUCAAAAAACCAUUUAUUAAGUGCCCUUGCAAUAUCAAUCGC UGUGCCAGGCAUUGAAUCUACAGAUGUGAGCAAGACAAAGUACCUGUCCUCAAGGAGCUCAUAGUAUAAUGAGGAGAUUA ACAAGAAAAUGUAUUAUUACAAUUUAGUCCAGUGUCAUAGCAUAAGGAUGAUGCGAGGGGAAAACCCGAGCAGUGUUGCC AAGAGGAGGAAAUAGGCCAAUGUGGUCUGGGACGGUUGGAUAUACUUAAACAUCUUAAUAA<mark>UCAGAG</mark>UAAUUUUCAUUUA CAAAGAGAGGUCGGUACUUAAAAUAACCCUGAAAAAUAACACUGGAAUUCCUUUUCU**AGCAUUA**UAUUUAUUCCUGAUUU GCCUUUGCCAUAUAAUCUAAUGCUUGUUUAUAUAGUGUCUGGUAUUGUUUAACAGUUCUGUCUUUUCUAUUUAAAUGCCA CUAAAUUUUAAAUUCAUACCUUUCCAUGAUUCAAAAUUCAAAAGAUCCCAUGGGAGAUGGUUGGAAAAUCUCCACUUCAU UUUGGAAAUGUAUGUUAAAAGCACGUAUUUUUAAAAUUUUUUUCCUAAAUAGUAACACAUUGUAUGUCUGCUGUGUACUU UCUUUGUUUCUAAGUUAUCUUUCCCAUAGCUUUUCAUUAUCUUUCAUAUGAUCCAGUAUAUGUUAAAUAU **GUCCUA**CAUA UACAUUUAGACAACCACCAUUUGUUAAGUAUUUGCUCUAGGACAGAGUUUGGAUUUGUUUAUGUUUGCUCAAAAGGAGAC CCAUGGGCUCUCCAGGGUGCACUGAGUCAAUCUA<mark>GUCCUA</mark>AAAAGCAAUCUUAUUAUUAACUCUGUAUGACAGAAUCAUG GGAAAUUCCGGCAGUGUACCUUGACUGCUAGCUACCCUGUGCCAGAAAAGCCUCAUUCGUUGUGCUUGAACCCUUGAAUG CCACCAGCUGUCAUCACUACACAGCCCUCCUAAGAGGCUUCCUGGAGGUUUCGAGAUUCAGAUGCCCUGGGAGAUCCCAG AGUUUCCUUUCCCUCUUGGCCAUAUUCUGGUGUCAAUGACAAGGAGUACCUUGGCUUUGCCA<u>CAUGUC</u>AAGGCUGAAGAA ACAGU<mark>GUCUCC</mark>AACAGAGCUCCUUGUGUUAUCUGUUUGUACAUGUGCAUUUGUACAGUAAUU<mark>GGUGUG</mark>ACAGUGUUCUUU GUGUGAAUUACAGGCAAGAAUUGUGGCUGAGCAAGGCACAUAGUCUACUCAGUCUAUUCCUAA<mark>GUCCUA</mark>ACUCCUCCUUG UGGUGUUGGAUUUGUAAGGCACUUUAUCCCUUUUGUCUCAUGUUUCAUCGUAAAUGGCAUAGGCAGAGAUGAUACCUAAU UCUGCAUUUGAUUGUCACUUUUUGUACCU<mark>GCAUUA</mark>AUUUAAUAAAAUAUUCUUAUUUAUUUGUUACUUGGUACACCAGC AUGUCCAUUUUCUUGUUUAUUUUGUGUUUAAUAAAAUGUUCAGUUUAACAUCCCAGUGGAGAAAGUUA-3'



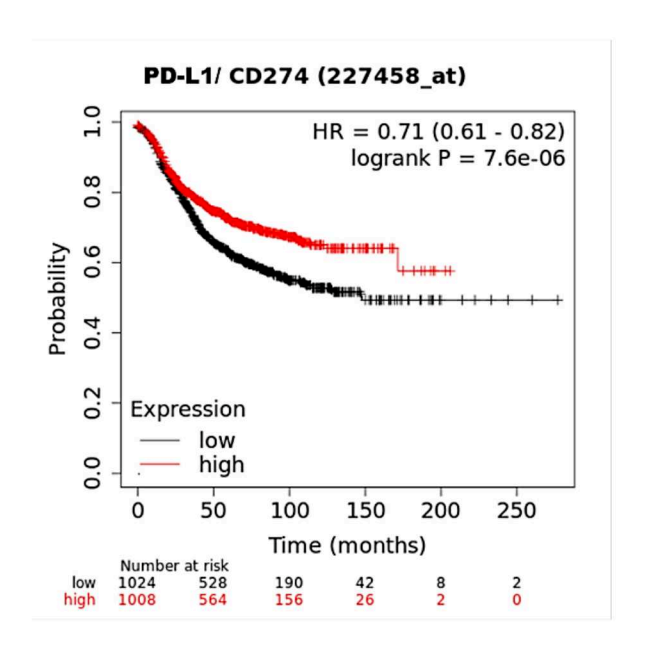
**Supplementary Figure 6: PD-L1 3'-UTR Sequence.** The shortened PD-L1 3'-UTR sequence fragment included in pLS-PD-L1-3'-UTR is highlighted in grey (Active Motif, 2023). The highlighted miRNA binding sites were predicted using miRmap web **(Vejnar & Blum, 2013)**.

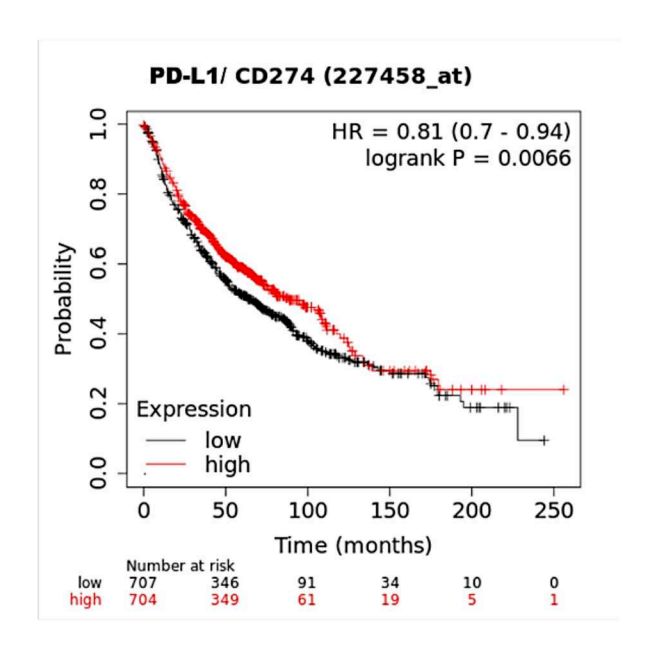


**Supplementary Figure 7: Brightfield microscopy of 3'-UTR PD-L1 reporter assay.** Qualitative imaging of cell growth in untreated and pLS-PD-L1-3'-UTR transfected MDA-MD-231, MaMel86b, HK-2 and CRL-5826 cells captured by a Leica DM1L Microscope using a 4x/ 0.1 NA non-immersion objective.

### Breast cancer

## Lung cancer





Expression range: 6 - 3390

Expression range: 6 - 6880

### Supplementary Figure 8: Kaplan-Meier curve based on PD-L1 expression in breast and lung cancer.

High PD-L1 expression is very significantly associated with better prognosis of breast and lung cancer patients. The Kaplan-Meier plots were generated with the Kaplan-Meier Plotter online tool (Győrffy, 2021; Győrffy et al., 2013).

# 8.2. Figures

8.2.1.	Lis	t of	fic	iures
--------	-----	------	-----	-------

Figure 1: Summary of miRNA effects on PD-L1 and NT5E mRNA and surface level expressio
Display of miRNAs significantly affecting both immunoregulatory target molecules in three huma
tumor entities. Flow cytometric and RT-qPCR data was acquired for the breast cancer cell line MD.
MB-231, the lung adenocarcinoma cell line CRL-5826 and the metastatic melanoma cell line
MaMel86b, as well as the normal proximal tubular kidney cell line HK-2.
Figure 2: Zusammenfassung der miRNA Effekte in der Brustkrebslinie MDA-MB-231. In grün od
rot markiert sind mRNAs, die die Expression eines Immun-Checkpoint-Moleküls verstärkten od
hemmen. miRNAs mit gemischten Effekten sind in orange dargestellt. Beobachtungen, die nur a
der FACS-Analyse basieren sind mit gestrichelten Linien dargestellt, während RT-qPCR validier
intrazelluläre Effekte mit durchgehenden Linien dargestellt sind
Figure 3: Biogenesis of miRNAs through canonical and non-canonical pathways. Mature miRNA
are incorporated into the miRNA-induced silencing complex (miRISC) targeting the 3'-UTR
mRNA transcripts, blocking translation or inducing mRNA degradation (adapted from O'Brien
al., 2018)
Figure 4: Structure and function of PD-1 and its ligand PD-L1. The ligation of PD-1 / PD-L1 induc
the phosphorylation of the immunoreceptor tyrosine-based switch motif (ITSM) and the
immunoreceptor tyrosine-based inhibitory motif (ITIM), recruiting SHP-2 protein tyrosin
phosphatases for the dephosphorylation of the co-stimulatory receptor CD28. Overall, the binding
of PD-1 to its ligand PD-L1 results in the inhibition of T cell signaling and survival (adapted fro
Farrukh et al., 2021).
Figure 5: Structure and function of NT5E. The membrane bound enzymes ectonucleoside triphospha
diphosphohydrolase 1 (ENTPD1) and ecto-5'-nucleotidase (NT5E) cooperatively cataboli
extracellular adenosine triphosphate (ATP) to free adenosine. In T cells, natural killer (NK) ar
dendritic cells (DCs) the produced adenosine is bound by the adenosine A2A receptor and induc
anti-inflammatory effects. In cancer cells A2B receptors are stimulated, resulting in increased tum
cell proliferation and survival (Kordaß et al., 2018).
Figure 6: XTT assay. The mitochondrial reduction of yellow XTT forms orange XTT formazan salt2
Figure 7: NT5E surface expression among human cell lines of different non-/tumor entities. Resul
show mean fluorescence intensities of Mimic Control-1 normalized to the isotype control of NT5
Figure 8: PD-L1 surface expression among human cell lines of different non-/tumor entities
Display of mean fluorescence intensities of Mimic Control-1 normalized to the isotype control
PD-L12

Figure 9: Log2 fold change of target MFIs for miRNA library transfection in MDA-MB-231. Result	ts
show the relative NT5E (A) and PD-L1 (B) surface levels 72 h post transfection. The graph displa	ys
mean values and SEM of $>$ 3 independent experiments in MDA-MB-231 cells. Fold changes we	re
calculated compared to Mimic Control-1. Significances were assessed by One-sample T-Te	st
$(* = P \le 0.05; ** P \le 0.01; *** = P \le 0.001; **** = P \le 0.0001)$	26
Figure 10: Log2 fold change of target MFIs after miRNA library transfection of CRL-5826 cell	s.
Results show the relative NT5E (A) and PD-L1 (B) surface levels 72 h post transfection. The grap	h
displays mean values and SEM of $>$ 3 independent experiments in CRL-5826 cells. Fold chang	es
were calculated compared to Mimic Control-1. Significances were assessed by One-sample T-Te	st
$(* = P \le 0.05; ** P \le 0.01; *** = P \le 0.001; **** = P \le 0.0001)$	27
Figure 11: Log2 fold change of target MFIs for miRNA library transfection in MaMel86b. Result	ts
show the relative NT5E (A) and PD-L1 (B) surface levels 72 h post transfection. The graph displa	ys
mean values and SEM of 4 independent experiments in MaMel86b cells. Fold changes we	re
calculated compared to Mimic Control-1. Significances were assessed by One-sample T-Te	st
$(* = P \le 0.05; ** P \le 0.01; *** = P \le 0.001).$	28
Figure 12: Log2 fold change of target MFIs for miRNA library transfection in HK-2. Results sho	w
the relative NT5E (A) and PD-L1 (B) surface levels 72 h post transfection. The graph displays mea	ın
values and SEM of 4 independent experiments in HK-2 cells. Fold changes were calculated compare	ed
to Mimic Control-1. Significances were assessed by One-sample T-Test (* = $P \le 0.05$ ; ** $P \le 0.0$	1;
*** = $P \le 0.001$ ).	30
Figure 13: RT-qPCR examination of PD-L1 and NT5E mRNA levels for miRNA library transfectio	n.
The graph displays mean values and SEM of 3 independent experiments in MDA-MB-231, CRl-582	6,
MaMel86b and HK-2 cells. Samples were normalized on the housekeeping gene RPL19 and fo	ld
changes were calculated using Mimic Control-1. Significances were assessed by a One-sample T-Te	st
$(* = P \le 0.05; ** P \le 0.01).$	32
Figure 14: Effect of miRNAs on viability of transfected MDA-MB-231 cells 24-72 h post transfectio	n.
The box-and-whiskers plots display minimum, maximum and median values of two independe	nt
experiments (N1 and N2) with at least 4 technical replicates. All samples were compared to Mim	ic
Control-1. Significance was assessed by one-way ANOVA using Dunnett's multiple comparison to	st
$(* = P \le 0.05; ** P \le 0.01; *** = P \le 0.001; **** = P \le 0.0001).$	35
Figure 15: Effect of miRNAs on viability of transfected MaMel86b cells 24-72 h post transfectio	n.
The box-and-whiskers plots display minimum, maximum and median values of two independe	nt
experiments with at least 4 technical replicates. Most samples were compared to Mimic Control-	1.
Significance was assessed by one-way ANOVA using Dunnett's multiple comparison to	st
$(* = P \le 0.05; ** P \le 0.01; *** = P \le 0.001; **** = P \le 0.0001).$	36

Figure 16: PD-L1 3'-UTR reporter assay. The graph displays mean values and SEM of at least 4
technical replicates in MDA-MB-231, MaMel86b, HK-2 and CRL-5826 cells. All samples were
compared to Mimic Control-1. Significance was assessed by one-way ANOVA using Dunnett's
multiple comparison test (* = $P \le 0.05$ ; ** $P \le 0.01$ ; *** = $P \le 0.001$ ; **** = $P \le 0.0001$ )38
Figure 17: Venn diagram of miRNAs affecting mRNA and surface expression of PD-L1 and NT5E.
Overlap of miRNAs significantly up- or downregulating immunomodulatory target molecules in
MDA-MB-231, CRL-5826, MaMel86b and HK-2 cells40
8.2.2. List of supplementary figures
<b>Supplementary Figure 1: Vector map of pLS-PD-L1-3'-UTR plasmid.</b> The human PD-L1 3'-UTR sequence is fused to the gene encoding renilla firefly luciferase (Active Motif, 2023)
Supplementary Figure 2: Representative gating strategy on isotype control. Investigated human cell
lines were selected for cells, single and live cells with gates for the targets PE::NT5E and APC::PD-L1.
Sumlamentary Figure 2. Democratative regular chaving confess expression of NTEE and DD 11
Supplementary Figure 3: Representative results showing surface expression of NT5E and PD-L1
<b>for Mimic Control-1.</b> For all investigated human cell lines positive target signals were gated on the
isotype control and further applied onto remaining samples
Supplementary Figure 4: Surface expression of NT5E (top) and PD-L1 (bottom) on HT-29 cells.
Display of Mimic Control-1 histogram and dot plot with respective gates for NT5E and PD-L168
Supplementary Figure 5: Representative flow cytometric profiling of NT5E and PD-L1 surface
expression on investigated human cells. Display of histograms of a single miRNA library
transfection experiment for MDA-MB-231, CRL-5826, MaMel86b and HK-2 cells
Supplementary Figure 6: PD-L1 3'-UTR Sequence. The shortened PD-L1 3'-UTR sequence fragment
included in pLS-PD-L1-3'-UTR is highlighted in grey (Active Motif, 2023). The highlighted
miRNA binding sites were predicted using miRmap web (Vejnar & Blum, 2013)70
Supplementary Figure 7: Brightfield microscopy of 3'-UTR PD-L1 reporter assay. Qualitative
imaging of cell growth in untreated and pLS-PD-L1-3'-UTR transfected MDA-MD-231, MaMel86b,
HK-2 and CRL-5826 cells captured by a Leica DM1L Microscope using a 4x/ 0.1 NA non-immersion
objective71
Supplementary Figure 8: Kaplan-Meier curve based on PD-L1 expression in breast and lung cancer.
High PD-L1 expression is very significantly associated with better prognosis of breast and lung
cancer patients. The Kaplan-Meier plots were generated with the Kaplan-Meier Plotter online tool
(Győrffy, 2021; Győrffy et al., 2013)72

# 8.3. List of tables

Table 1: microRNA library and short reference names used for Lipofectamine $^{ ext{TM}}$ transfection	15
Table 2: Composition of assay tubes for Qubit <sup>TM</sup> 4 Fluorometer measurements	16
Table 3: cDNA Synthesis components and thermal conditions.	17
Table 4: <i>Power</i> SYBR® Green RT-qPCR components and program	18
Table 5: Primer sequences for <i>Power</i> SYBR® Green RT-qPCR	18
Table 6: Fluorescent dyes and antibodies with short reference names used in this study	20
Table 7: Applied significance levels.	22
Table 8: miRNAs of interest decreasing PD-L1 and NT5E surface expression in human cell lines	31
Table 9: miRNAs increasing NT5E surface expression in human cell lines	34
Table 10: List of abbreviations	77
Table 11: List of units and prefixes.	80
Table 12: Chemicals and kits with manufacturers.	80
Table 13: Cell lines and origins	81
Table 14: Materials and manufacturers	81
Table 15: microRNA, plasmids and antibodies with manufacturers	82
Table 16: Devices and manufacturers	83
Table 17: Composition of cell culture medium and buffers.	83

# 8.4. Abbreviations

Table 10: List of abbreviations.

Abbreviations	Meaning
A	Absorbance
Ago	Argonaute protein
AKT	Protein kinase B
AKT1	RAC-alpha serine/threonine-protein kinase
APC	Allophycocyanin
ATCC	American Type Culture Collection
ATP	Adenosine triphosphate
AMP	Adenosine monophosphate
A.U.	Arbitrary unit
cAMP	Cyclic adenosine monophosphate
ccRCC	Clear cell renal cell carcinoma
CD73	Cluster of differentiation 73
	Gene name: Ecto-5'-nucleotidase (NT5E)
CD273	Cluster of differentiation 273
	Gene name: Programmed death-ligand 2 (PD-L2)
CD274	Cluster of differentiation 274
	Gene name: Programmed death-ligand 1 (PD-L1) or B7 homolog (B7-H1)
CD279	Cluster of differentiation 279
	Gene name: Programmed cell death-protein 1 (PD-1)
DGCR8	DiGeorge Syndrome Critical Region 8
DNA	Deoxyribonucleic acid
DSPC	1,2-diestearoyl-sn-glycero-3-phosphocholine
ENTPD1	Ectonucleoside triphosphate diphosphohydrolase 1
FACS	Fluorescence-activated cell sorting
FCS	Fetal calf serum
FSC	Forward scatter
GAPDH	Glyceraldehyde-3-phophate dehydrogenase
GLUT-1	Glucose transporter 1
GOI	Gene of interest
НК	Housekeeping genes

Abbreviations	Meaning
Ig	Immunoglobulin
KIF18B	Kinesin Family Member 18B
MFI	Median fluorescence intensity
miR	MicroRNA
miRNA	
miRISC	miRNA-induced silencing complex
mRNA	Messenger RNA
MAPK	Mitogen-activated protein kinase
MEK	Mitogen-activated extracellular signal-regulated kinase
MQ	Milli-Q distilled water
NOB1	NIN1/RPNI2 binding protein 1 homolog
NSCLC	Non-small-cell lung cancer
nt	Nucleotide
NT5E	Ecto-5'-nucleotidase
	Cell surface molecule nomenclature: CD73
PBS	Phosphate buffered saline
PD-1	Programmed cell death-protein 1
	Cell surface molecule nomenclature: CD279
PD-L1/2	Programmed death-ligand 1/2
	Cell surface molecule nomenclature: CD274/ CD273
PE	R-Phycoerythrin
pERK	Propylated extracellular signal-regulated kinase
PITX1	Paired like homeodomain 1
PI3K	Phosphatidylinositol 3-kinase
PKA	Protein kinase A
PLAC8	Placenta associated 8 protein
PLC	Phospholipase C
PTTG1	Pituitary tumor-transforming gene 1- oncogene
p.	Page
p.t.	Post transfection
RAB	Ras-related protein
RAF	Rapidly accelerated fibrosarcoma
RAS	Rat sarcoma virus
RNA	Ribonucleic acid

Abbreviations	Meaning
RPL19	Ribosomal protein 19
RPMI	Roswell Park Memorial Institute
RT	Room temperature
SEM	Standard error of the mean
shRNA	Short hairpin RNA transcript
SI	International System of Units
siRNA	Small interfering RNA
SOCS1	Suppressor of cytokine signaling 1
SOX-5	Sry-related HMG box
SSC	Side scatter
TTN-AS1	TTN antisense RNA 1
USA	United States of America
VEGF	Vascular endothelial growth factor
VHL	Von Hippel-Lindau
Wnt	Wingless and Int-1
Wnt5A	Wnt Family Member 5A
XPO5	Exportin 5
XTT	2,3-bis (2-methoxy-4-nitro-5-sulfophenyl)-5-[(phenylamino) carbonyl]-
	2H-tetrazolium hydroxide
ZAP70	Zeta-chain-associated protein kinase 70

Table 11: List of units and prefixes.

SI prefix	Meaning	Multifaction factor	
k	kilo	$10^{3}$	
m	milli	10-3	
$\mu$	micro	10-6	
n	nano	10-9	
p	pico	10 <sup>-12</sup>	
Units	ľ	Meaning	
Da		daltons	
g		grams	
h	hours		
L		liters	
min		minutes	
s		seconds	

## 8.5. Chemicals and materials

Table 12: Chemicals and kits with manufacturers.

Chemicals	Company	Headquarters
DharmaFECT Duo Transfection Reagent	Dharmacon <sup>TM</sup>	Lafayette, USA
Ethanol	Carl Roth	Karlsruhe, Germany
Fetal calf serum (FCS)	Sigma Aldrich	St. Louis, USA
High-Capacity cDNA Reverse Transcription Kit	Thermo Fischer Scientific	Waltham, USA
LightSwitch™ Luciferase Assay Kit	Active Motif	La Hulpe, Belgium
Lipofectamine™ RNAiMAX Transfection Reagent	Thermo Fischer Scientific	Waltham, USA
miRNeasy Mini Kit	Qiagen	Hilden, Germany
Penicillin-Streptomycin	Thermo Fischer Scientific	Waltham, USA
Phospahte Buffered Saline (PBS)	Gibco	Carlsbad, USA
PowerSYBR® Green PCR Master Mix	Applied Biosystems <sup>TM</sup>	Foster City, US
RNaseZap™	Thermo Fischer Scientific	Waltham, USA
Roswell Park Memorial Institute 1640 medium	Gibco™	Carlsbad, USA
TrpLE <sup>TM</sup>	Gibco <sup>™</sup>	Carlsbad, USA
Trypan blue (0.4 %)	Carl Roth	Karlsruhe, Germany

Chemicals	Company	Headquarters
Trypsin/EDTA (0.25 %)	Gibco	Carlsbad, USA
Qubit™ microRNA Assay Kit	Thermo Fisher Scientific	Waltham, USA
XTT Cell Proliferation Assay	SERVA Electrophoresis	Heidelberg, Germany
	GmbH	
Yellow fluorescent reactive dye	Invitrogen <sup>TM</sup>	Carlsbad, USA

Table 13: Cell lines and origins.

Cell line	Origin/ provided by	Headquarters
CRL-5826 (NCI-H226)	ATCC®	Manassas, USA
MaMel86b	Universitätsklinik Mannheim (Hauttumorzentrum)	Mannheim, Germany
MDA-MB-231 (HTB-26)	ATCC®	Manassas, USA
HK-2 (CRL-2190)	Curtesy of Prof. Dr. Ilse Hoffmann, DKFZ	Heidelberg, Germany
HT-29 (HTB-32)	ATCC®	Manassas, USA

Table 14: Materials and manufacturers.

Disposables	Company	Headquaters
Aluminum foil	VWR International	Radnor, USA
Cell culture flask (75 cm <sup>2</sup> )	Greiner Bio-One	Frickenhausen, Germany
C-CHIP disposable hemocytometer	Kisker Biotech,	Steinfurt, Germany
Eppendorf reaction tubes (1.5, 2 ml)	Eppendorf AG	Hamburg, Germany
Gloves	Starlab International GmbH	Hamburg, Germany
Polystyrene round-bottom tubes	Corning Incorp.	New York, US
with cell-strainer cap		
Qubit <sup>™</sup> assay tubes	Thermo Fischer Scientific	Waltham, USA
RNase free filter-tips (10, 20, 100,	Starlab International GmbH	Hamburg, Germany
200, 1000 $\mu$ l)		
Serological pipettes (5, 10, 25 ml)	Greiner Bio-One GmbH	Frickenhausen, Germany
12-well plates	TPP Techno Plastic Products	Trasadingen, Switzerland
96-well flat bottom plates	TPP Techno Plastic Products	Trasadingen, Switzerland
96-well flat bottom plates (opaque)	PerkinElmer <sup>TM</sup>	Waltham, USA
96-well round bottom plates	TPP Techno Plastic Products	Trasadingen, Switzerland

Table 15: microRNA, plasmids and antibodies with manufacturers.

microRNAs	Company	Headquarters
miRIDIAN® microRNA Mimic:	Dharmacon <sup>TM</sup>	Lafayette, USA
1. hsa-miR-139-3p		
2. hsa-miR-139-5p		
3. hsa-miR-146a-3p		
4. hsa-miR-146a-5p		
5. hsa-miR-155-5p		
6. hsa-miR-374b-3p		
7. hsa-miR-512-3p		
8. hsa-miR-1204		
9. hsa-miR-1228-3p		
10. hsa-miR-1273c		
11. hsa-miR-3117-3p		
mirVana™ miRNA Mimic: Negative Control #1 (ath-miR-416)	$Invitrogen^{\rm TM}$	Carlsbad, USA
ON-TARGETplus SMART pool Human CD274	Dharmacon <sup>TM</sup>	Lafayette, USA
ON-TARGETplus SMART pool Human NT5E	Dharmacon <sup>TM</sup>	Lafayette, USA
Plasmids	Company	Headquarters
pLS-PD-L1-3'-UTR	Active Motif	La Hulpe,
		Belgium
Antibodies	Company	Headquarters
Anti-Hu CD274 (PD-L1, B7-H1)	Invitrogen <sup>TM</sup>	Carlsbad, USA
Clone: MIH1, REF. 17-5983-48		
PE anti-human CD73 (Ecto-5'-nucleotidase)	BioLegend®	San Diego, USA
Clone: AD2, Cat. 344044		
Mouse IgG1 kappa Isotype Control eFluor 660	Invitrogen <sup>TM</sup>	Carlsbad, USA
Clone: P3.6.2.8.1 REF.50-4714-82		
Mouse IgG1 kappa Isotype Control PE	Invitrogen <sup>TM</sup>	Carlsbad, USA
Clone: P3.6.2.8.1, REF. 12-4714-82		

82

Table 16: Devices and manufacturers

Machines	Company	Headquaters
BD FACSCanto™ II Flow Cytometer	Becton Dickinson Bioscience	Franklin Lakes, USA
CLARIOstar® <i>Plus</i> microplate reader	BMG LABTECH GmbH	Ortenberg, Germany
CO <sub>2</sub> incubator CB210	BINDER	Tuttlingen, Germany
Centrifuge 5810 R	Eppendorf AG	Hamburg, Germany
Fluoroskan <sup>TM</sup> Ascent Microplate	Thermo Fischer Scientific	Waltham, USA
Fluorometer		
Leica DM1L Microscope	Leica	Wetzlar, Germany
QuantStudio™ 3 Real-Time PCR System	Applied Biosystems <sup>TM</sup>	Foster City, US
Qubit™ 4 Fluorometer	Thermo Fischer Scientific	Waltham, USA
Refrigerator	Liebherr	Bulle FR, Switzerland
Thermomixer comfort	Eppendorf AG	Hamburg, Germany
Veriti™ 96 Well Thermal Cycler	Applied Biosystems™	Foster City, US

Table 17: Composition of cell culture medium and buffers.

Solutions	Composition
Culture medium	10 % FCS
	1 % Penicillin-streptomycin
	in RPMI 1640
FACS buffer	3 % FCS
	in PBS

### 8.6. Acknowledgements

An dieser Stelle möchte ich mich bei all denjenigen bedanken, die mich während meines Studiums und der Anfertigung dieser Masterarbeit unterstützt und motiviert haben:

Zuerst möchte ich mich recht herzlich bei **Prof. Dr. Beatrix Süß** bedanken. Ihre interessanten Vorlesungen und Praktika begleiten mich seit dem ersten Semester und haben mein Interesse an der Genetik und der RNA geweckt. Sie sind ein integraler Teil meiner Entwicklung an dieser Universität gewesen und sind als Professorin ein großes Vorbild für mich! Vielen Dank für das vermittelte Wissen und die netten Gespräche, die ich mit Ihnen in den letzten Jahren führen durfte.

Des Weiteren gilt mein Dank **Prof. Dr. Stefan Eichmüller** vom Deutschen Krebsforschungszentrum (DKFZ). Ich habe in Heidelberg viele neue Erfahrungen sammeln können, die mir geholfen haben mich fachlich und persönlich weiterzuentwickeln. Ich schätze Ihre Investition in mich als junge Naturwissenschaftlerin sehr und habe mich besonders gefreut, an so interessanten Forschungsthemen mitarbeiten zu dürfen.

Ein besonderes Dankeschön gilt **Dr. Theresa Kordaß** für die gute Betreuung und die tolle Zeit im Labor. Gerne möchte Ich mich auch beim gesamten **Eichmüller Labor** bedanken. Ich wurde von euch herzlich aufgenommen und habe mich immer über eure hilfreichen Tipps und eure Unterstützung gefreut.

Ebenfalls möchte ich mich recht herzlich bei **meinen Freunden** bedanken. Vielen Dank für eure Freundschaft und das stetige gemeinsame Durchstehen der persönlichen und akademischen Herausforderungen.

Abschließend möchte ich mich bei **meinen Eltern** bedanken, die mir mein Studium durch ihre Unterstützung ermöglicht haben. Ihr habt mir stehts mit Rat und Tat zur Seite gestanden und hattet immer ein offenes Ohr für mich. Vielen Dank, dass ihr an mich geglaubt habt und mich immer wieder neu motiviert habt meine Ziele und Träume zu verfolgen.